SYNAPTIC DYSREGULATION OF INHIBITION IN THE DENTATE GYRUS AFTER TRAUMATIC BRAIN INJURY

Kaitlin A. Folweiler

A DISSERTATION

in

Neuroscience

Presented to the Faculties of the University of Pennsylvania

in

Partial Fulfillment of the Requirements for the

Degree of Doctor of Philosophy

2019

Supervisor of Dissertation

_____

Dr. Akiva S. Cohen

Professor of Anesthesiology and Critical Care Medicine

Graduate Group Chairperson

_____

Dr. Joshua I. Gold, Professor of Neuroscience

Dissertation Committee

Dr. D. Kacy Cullen, Committee Chair, Research Associate Professor of Neurosurgery

Dr. Minghong Ma, Professor of Neuroscience

Dr. Diego Contreras, Professor of Neuroscience

Dr. Marc V. Fuccillo, Assistant Professor of Neuroscience

Dr. Corina O. Bondi, Assistant Professor of Physical Medicine and Rehabilitation, University of Pittsburgh School of Medicine

SYNAPTIC DYSREGULATION OF INHIBITION IN THE DENTATE GYRUS AFTER TRAUMATIC

BRAIN INJURY

To my parents Judy and Joe, and my grandmothers Lucy and Ann.

Thank you for the love and encouragement, always.

ACKNOWLEDGEMENTS

I am extremely grateful for the excellent scientific training I have received as a graduate student in the Neuroscience Graduate Group at the University of Pennsylvania. The NGG would not be what it is without its graduate students, who I want to thank for creating such a fun and supportive community. I also would like to thank the NGG administrators, Josh Gold, Jane Hoshi, Christine Clay, as well as all the faculty instructors for their expertise and time devoted to teaching. This includes the members of my thesis committee, who have always provided constructive feedback and insight.

To the members of the Cohen laboratory, past and present, I am very appreciative of your patience, wisdom and willingness to help me throughout my graduate research. Thank you to my family and friends for the good times and the laughs outside of lab. To my boyfriend Brian, I am so lucky to have such a caring and supportive partner since the beginning of this journey. Thanks for always encouraging me to achieve my goals.

I am honored to have had two amazing mentors throughout my training. I want to thank my undergraduate mentor, Anthony Kline, for instilling an attention to detail and for inspiring me to go to graduate school. And to Kiva—you are an “n of 1” among graduate advisors. No other graduate advisor devotes more time to, and cares more about his students. Thank you for your eternal optimism, putting up with my sass, and always having an open door. I am truly grateful for the opportunity to have learned and grown as a scientist in your lab. Go Eagles!

ABSTRACT

SYNAPTIC DYSREGULATION OF INHIBITION IN THE DENTATE GYRUS

AFTER TRAUMATIC BRAIN INJURY

Kaitlin A. Folweiler

Akiva S. Cohen, PhD

Traumatic brain injury (TBI) is a leading cause of death and disability in the United States, with an estimated 2.8 million new cases annually resulting from falls, motor vehicle accidents, sports, and other traumatic events. About 75-80% of new cases are considered to be mild (mTBI). Of the sequelae of neurological symptoms that result from mTBI, memory impairments are among the most prevalent and long-lasting consequences. The encoding and consolidation of episodic memories relies on spatial information processing within the hippocampus. The dentate gyrus hippocampal sub-region is one of the primary entryways of cortical input to the hippocampus and is thought to act as a gate or filter of incoming excitation, as well as play a role in specific cognitive processes such as pattern separation. After brain injury, the dentate gyrus exhibits increased network hyperexcitability, however the underlying mechanisms and impact of this circuit alteration on downstream hippocampal function are poorly understood. In this body of work, we evaluated the physiological effects of TBI on dentate gyrus function in a mouse model of lateral fluid percussion injury. One week after injury, our results indicate that network hyperexcitability leads to diminished dentate filtering efficacy and consequently, increased network excitation in downstream area CA3. Additionally, we evaluated the effects of brain injury on the intrinsic and synaptic properties of GABAergic, parvalbumin-expressing inhibitory interneurons in the dentate gyrus. The data demonstrate that increased synaptic inhibition onto these interneurons decreased their likelihood of firing action potentials and suggests a potential mechanism contributing to dentate

network hyperexcitability. These findings have important implications for understanding hippocampal vulnerability and associated memory impairments following TBI.

TABLE OF CONTENTS

LIST OF TABLES AND FIGURES

Chapter 2: Diminished dentate gyrus filtering of cortical input leads to enhanced area CA3 excitability after mild traumatic brain injury

Chapter 3: Traumatic brain injury reduces feedforward activation of parvalbumin-expressing interneurons in the dentate gyrus

CHAPTER 1

INTRODUCTION

Traumatic brain injury

Traumatic brain injury (TBI) is a frequent occurrence in the United States, with an estimated 2.8 million new cases reported each year (Taylor et al., 2017). TBI is generally defined as any disruption in normal brain functioning resulting from a physical blow to, or rapid acceleration and deceleration of the head (Kay et al., 1993; R. M. Ruff et al., 2009). On the severity spectrum of TBI, mild traumatic brain injury (mTBI), also known as concussion, is the most common type of brain injury and accounts for 75-80% of all cases (Thomas R. Frieden, Debra Houry, 2015). In the acute-subacute injury period lasting up to 3 months after mTBI, patients can experience a range of neurological symptoms. These include physical or sensory disturbances (e.g., headaches, dizziness, nausea, photophobia, etc.), affective symptoms such as irritability, anxiety and depression, and cognitive deficits, which include problems with attention and memory, slow processing speed and a feeling of fogginess (Prince & Bruhns, 2017).

While the majority of mTBI patients recover within 3 months, about 10-20% of cases experience post-concussive syndrome, with prolonged symptoms occurring for months or years after the initial injury (Ruff 2005). Currently, there are no FDA-approved therapeutic treatments available to mitigate mTBI symptoms or to prevent development of post-concussion syndrome. Therefore, there is a critical need to understand the underlying mechanisms of mTBI symptoms and to identify potential therapeutic targets.

Memory impairments after mTBI

Regarding the sequelae of mTBI symptoms, memory impairments are extremely common (Nicholl & LaFrance, 2009; Pierce et al., 1998; Rutland-Brown et al., 2006). Indeed, memory and TBI appear to be intrinsically linked, as the hippocampus and cortex, brain regions involved in the physiological circuits of memory, are often damaged after TBI (Adams et al., 1989; Graham et al., 1995; Paterno et al., 2017). Memory is a dynamic neural and cognitive progression characterized by three separate processes: encoding, maintenance and retrieval (Tulving, 1985). Encoding is the transformation of an experience into a discrete neural representation, known as the memory engram. Maintenance refers to the endurance of the engram across time, and retrieval is the ability to voluntarily reinstate the engram into the forefront of consciousness. It is widely accepted that the hippocampus plays a major role in all three of these memory processes (Josselyn et al., 2015; Tonegawa et al., 2015). However, it is unknown how, and whether, TBI disproportionately alters one of these processes compared to the others.

While several types of memory are disrupted after TBI, our laboratory is interested in the effects of brain injury on episodic and spatial memory (Coronado et al., 2012; Shum et al., 1999; Wammes et al., 2017) . Episodic and spatial learning and memory deficits have been well-established using spatial and contextual behavioral tasks in many TBI animal models (see Paterno et al., 2017 for comprehensive review of behavioral studies). Episodic memory refers to the recall of personal experiences or events that contain information on what has happened and also where and when it happened (Pause et al., 2013; Tulving & Markowitsch, 1998). That is, episodic memory receives and stores information about temporally-dated episodes or events, and temporal-spatial relations among these events (Tulving, 1972). Spatial navigation memory, represented in episodic

memory, is a subtype of memory that records information about a subject's environment and navigation within that environment.

Episodic and spatial memory predominantly rely on the function of the hippocampus, which plays a central role in a large network of brain areas that interact to store and retrieve memory engrams (Josselyn et al., 2015; Tonegawa et al., 2015). Specifically, the hippocampus receives spatial and non-spatial information about the environment via projections from the superficial layers of the medial and lateral entorhinal cortex, respectively. The hippocampus then encodes this information into the memory engram, which undergoes consolidation over time in a process that involves transfer to and storage in the cerebral cortex. Retrieval of episodic memories, leading to conscious recall of the memory engram is also mediated by the hippocampus. Recently, it has been demonstrated that retrieved memory engrams from the hippocampus are returned to deep layers of the entorhinal cortex and then re-presented as new input to the superficial entorhinal layers in order to loop back into hippocampus (Koster et al., 2018). This "big-loop" reoccurrence, whereby hippocampal outputs are recirculated as new inputs, simultaneously allows for the storage of distinct episodic memories, as well as the ability for linking associations across episodes.

The hippocampal circuit

The hippocampus is comprised of three sub-regions: the dentate gyrus, area CA3, and area CA1. This is classically referred to as the "tri-synaptic circuit", where cortical information entering the hippocampus flows from dentate gyrus to CA3 to CA1, though CA3 and CA1 both receive direct projections from the entorhinal cortex, as well (D. G. Amaral & Witter, 1989). Each of these sub-regions is thought to have distinct functional

roles in hippocampal-dependent memory processing. For instance, the dentate gyrus is thought to be implicated in pattern separation, the ability to receive a pattern of afferent inputs and 'separate' them so that the outputs are less similar than the inputs (Bakker et al., 2008; Leutgeb et al., 2007b; Marr, 1971; McNaughton & Morris, 1987; O'Reilly & McClelland, 1994; A. Treves & Rolls, 1994). Pattern separation in the dentate gyrus is important for memory encoding in area CA3 because it its thought to allow similar experiences to be stored in different subsets of CA3 pyramidal cells (Yassa & Stark, 2011).

In addition to memory storage, area CA3 plays a critical role in memory retrieval via the process of pattern completion. Pattern completion allows for the reactivation of full memory engrams using partial information as recall cues and is thought to be conferred through rich auto-associational inputs from recurrent CA3 pyramidal cell axon collaterals (Hasselmo et al., 1995; Marr, 1971; McNaughton & Morris, 1987; Nakashiba et al., 2012; O'Reilly & McClelland, 1994; Treves et al., 1994). Area CA1 is also heavily implicated in the storage and retrieval of spatial information. Specifically, cells in the CA1 region, known as place cells, encode spatial representations of the environment and are important for long-term memory involving space (I. Lee & Kesner, 2004; Moser et al., 2008). Overall, each hippocampal area plays many vital subspecialty roles in memory processing, and physiological disruption of any of these sub-regions or their connections, is thought to be largely responsible for disruption of episodic and spatial memory after TBI (David G Amaral et al., 1996; Bohbot et al., 2000; Cave & Squire, 1991; Deweer et al., 2001; Miller et al., 1998; Reed & Squire, 1997).

The dentate gyrus circuit

At the forefront of the hippocampal circuit, the dentate gyrus is a crucial regulator of incoming cortical excitability to the hippocampus. The dentate gyrus has a laminar structure with three predominant layers: the molecular layer, the granule cell layer, and the hilus (Chapter 2, Figure 2). The dentate gyrus laminar structure has a characteristic "V-shape", which splits the granule cell and molecular layers into a suprapyramidal blade above the pyramidal cell layer of area CA3, and an infrapyramidal blade running below it.

Dentate granule cells, whose cell bodies comprise the granule cell layer, are the principal glutamatergic cells within the dentate gyrus circuit. The rodent hippocampus contains approximately 800,000 to 1 million granule cells (David G. Amaral et al., 2007; Amrein et al., 2004; Witgen et al., 2005). Granule cell dendrites extend into the molecular layer where they receive synaptic input from axons originating in superficial entorhinal cortex layers, known as the perforant path. While the perforant path is considered to be the major input to the dentate gyrus, this region also receives extrinsic, neuromodulatory inputs from the septal nuclei (cholinergic), supramammillary area of the hypothalamus (glutamatergic), and the brainstem (noradrenergic and dopaminergic) (D. G. Amaral & Kurz, 1985; Dent et al., 1983; Lübke et al., 1997; Maglóczky et al., 1994; Moore & Halaris, 1975; Pickel et al., 1974; Swanson & Hartman, 1975; Wyss et al., 1979). Granule cell axons, known as mossy fibers, then pass through the hilus and synapse onto cells in downstream area CA3. The interface between the hilus and the granule cell layer, called the subgranular zone, is also one of two sites of adult neurogenesis in the mammalian brain (Kempermann & Gage, 2000).

In addition to granule cells, the dentate gyrus contains a diverse array of interneurons, which exert a balance of excitation and inhibition onto granule cells and regulate their firing output (Houser, 2007). The majority of these interneurons are GABAergic, though there are two glutamatergic types: mossy cells and semilunar granule cells (Helen E. Scharfman & Myers, 2013; Helen E Scharfman, 2016; Williams et al., 2007). Mossy cells are found in the hilus and receive excitatory input from granule cells as well as CA3 backprojections to the hilus (H. E. Scharfman, 1994; Helen E Scharfman, 2016). These neurons provide feedback excitation onto granule cells and GABAergic interneurons, and it is unclear whether they have a net excitatory or inhibitory effect on granule cells due to their complex role in the dentate circuit. Semilunar granule cells reside in the inner molecular layer and provide glutamatergic input to hilar interneurons as well as neighboring granule cells (Larimer & Strowbridge, 2010).

The GABAergic interneuron types in the dentate gyrus can classified broadly by whether they form synapses onto granule cells at perisomatic or dendritic locations (Freund & Buzsáki, 1996; Halasy & Somogyi, 1993; Han et al., 1993; Houser, 2007). Basket cells and axo-axonic cells, two interneuron types both expressing the calcium-binding protein parvalbumin (PV+), form synapses directly onto granule cell soma and axon initial segment, respectively. Basket cells are most concentrated in the subgranular zone, while axo-axonic cells have their cell bodies in the molecular layer. Both types are directly innervated by perforant path and mossy fiber axons, and therefore are strong sources of rapid feed-forward and feedback inhibition onto granule cells. Another source of granule cell feed-forward inhibition comes from an interneuron population in the molecular layer known as molecular layer perforant path-associated (MOPP) cells (Halasy & Somogyi, 1993; Li et al., 2013). The location of MOPP cell bodies is primed to receive afferent

glutamatergic synapses from the perforant path and also potentially from commissural-association fibers from the contralateral hippocampus (Freund & Buzsáki, 1996).

The hilus contains both somatostatin-positive hilar perforant path-associated (HIPP) cells and cholecystokinin-positive (CCK) hilar commissural-associational pathway (HICAP) cells. Because of the location of their cell bodies, both HIPP and HICAP cells primarily receive excitatory input from granule cell mossy fibers. HIPP and HICAP cell axons project back onto the distal dendrites of granule cells, close to the sites of perforant path and commissural-associative synapses, respectively. Functionally, these neurons provide feedback inhibition as well as finely-tuned regulation of excitatory synapses onto granule cells (Bakst et al., 1986; Katona et al., 1999; Leranth et al., 1990).

The dentate gyrus as a gate or filter of cortical input to the hippocampus

The physiological properties of the dentate gyrus support the theory that this sub-region acts as a gate, or filter, of afferent input into the hippocampus and regulates perforant path excitation to downstream area CA3 (Hsu, 2007). Under normal conditions *in vivo*, granule cells exhibit sparse, spatially-selective firing activity, which is thought to support dentate-mediated cognitive functions such as pattern separation, novelty detection, and spatial learning (Chawla et al., 2005; Gilbert et al., 2001; Hunsaker et al., 2008; Jung & McNaughton, 1993; Leutgeb et al., 2007a; Morris et al., 2012). Previous studies using perforant path electrical stimulation determined that the dentate gyrus largely remains silent in response to afferent excitation, and that network activation only occurs with longer duration stimuli within the 10-15 Hz frequency range (Alger & Teyler, 1976; Andersen et al., 1966; Teyler & Alger, 1976). The Infrequent action potential firing of dentate granule cells is due to a combination of cellular- and circuit-level attributes, including low granule

cell intrinsic membrane excitability such as an extremely hyperpolarized resting membrane potential and low input resistance, little direct connectivity between granule cells, as well as strong inhibitory control from the local network of GABAergic interneurons (Coulter & Carlson, 2007; Fricke & Prince, 1984). As a secondary consequence of low network excitability, the dentate gyrus has been shown to restrict the relay of pathological cortical seizure activity into the hippocampus (Dengler & Coulter, 2016; Lothman et al., 1992). These circuit properties are maintained by excitatory-inhibitory (E/I) balance within the dentate gyrus and contributes to its physiological filtering function.

After TBI, the dentate gyrus is tipped into a hyperexcitable state. Animal studies show that the dentate gyrus experiences an increase in network excitability associated with an imbalance of E/I synaptic transmission onto granule cells (Lowenstein et al., 1992; Santhakumar et al., 2000; Santhakumar et al., 2001; Toth et al., 1997; Witgen et al., 2005). Posttraumatic E/I disruption has also been shown to occur alongside hippocampal-dependent memory impairments and interneuron cell loss in the hilus (Cole et al., 2010; Lowenstein et al., 1992; V Santhakumar et al., 2000; Toth et al., 1997; Witgen et al., 2005). Interestingly, the intrinsic membrane properties of granule cells appear to be unaffected by injury (Hunt et al., 2011; Lowenstein et al., 1992; V Santhakumar et al., 2000; Santhakumar et al., 2003).

Inhibitory transmission onto granule cells, comprised of phasic and tonic components, is altered as well. The frequency of phasic $GABA_e$rgic synaptic currents onto the granule cells is diminished one week after experimental TBI (Santhakumar et al., 2000; Toth et al., 1997; Witgen et al., 2005). One month after TBI phasic inhibition recovers; however in more severe injury models, inhibition remains diminished for several months post-injury (Hunt et al., 2011; Santhakumar et al., 2001). Compromised phasic inhibition is associated

with reduced expression of the potassium-chloride membrane transporter KCC2, thus decreasing the driving force of chloride through $GABA_A$ receptors (Bonislawski et al., 2007). A reduction in phasic $GABA_e$rgic inhibition appears to be present across TBI models, but the duration of these changes varies with injury severity. In contrast, tonic inhibition is altered in opposite directions depending on the cell type. For example, tonic inhibition is enhanced onto granule cells, while it is diminished onto semilunar granule cells (Boychuk et al., 2016; Gupta et al., 2012; Langlois et al., 2015; Mtchedlishvili et al., 2010; Pavlov et al., 2011). Therefore, alteration in inhibition leads to a complicated dysfunction of granule cell activity regulation.

In order to understand alterations in granule cell firing, it is imperative to examine alterations in DG interneurons. Of the $GABA_e$rgic interneuron subtypes, only hilar somatostatin-positive interneurons, which supply dendrite inhibition onto granule cells, have been examined physiologically after TBI. A study by Hunt and colleagues demonstrated that somatostatin-expressing interneurons in the hilus receive more glutamatergic synaptic input after injury, and fire more action potentials (Hunt et al., 2011). In addition, glutamatergic mossy cells have been shown to fire more action potentials, resulting in delayed excitatory postsynaptic currents in granule cells (Santhakumar et al., 2000). Increased mossy cell firing is due to a shift in enhanced afferent excitatory input as well as homeostatic compensation of intrinsic properties after TBI (Howard et al., 2007). In summary, the current literature suggests that posttraumatic dentate hyperexcitability is primarily due to changes in $GABA_e$rgic and glutamatergic (i.e., E/I) synaptic transmission within this sub-region.

Although dentate gyrus hyperexcitability has been well-studied after TBI, there is still much

to be understood about the underlying mechanisms of network E/I imbalance, and its downstream effects on the hippocampal function and hippocampal-dependent memory processing. As previously mentioned, phasic inhibition onto granule cells is diminished one week following experimental mTBI, suggesting potential alterations in the function of GABAergic interneurons within the network (Toth et al., 1997; Witgen et al., 2005). A potential source of reduced granule cell inhibition is the fast-spiking, parvalbumin-positive interneuron (PV-INs) population, which provide robust inhibition onto granule cells via perisomatic synapses. Functional changes in PV-INs have been observed in the cerebral cortex after experimental TBI (Vascak et al., 2018), however the effects of injury on PV-INs in the dentate gyrus have yet to be explored.

In the present work, we aimed to understand the functional effects of mTBI on PV-INs within the dentate gyrus and the downstream consequences of dentate network hyperexcitability during the acute injury period. Our primary hypothesis was that dentate hyperexcitability does not remain isolated in this region but spreads to downstream area CA3, thus disrupting the physiological filtering function. Our secondary hypothesis, to address a potential source of decreased granule cell inhibition, was that GABAergic PV-IN cells experience synaptic and intrinsic alterations in their E/I balance which reduces their firing output.

To test our hypotheses, we performed a series of behavioral and electrophysiological experiments one week after lateral fluid percussion injury, a mouse model of mTBI. Lateral fluid percussion injury (LFPI) is a well characterized and commonly used rodent model of brain injury that reproduces key features of human TBI, including neuronal cell loss, gliosis, ionic perturbation, and memory deficits (Carbonell et al., 1998; Dixon et

al., 1987; McIntosh et al., 1989; Smith et al., 1991). LFPI produces an injury that has both focal and diffuse components, and despite subtle differences has largely been replicated across laboratories (Thompson et al., 2005). The LFPI model utilizes a fluid pressure wave impact, initiated by the release of a pendulum onto the end of a water-filled cylinder, which then travels down the length of the cylinder and directly impacts craniotomy-exposed dura mater over the right parietal cortex. The pendulum height of the device can be set to increase the amplitude of the pressure wave and thus can create a range of injury severities. To recapitulate human mTBI, our LFPI model uses a fluid pressure wave with amplitudes between 1.4-1.6 atmospheres that does not rupture the dura mater (See Chapter 1 Materials and Methods). These injury parameters prevent dural breaches and bleeding typically not seen in human mTBI cases, while also producing behavioral cognitive deficits similar to postconcussive symptoms (Palmer et al., 2016; C. J. Smith et al., 2015; Witgen et al., 2005). Behavioral and physiological evaluation was performed at one week after LFPI for two main reasons. First, this time period mimics the acute injury period after transient metabolic and pathophysiological cascades have stabilized. Secondly, this time point falls within the clinically relevant "therapeutic time window" when potential mechanisms can be targeted for intervention (Cole et al., 2010; Grady MS, 1995).

In Chapter 2, we investigated the effects of network hyperexcitability on the physiological filtering function of the dentate gyrus. We first established that LFPI induced impairments in a behavioral task of spatial novelty detection, which is reliant on interplay between the dentate gyrus and area CA3. To evaluate dentate filtering efficacy, we performed voltage-sensitive dye imaging and extracellular field recordings in acute brain slices to assess network excitability in both the dentate gyrus and area CA3 in response to perforant path electrical stimulation. Voltage-sensitive dye imaging revealed the aberrant spatial spread

of depolarization from the dentate gyrus into area CA3. Extracellular field recordings confirmed that this spread of depolarization led to increased population spikes in area CA3 and that this was due to mossy fiber synaptic transmission. From these data, we conclude that dentate network hyperexcitability leads to an aberrant spread of excitability into area CA3, thereby indicating a diminished DG filtering efficacy and disrupting E/I balance in its downstream target.

In Chapter 3, we investigated physiological alterations in PV-IN intrinsic membrane properties, as well as synaptic inputs onto PV-INs in the dentate gyrus one week after lateral fluid percussion injury using whole-cell patch clamp recordings. We first determined that there was no significant loss of PV-INs in the injured dentate gyrus. Next, whole-cell recordings from PV-INs demonstrated that while LFPI did not disturb PV-IN intrinsic membrane properties, synaptic E/I balance onto these neurons was greatly perturbed. LFPI slices demonstrated a significant reduction in the amplitude and charge transfer of evoked excitatory postsynaptic currents (EPSCs) in response to perforant path stimulation. Spontaneous and miniature EPSCs showed increased amplitudes but opposing shifts in frequency, suggesting alterations in different mechanisms of synaptic transmission. On the inhibitory side, miniature inhibitory postsynaptic currents (IPSCs) also experienced an increase in size following LFPI, however only spontaneous, action potential-mediated IPSCs showed an increase in frequency. To understand the net effects of these alterations in E/I synaptic transmission on PV-IN firing output, we applied minimal perforant path stimulation in LFPI and sham control slices and recorded the number of action potentials that resulted from each stimulation. Under normal conditions, PV-INs from LFPI slices fired significantly fewer action potentials than control PV-INs. When GABAergic synaptic transmission was blocked in the presence of picrotoxin, PV-IN cells

from both sham and LFPI slices fired the same number of action potentials in response to minimal stimulation. Therefore, the results of these experiments indicate that alterations in E/I balance onto PV-INs in the dentate gyrus have a net inhibitory effect and decrease the propensity for these interneurons to fire action potentials.

Altogether, our findings demonstrate that there are functional consequences to dentate network E/I imbalance which may due to alterations in synaptic transmission onto inhibitory interneurons. Diminished PV-IN firing activity may suggest that GABAergic signals from these neurons is also decreased and could be a potential mechanism underlying decreased granule cell inhibition after LFPI. In sum, this dissertation work has important implications for further understanding network shifts in excitability and synaptic reorganization within this circuit after injury, and identifies a potential cellular mechanism that can be explored therapeutically to restore dentate physiological and cognitive function.

CHAPTER 2

DIMINISHED DENTATE GYRUS FILTERING OF CORTICAL INPUT LEADS TO ENHANCED AREA CA3 EXCITABILITY AFTER MILD TRAUMATIC BRAIN INJURY

Kaitlin A. Folweiler,[1,2,3] Sandy Samuel,[1,2] Hannah E. Metheny,[1,2]

Akiva S. Cohen[1,2,3]

[1]Department of Anesthesiology and Critical Care Medicine, Children's Hospital of Philadelphia, Philadelphia, PA 19104. [2]Department of Anesthesiology, Perelman School of Medicine, University of Pennsylvania, Philadelphia, PA 19104. [3]Neuroscience Graduate Group, University of Pennsylvania, Philadelphia, PA 19104

Abstract

Mild traumatic brain injury (mTBI) disrupts hippocampal function and can lead to long-lasting episodic memory impairments. The encoding of episodic memories relies on spatial information processing within the hippocampus. As the primary entry point for spatial information into hippocampus, the dentate gyrus is thought to function as a physiological gate, or filter, of afferent excitation before reaching downstream area CA3. While injury has previously been shown to alter dentate gyrus network excitability, it is unknown whether mTBI affects dentate gyrus output to area CA3. In this study, we assessed hippocampal function, specifically the interaction between the dentate gyrus and CA3, using behavioral and electrophysiological techniques in *ex vivo* brain slices one week following mild lateral fluid percussion injury (LFPI). Behaviorally, LFPI mice were found to be impaired in an object-place recognition task, indicating that spatial information processing in the hippocampus is disrupted. Extracellular recordings and voltage-sensitive dye imaging demonstrated that perforant path activation leads to the aberrant spread of excitation from the dentate gyrus into area CA3 along the mossy fiber pathway. These results suggest that after mTBI the dentate gyrus has a diminished capacity to regulate cortical input into hippocampus, leading to increased CA3 network excitability. The loss of the dentate filtering efficacy reveals a potential mechanism by which hippocampal-dependent spatial information processing is disrupted, and may contribute to memory dysfunction after mTBI.

Introduction

Mild traumatic brain injury (mTBI) leads to an array of long-lasting cognitive symptoms, notably including episodic memory dysfunction (Tsirka et al., 2010). In the healthy brain, episodic memory relies on cortical input of spatial information to the hippocampus for memory encoding and consolidation. Experimental mTBI models have specifically demonstrated that hippocampal disruption is associated with spatial memory impairments (Milman et al., 2005; Paterno et al., 2017; Tweedie et al., 2013; Witgen et al., 2005; Zohar et al., 2011). The dentate gyrus is poised to receive incoming signals from layer II/III entorhinal cortex via perforant path axons and transmit signals to the CA3 region of the hippocampus via the mossy fiber axonal pathway (Witter, 2007b, 2007a). Synaptic transmission through this di-synaptic pathway plays a critical role in the processing of spatial information received by the hippocampus, as well as in pattern separation and completion (Bakker et al., 2008; Gilbert et al., 2001; Hunsaker et al., 2008; Leutgeb et al., 2007b; Marr, 1971; McHugh et al., 2007; McNaughton & Morris, 1987; Nakashiba et al., 2012; O'Reilly & McClelland, 1994; A. Treves & Rolls, 1994).

The dentate gyrus (DG) is thought to act as a physiological gate, or filter, of afferent input into the hippocampus, limiting afferent cortical excitation to area CA3 (Hsu, 2007). This filtering property is distinctly exhibited by the sparse, action potential firing of dentate granule cells in response to perforant path stimulation (Alger & Teyler, 1976; Andersen et al., 1966; Teyler & Alger, 1976). Sparse granule cell activation is likely due to both the low intrinsic membrane excitability of granule cells, as well as robust GABAergic inhibition from interneurons within the DG network (Coulter & Carlson, 2007; Fricke & Prince, 1984; H E Scharfman, 1992; Staley et al., 1992; Williamson et al., 1993). As such, the putative

dentate filter may be functionally important for discerning relevant spatial information for further hippocampal memory processing and diminishing irrelevant inputs.

Lateral fluid percussion injury (LFPI) is a well characterized and commonly used rodent model of brain injury that reproduces key features of human TBI, including neuronal cell loss, gliosis, ionic perturbation, and memory deficits (Dixon et al., 1987; McIntosh et al., 1989; D. H. Smith et al., 1991). After LFPI, the DG experiences a net increase in network excitability associated with an imbalance of excitatory and inhibitory synaptic transmission onto dentate granule cells(Butler et al., 2015; Gupta et al., 2012; Hunt et al., 2009, 2010; Lowenstein et al., 1992; V Santhakumar et al., 2000; Vijayalakshmi Santhakumar et al., 2001; Toth et al., 1997; Witgen et al., 2005). Though posttraumatic alterations in individual DG cell types have been well characterized, it remains unknown how these circuit alterations affect the net output of the DG to area CA3. In this study, we investigated the physiological filtering ability of the dentate gyrus to limit afferent excitation to area CA3 using a mouse model of LFPI. We initially confirm spatial novelty detection impairments in a hippocampal-dependent behavioral task at one week after LFPI. To evaluate DG filtering efficacy, we used electrophysiological techniques in acute brain slices to assess network excitability in DG and area CA3 in response to perforant path stimulation. The results demonstrate that afferent excitation not only generates a hyperexcitable shift in the DG network response after LFPI, but causes aberrant propagation of excitation to CA3 via the mossy fiber pathway. From these data, we conclude that synaptic transmission through the dentate gyrus to area CA3 is altered after LFPI, indicating a diminished filtering capacity of the DG in the injured brain.

Materials and Methods

Mice

Experiments were performed on 6- to 8-week-old male C57/BL6 mice (Jackson Laboratory, Bar Harbor, ME, USA. IMSR Cat# JAX:000664, RRID: IMSR_JAX:000664). All experiments were carried out in accordance with protocols approved by the Institutional Animal Care and Use Committee of Children's Hospital of Philadelphia and the guidelines established by the NIH Guide for the Care and Use of Laboratory Animals. Separate cohorts of animals were used for behavioral and electrophysiological experiments due to the large number of animals necessary for electrophysiological experiments.

Surgical procedures

Animals were anesthetized with a mixture of ketamine (2.6mg/kg) and xylazine (0.6-0.16 mg/kg) via intraperitoneal injection. Once fully anesthetized, animals were placed in a stereotaxic frame (Stoetling, Wood Dale, IL, USA). The scalp was incised and pulled away to fully expose the right parietal bone. An ultra-thin Teflon disk, with the outer diameter equal to the inner diameter of a trephine was glued to the skull with Vetbond (3M, St. Paul, MN, USA) between lambda and bregma, and between the sagittal suture and the lateral ridge over the right hemisphere. Guided by the Teflon disk, a trephine was used to perform a 3-mm diameter craniectomy over the right parietal area. Following craniectomy, a Lure-lock needle hub (3-mm inner diameter) was secured above the skull opening with Loctite superglue and dental acrylic, filled with saline and capped. Lastly, animals were removed from stereotaxis, placed on a heating pad until fully recovered from anesthesia, and then returned to their respective home cage.

Lateral fluid percussion injury (LFPI)

Twenty-four hours following craniectomy, animals were placed under isoflurane anesthesia (2% oxygen in 500ml/min) in a chamber and respiration was visually monitored until animals reached a surgical plane of anesthesia (one respiration per 2 seconds). At this point, animals were removed from isoflurane, the needle hub was refilled with saline and connected to the fluid percussion injury device (Department of Biomedical Engineering, Virginia Commonwealth University, Richmond, VA, USA) via high-pressure tubing. The animal was placed onto a heating pad on its left side and upon resumption of normal breathing pattern but before sensitivity to stimulation, the injury was induced by a 20-millisecond pulse of saline onto the intact dura. The pressure transduced onto the dura was monitored with an oscilloscope, with injury severity ranging between 1.4 and 1.6 atmospheres. Immediately after injury, the hub was removed from the skull and the animal was placed in a supine position to assess righting reflex. After righting, the animal was subjected to inhaled isoflurane to suture the scalp. Animals were allowed to recover on a heating pad until mobile, at which point they were returned to their home cage. Sham animals underwent all surgical procedures including attachment to the FPI device with exclusion of the actual fluid pulse.

Object-place recognition memory behavioral task

One week after LFPI or sham surgery, hippocampal-dependent spatial information processing was assessed an object-place recognition memory task adapted from Oliveira and colleagues(Oliveira et al., 2010). The task consisted of a respective training and testing day, spanning a total of two days. Mice were handled for five minutes each day for four days prior to training. During the training day, mice first received one six-minute habituation trial followed by three identical six-minute training trials with three-minute inter-

trial intervals in their home cage. Habituation consisted of six-minutes in a rectangular open field box (12 x 20 x 12 inches) with visual cues placed on each of the arena walls in the absence of objects. Subsequent training trials took place in the same box but now with three identical, complex objects positioned diagonally in the box. Corner objects were placed three inches away from each wall. Mice were allowed to freely explore the environment and the objects for the duration of each trial. Twenty-four hours from the first training trial, mice were placed back in the box for a single six-minute testing trial. The three objects were again present, but one of the outer two objects was now displaced to a novel spatial location (Figure 1A). Time spent exploring the displaced and non-displaced objects was measured in the third training trial and testing trial. The initial diagonal orientation of the objects, as well as the testing object selected for displacement was counterbalanced between mice. Testing was always performed in the morning at the end of the dark phase of a 12-hour light-dark cycle.

Behavioral analysis

All testing and training sessions were videotaped and analyzed by an experimenter blinded to the injury conditions of the animals. Object interaction times were independently calculated by both manual observation of video recordings, and automated open-source behavioral software developed by Patel and colleagues (Patel et al., 2014). The results of the manual and automated behavioral analysis were then subsequently averaged together. Total object interaction time, as well as time spent with each object, were recorded for each trial. Each animal's exploratory response to the spatial object displacement was measured with a normalized discrimination index (Oliveira et al., 2010). The discrimination index was calculated by subtracting the percent of total interaction time a mouse spent exploring the respective object category (i.e., displaced and the non-

displaced), in the testing trial from the percent of total interaction time exploring the same object category in the third training trial. Therefore; a positive index percentage value indicates that the animal spent more time with that object in testing than in training. Criteria for what was considered as object interaction was limited to the times when mice were facing and sniffing the objects within a 2-centimeter radius and/or touching them; sitting on the objects did not count as an exploration interaction. The first 2 minutes in the third training and testing trials were used for analysis, as preliminary testing in naïve mice showed a significant decrease in total object interaction time after the first 2 minutes of each trial. Animals that did not explore the objects for more than 3 seconds during training or testing were excluded from analysis.

Slice preparation

All electrophysiological experiments were performed on days 6–8 after LFPI or sham surgery. Slice preparation was performed as previously described (Johnson et al., 2014). Briefly, animals were anesthetized with isoflurane, the brain was dissected out and placed in ice-cold oxygenated (95% O_2/5% CO_2) sucrose-containing artificial cerebrospinal fluid (aCSF) containing (in mM): sucrose 202, KCl 3, NaH_2PO_4 2.5, $NaHCO_3$ 26, glucose 10, $MgCl_2$ 1, and $CaCl_2$ 2. The hemisphere contralateral to the craniectomy was removed prior to vibratome slice cutting. Hippocampal-entorhinal slices (HEC) slices 350 μm thick were cut on a vibratome (VT1200S, Leica Microsystems, Buffalo Grove, IL, USA). HEC slice orientation was used in an effort to maximally preserve intact perforant path and mossy fiber pathway axons. In a subset of slices (n = 2 slices per group), the hilus was transected with a scalpel at the terminal ends of DG stratum granulosum immediately following vibratome slicing to sever mossy fiber axons traveling to area CA3. Slices were transferred to 33–37 °C oxygenated (95% O_2/5% CO_2) control aCSF containing (in

millimolar): NaCl 130, KCl 3, NaH_2PO_4 1.25, $NaHCO_3$ 26, glucose 10, $MgCl_2$ 1, $CaCl_2$ 2. Slices were allowed to incubate and equilibrate for at least 60 minutes before recording. Voltage-sensitive dye (VSD) imaging and extracellular field potential recordings were performed in an interface chamber with a flow rate of 2.0 ml/min and maintained at 27–30 °C.

Extracellular field recordings

Electrodes for recordings field excitatory post-synaptic potentials (fEPSPs) were fabricated from borosilicate glass (World Precision Instruments, Sarasota, FL, USA, #1B150F-4), pulled to a tip resistance of 2–6 MΩ when filled with aCSF. Field EPSPs were recorded from an electrode placed in the suprapyramidal blade of DG middle stratum moleculare. Stimulating electrodes were non-concentric bipolar (World Precision Instruments, Sarasota, FL, USA, #ME12206) and placed at the apex of the stratum moleculare. Electrical stimuli were 100 μs in duration. Field potential input–output relationships (50–500 μA stimulation, 50 μA increments, 8 second inter-stimulus interval) were performed prior to VSD recordings. Field potential recordings were also recorded simultaneously with VSD recordings. The inter-stimulus interval for field potentials recorded during the VSD trials was 20 seconds. This duration was necessary to accommodate every other trial subtraction method used for VSD analysis. Simultaneous VSD and field recordings were performed at 200 μA, 300 μA and 400 μA stimulation intensities in aCSF.

In a separate experiment, extracellular recordings of orthodromic population spikes from the stratum granulosum of the dentate infrapyramidal blade and CA3 stratum pyramidale were recorded simultaneously. A non-concentric bipolar electrode was again placed at the

apex of the dentate stratum moleculare to stimulate afferent perforant path fibers from entorhinal cortex. Paired-pulse stimulation (100-millisecond inter-stimulus interval), each pulse 100 μsec in duration, was used to elicit population spikes in both DG stratum granulosum and CA3 stratum pyramidale, and subsequently fEPSPs in CA3 stratum lucidum and stratum radiatum (Figure 2). A paired-pulse protocol was chosen in order to increase the probability of eliciting a population spike in CA3 as compared to a single stimulation (preliminary data, not shown). Field potential input–output relationships (20–500 μA stimulation, 8 second inter-stimulus interval) were performed for each cell layer. Recordings were obtained with an Axoclamp 900 A amplifier and pClamp10 data acquisition software (Molecular Devices, Sunnyvale, CA, USA), filtered at 2 kHz. Population spike amplitude was measured as the amplitude of the first negative deflection overriding the field EPSP waveform (Neuberger et al., 2014). Field potential data was analyzed using pClamp10 and custom-written MATLAB scripts.

Voltage-sensitive dye imaging acquisition

Dye stock solutions of di-3-ANEPPDHQ (Invitrogen) were prepared at a concentration of 20 mg/ml in ethanol and stored at −20°C. Dye working solutions were prepared at a concentration of 67 μg/ml by diluting dye stock solution 1:300 in aCSF on the day of recording. Slices were stained for 16 minutes, and afterwards rinsed thoroughly with aCSF before being transferred to the recording chamber. Stained slices were then washed for another 15–20 min prior to commencing VSD recording. As in extracellular field recordings, a non-concentric bipolar electrode was placed at the apex of the stratum moleculare to elicit electrical stimulation. The dye was excited by seven high-power green LEDs (Luxeon Rebel LXML-PM01-0100, Philips) coupled to a 535 ± 25 nm bandpass filter and 565 nm dichroic mirror. Emitted VSD fluorescence was isolated with a 610 nm long-

pass filter and recorded at 0.5 kHz with a fast video camera with 80 × 80 pixel resolution (NeuroCCD, Redshirt Imaging, Decatur, GA, USA) through a reverse-lens macroscope with a 50 mm f/1.3 M46 lens (Dark Invader). Each camera pixel imaged a 25 μm × 25 μm region of tissue. The fluorescence light source was triggered 230 milliseconds prior to the acquisition of the fluorescence signal to allow the light onset emission transient to stabilize, and the electrical stimulus was delivered 170 milliseconds after commencing fluorescence data acquisition. All VSD recordings were 13 trials, 1.0 s in duration (1000 samples), with a 20 second interval between electrically stimulated trials. Each stimulated trial was followed 10 seconds later, by a non-electrically stimulated trial that was used to subtract photo-bleaching from the active signal. All VSD figures and statistics reported here are from recordings at 200 μA stimulation, as this elicited an approximately half maximal field potential response, while providing a high enough signal to noise ratio for VSD analysis.

Voltage-sensitive dye imaging analysis

Initial processing of VSD signals was performed as described previously (Johnson et al., 2014; Palmer et al., 2016). All VSD measurements were recorded as fractional change in fluorescence values (ΔF/F), which were calculated as follows: fluorescence values for each pixel in each trial were normalized according to the average fluorescence in the pixel during a 64-millisecond window immediately preceding the electrical stimulus. Then, the average from the corresponding pixel in the non-electrically stimulated trial was normalized and subtracted from the individual electrically stimulated trials to correct for photo-bleaching. VSD recordings were filtered in x and y spatial coordinates by convolution with a 5 pixels × 5 pixels Gaussian filter (Σ = 1.2 pixels), and in time by convolution with a five-sample median filter. No additional filtering was applied to any of the images or analysis of VSD data. For VSD videos and representative movie frames,

the ΔF/F for each pixel for the given sample (1 millisecond) is displayed as pseudocolor superimposed onto the image of the brain slice, where warm colors (i.e., red and orange) indicate depolarization and cool colors (i.e., blue and purple) indicate hyperpolarization. Time points selected for the representative movie frames correlate to fluorescence peaks analyzed in the regional average line plots. Peak maps were generated by pseudo-coloring and plot the maximum ΔF/F value at each pixel regardless of time for that slice.

Raster plot construction, analysis, and statistics were performed using the MATLAB VSD analysis toolbox (Bourgeois et al., 2014). To begin raster construction, regions of interest (anatomical regions) were defined for segmentation. In these experiments, the anatomical boundaries of the DG stratum moleculare, stratum granulosum and hilus, as well as CA3 stratum pyramidale, radiatum/lucidem, and oriens, were clearly visible and used to draw region boundaries. DG strata granulosum and moleculare were subdivided into suprapyramidal and infrapyramidal blades, as these blades have been found to have different circuit properties and connections (David G. Amaral et al., 2007). There was no clear visual division between the subregions CA3a,b, or c, so approximate geometric divisions were made consistently across slices to include the regions closest to the dentate, putatively CA3b/c.

Regions were then split into 100 μm segments along the rostrocaudal axis, numbering segments in ascending order from rostral to caudal ends of each region. Average ΔF/F values were calculated for each spatiotemporal site and plotted as pseudocolor in the distance from stimulating electrode versus time raster plots. To account for slight variability in region of interest size when creating average raster plots, all individual slice raster plots were stretched or compressed to have the same number of segments. That number was

set as the mean number of segments from the individual slices. VSD recordings were done in a maximum of two slices per animal, and so ΔF/F values for each anatomical region of interest were averaged to create a raster plot for each animal for group analysis. Statistical comparison of group raster plots was performed at each individual spatiotemporal site using a permutation test (t = 1000). Permutation is a non-parametric test that randomly resamples data to generate a null distribution describing variability in the data. Significant differences ($\alpha < .05$) were registered at sites where injury versus sham groupings explain the variability in the data. The P-values generated are displayed in pseudocolor on the P-value raster plots. Multi-segment averages were calculated for each anatomical region by averaging the mean ΔF/F value for each signal to generate a regional average, and are plotted as line plots (i.e., multi-segment regional average line plots). Line plots show the average ΔF/F (dark line) surrounded by ellipses marking the standard error of the mean (shaded surrounding). The initial fast depolarization peak (max ΔF/F between 0–35 milliseconds), was used for analysis since it roughly corresponds to the time scale of synaptic transmission. The segments selected for line plots were the same between conditions and consistent by region.

Statistical procedures

All statistical analyses and calculations were performed using MATLAB and/or GraphPad Prism. *A priori* power calculations were performed using G*Power based on variability from similar previous experiments (Faul et al., 2007). The spatial object recognition task discrimination index was analyzed with one-way ANOVA with *post hoc* Tukey's multiple comparisons test. Student's t-tests were used to compare total object interaction times in training and testing, respectively. All statistical tests for fEPSP data were conducted using Mann–Whitney U-tests, or two-way repeated measures ANOVA with Sidak's multiple

comparison test in order to test for injury effect and stimulation intensity effect. VSD data was analyzed spatiotemporally with the permutation test described in Bourgeois et al. where applicable (Bourgeois et al., 2014). Statistical significance is considered: $P < 0.05$*, $P < 0.01$**, $P < 0.001$***. N values represent number of animals in each condition, with a maximum of 2 slices per animal. For physiological experiments (fEPSP and VSD) when multiple brain slices from a single animal were used, data from individual brain slices generated from the same animal were averaged yielding a single animal value for each given measure. The value generated was used in group analysis and statistics, based on the animal N. Data in the figures are presented as group means ± SEM.

Results

LFPI diminishes object-place recognition memory

To evaluate the effect of mTBI on ability to detect spatial change within an environment (i.e., spatial novelty), we utilized an object-place recognition memory task based on a previously established paradigm (Oliveira et al., 2010). In this version of the task, all three objects were identical, and the spatial change consisted of the displacement of one object to a novel location within the chamber during the testing trial while keeping constant the locations of the remaining two objects (Figure 1A). There was no difference in total object interaction time between the two groups during training (Sham: 8.14 ± 1.12 seconds, LFPI: 8.07 ± 0.82 seconds, $p = 0.95$, n.s.) or testing (Sham: 9.56 ± 0.74 seconds, LFPI: 9.70 ± 1.05 seconds, $p = 0.91$, n.s.). During the testing trial, sham animals spent significantly more time interacting with the displaced object versus the non-displaced objects (Figure 1B. Displaced object mean discrimination index score: 22.46%, non-displaced objects

mean discrimination index score: -10.17 %, $p < 0.001$; n = 10 animals). Conversely, there was no significant difference in the time spent between displaced and non-displaced objects for the LFPI animals (displaced mean discrimination index score: -5.88%, non-displaced mean discrimination index score: 2.82%, $p = 0.5970$, n.s.; n = 10 animals). Comparing between groups, LFPI animals spent less time with the displaced object versus sham (Sham: mean discrimination index score: 22.46%, LFPI mean discrimination index score: -5.88%, $p < 0.01$). There was no difference in the discrimination index scores of the non-displaced objects between the groups (Sham: mean discrimination index score: -10.17%, LFPI: mean discrimination index score: 2.82%, p=0.26, n.s.).

Mild LFPI causes an increase in DG network excitability

Next, we investigated dentate gyrus physiological function to determine if alterations in this region may contribute to the behavioral deficits observed. In order to confirm that the DG experiences a net shift in network excitability as seen in previous studies, we recorded field excitatory postsynaptic potentials (fEPSPs) from the DG stratum moleculare in response to perforant path stimulation (Sham n = 7 animals, LFPI n = 8 animals, 2 slices per animal). fEPSP responses were recorded over a range of stimulation intensities (50-300uA) to generate input/output (I/O) curves (Figure 3A). The I/O curve of the DG shows that as stimulation intensity increases, there is an increase in the fEPSP slopes from LFPI animals (two-way repeated measures ANOVA, (injury effect) $F(1,13) = 8.694$, $p < 0.05$; (stimulus intensity effect) $F(3,39) = 23.48$, $p < 0.0001$; (interaction) $F(3,39) = 4.099$, $p < 0.05$). Multiple comparisons show a statistically significant shift in the fEPSP response to the upper range of stimulation intensities (Sidak's multiple comparisons test, 200μA, $p < 0.01$; 300μA, $p < 0.01$).

To visualize the spatiotemporal characteristics of the DG physiological response to perforant path stimulation, we performed voltage-sensitive dye imaging (VSD). VSD is an advantageous tool for measuring population neuronal activity by recording changes in transmembrane potential with high spatial and temporal resolution. VSD dyes absorb into cell membranes where they emit fluorescence as a function of the transmembrane voltage. Changes in this fluorescence (ΔF/F) are linearly proportional to changes in membrane voltage, and in hippocampal slices, the voltage-sensitive dye di-3-ANEPPDHQ emits fluorescence for which 1×10^{-4} ΔF/F equals a roughly 1 mV change in transmembrane voltage (Ang et al., 2006). All ΔF/F values are visually represented by pseudo-coloring of spatial regions where warm colors (i.e., red and orange) indicate depolarization and cool colors (i.e., blue and purple) indicate hyperpolarization, as exhibited by representative video frames from sham and LFPI slices in Figure 3C (See supplemental materials for full videos).

In order to interpret group data, VSD videos were used to create regional raster plots and multi-segment regional average line plots for analysis. Rasterization of anatomical regions is a way to average ΔF/F for 100μm wide segments within each region thus quantifying the spatial response of the VSD signal in raster plots. The dentate gyrus was separated into five regions for analysis, the suprapyramidal and infrapyramidal branches of the stratum moleculare and stratum granulosum, respectively, and the hilus. Raster plots from the suprapyramidal stratum granulosum and stratum moleculare, shown in Figure 3 (D and E), demonstrated enhanced and prolonged depolarization throughout this layer. Statistical differences for each spatiotemporal point between the sham and LFPI group rasters are shown in the p-value raster plot generated by permutation testing (Figure 3G).

While rasters provide a way to measure the spatial response of the signal, multi-segment regional average line plots provide a way to measure the fast depolarizing peak of the fluorescence signal in each region. The multi-segment regional average line plot from the stratum granulosum revealed a significantly higher fast-depolarizing peak in LFPI slices (all ΔF/F values are reported in (10^{-4}) notation, Sham (ΔF/F): 15.9 $\pm$ 26.6, LFPI (ΔF/F): 22.5 $\pm$ 1.5; $p < 0.05$. Sham, n = 11, LFPI, n = 9). Subsequent analyses of line plot fast-depolarizing peaks showed that all cell layers of the DG showed enhanced depolarization in the LFPI group versus sham (for fast depolarizing peak ΔF/F values from each region, see Table 1).

Mild LFPI leads to spread of excitation through DG into area CA3

Another advantage of VSD is that it can detect the spatial propagation of activity from one region to another. To assess the functional efficacy of the DG as a filter of perforant path input, we examined the spread of the VSD signal into area CA3. Representative VSD peak maps revealed that perforant path activation lead to an aberrant spread of depolarization into area CA3 in slices from LFPI animals (Figure 4D). Multi-segment regional average line plots also indicate a significant increase in the fast depolarizing peaks in all area CA3 cellular layers from LFPI slices, compared to sham (Table 1; Sham n = 6, LFPI n = 6).

Next, we asked if the spread of depolarization to area CA3 could translate to a functional increase in action potential firing. To test this possibility, we simultaneously recorded extracellular population spikes in the DG stratum granulosum and area CA3 stratum pyraamidale while stimulating the perforant path. In order to reliably examine population spiking activity in CA3, paired-pulse stimulation (100-ms inter-stimulus interval) was used. Figure 5 shows I/O curves of population spike amplitudes in response to the second

stimulation. Interestingly, I/O curves recorded from the DG st. granulosum in response to the second pulse were not different between sham and LFPI animals (Two-way Repeated Measures ANOVA, Injury Factor: $F(1,11) = 0.3743$; $p = 0.5531$), however, I/O curves from the first pulse showed that LFPI animals had larger population spike amplitudes as stimulation intensity increased (Sham n = 7, LFPI n = 6, Stimuli 350-500μA Two-way Repeated Measures ANOVA: Stimulus Intensity Factor: $F(9,99) = 33.63$, $p < 0.0001$; Injury Factor: $F(1,11) = 5.089$, $p < 0.05$; Interaction: $F(9,99) = 4.432$, $p < 0.0001$, data not shown). In the subset of slices with CA3 population spikes, I/O curves demonstrated an increase in population spike amplitude for LFPI slices (Figure 5E. Two-way Repeated Measures ANOVA: Injury Factor: $F(1,10) = 5.594$, $p < 0.05$; Stimulus Intensity Factor: $F(9,90) = 9.900$, $p < 0.0001$; Interaction: $F(9,90) = 5.900$, $p < 0.0001$). In slices where the hilus was transected, CA3 population spikes were not observed, confirming that CA3 population spike activity was due to afferent excitation from DG mossy fibers as opposed to indirect stimulation of another afferent pathway (n = 2 slices per condition).

Next, we hypothesized that enhanced CA3 population spike activity could arise from two possibilities: an increase in synaptic transmission from mossy fibers located in CA3 stratum lucidum,(Acsády et al., 1998; Frotscher, 1985; Soriano & Frotscher, 1993) or alterations in the CA3 autoassociational network marked by net synaptic transmission from recurrent CA3 associational/commissural (A/C) synapses onto other CA3 neurons in stratum radiatum (D. A. Henze et al., 2000; Witter, 2007a). To test these alternative hypotheses, we again stimulated the perforant path using the same paired-pulse stimulation and placed recording electrodes in stratum lucidum and stratum radiatum, respectively. I/O curves from LFPI animals in response to the second stimulation were observed to have significantly larger fEPSP slopes in stratum lucidum (Figure 6A and 6C,

Sham n = 4, LFPI = 4, Stimuli: 20-500μA, Two-way Repeated Measures ANOVA: Injury Factor: $F(1, 135) = 108.2$, $p<0.0001$; Stimulus Intensity Factor: $F(24, 135) = 10.25$, $p<0.0001$; Interaction: $F(24, 135) = 3.426$, $p<0.0001$). Interestingly, there was no difference in the I/O curves from fEPSPs in stratum radiatum between sham and LFPI (Figure 6B and 6D, Sham n = 4, LFPI = 4. Stimuli: 20-500μA, Two-way Repeated Measures ANOVA: Injury Factor: $F(1, 135) = 1.419$, $p = 0.2356$; Stimulus Intensity Factor: $F(24, 135) = 5.209$, $p<0.0001$; Interaction: $F(24, 135) = 1.276$, $p = 0.1922$).

Discussion

In this study, we examined the ability of the dentate gyrus to regulate cortical input to the hippocampus one week after LFPI in mice. To first confirm hippocampal-dependent behavioral deficits and assess animals' ability to detect spatial novelty within their environment, we tested mice in a spatial memory object-place recognition task. While sham animals could discriminate the spatial object displacement, we found that LFPI mice could not. Total object interaction times during either training or testing trials were not significantly different between sham and LFPI, indicating that the observed deficit in spatial object discrimination was not due to a decrease in overall exploratory behavior after injury.

When the physiological function of the DG was assessed by stimulating cortical inputs in *ex vivo* brain slices, we found that the DG experienced increased network excitability, as indicated by higher levels of VSD fluorescence signals throughout all cellular layers, and larger fEPSP slopes in the stratum moleculare. Subsequently, we observed perforant path activation in LFPI animals to cause aberrant spread of depolarization into downstream area CA3. This was associated with greater population spike amplitudes in CA3 stratum

pyramidale and suggests enhanced action potential firing in this region. In addition, we observed that increased CA3 population spike activity was accompanied by larger fEPSPs in CA3 stratum lucidum, indicating augmented synaptic efficacy at mossy fiber synapses. Interestingly, enhanced excitability was not observed in CA3 stratum radiatum, which suggests that auto-associational activity due to CA3 A/C axon collaterals is not likely affected. In summary, our main finding that aberrant spread of afferent excitation from DG to area CA3 has functional consequences on CA3 network excitability is both novel and significant in understanding how synaptic transmission between localized circuits can lead to hippocampal disruption after mTBI.

DG hyperexcitability reflects a loss of excitatory/inhibitory (E/I) balance within the network. Departure from the endogenous state of E/I balance can cause network dysfunction, and ultimately manifest in behavioral impairments. After TBI, E/I imbalance has been observed in both the DG and area CA1 (reviewed in Paterno et al. 2017). The DG has intrinsically low network excitability (i.e., sparse granule cell firing), which is thought to confer its putative filtering property. Because of this low excitability under normal conditions, perturbations to the network tends to shift E/I balance toward hyperexcitability. This hyperexcitable shift within the DG is also seen in other neurological disorders, such as epilepsy and Alzheimer's disease, where it is associated with behavioral cognitive dysfunction (Bejanin et al., 2012; Dengler & Coulter, 2016; Heinemann et al., 1992; Hester & Danzer, 2013; Krook-Magnuson et al., 2015; Lothman et al., 1992; Marucci et al., n.d.; Nenov et al., 2014; Palop et al., 2007; Putcha et al., 2011). Our data demonstrate that mTBI causes E/I imbalance in the DG, leading to the diminished ability to regulate cortical input and behavioral dysfunction.

The results of our behavioral assessment substantiate an impairment in anterograde memory, recapitulating what is observed clinically in mTBI patients and experimentally in rodents after mild to moderate LFPI (Aiguo Wu et al., 2009; Eakin & Miller, 2012; Fedor et al., 2010; Gurkoff et al., 2013; Hylin et al., 2013; D. J. Lee et al., 2015; Pierce et al., 1998; Rutland-Brown et al., 2006; D. H. Smith et al., 1991; Witgen et al., 2005; Y. Zhang et al., 2015). Furthermore, alterations in object-place recognition memory and spatial novelty detection confirm that spatial information processing—as one component of episodic memory—is disrupted in our model of mTBI. These data are consistent with object-place recognition memory impairments seen in other TBI models one to two weeks post-injury (Beamer et al., 2016; Darwish et al., 2014; Gurkoff et al., 2013); however, are in contrast to one study using a mild CCI model, where no spatial object recognition deficits were observed (YungChia Chen et al., 2014). In previous behavioral studies, spatial novelty detection has been shown to rely on the DG and CA3 hippocampal sub-regions (Kesner et al., 2015; I. Lee et al., 2005). In a similar object exploration paradigm in rats, lesions of either DG or CA3 led to a decrease in the exploration of the displaced objects compared with controls, while CA1 lesions did not produce significant deficits (I. Lee et al., 2005). Another study, using the same task as that utilized in this study, found that chemogenetically silencing hyperactive dentate granule cells in a mouse model of epilepsy was able to restore behavioral spatial novelty detection, further implicating the role of the DG in spatial information processing (Kahn et al., 2016). The DG-CA3 pathway has also been implicated in pattern separation, i.e. the differentiation of similar, overlapping cortical input patterns, theorized to be a necessary computational step in episodic memory encoding (Bakker et al., 2008; Gilbert et al., 2001; Hunsaker et al., 2008; Kesner, 2013b; Leutgeb et al., 2007a; Marr, 1971; McHugh et al., 2007; McNaughton & Morris, 1987; Nakashiba et al., 2012; O'Reilly & McClelland, 1994; A. Treves & Rolls, 1994). Recently,

a study by Kim and colleagues demonstrated that pattern separation in an object-based recognition memory task is impaired after CCI in mice (Kim et al., 2016). While we do not provide direct evidence to support a causal link between diminished object-place recognition memory and DG-CA3 posttraumatic dysfunction in this study, these previous findings suggest that disruption to this pathway may underwrite the observed spatial novelty deficits after TBI, and should be explored in future experiments.

In addition to the hippocampus, other brain regions that contribute to object-place recognition memory may also be affected after LFPI. The hippocampus has been shown to functionally interact with the perirhinal cortex and medial prefrontal cortex during object-in-place memory tasks in rodents (G. R. I. Barker & Warburton, 2011; Gareth R I Barker et al., 2007; Bussey et al., 2000; Ennaceur & Aggleton, 1997; Hannesson, 2004; Kesner & Ragozzino, 2003). Additionally, the lateral entorhinal cortex and fornix play a role in recognition of object-context associations, i.e., whether familiar objects are in a familiar or novel environment (Bussey et al., 2000; Ennaceur & Aggleton, 1997; Langston & Wood, 2010; Wilson et al., 2013). Physiological, morphological and histological studies have shown that these regions have alterations in TBI models and human patients (Bolton & Saatman, 2014; Card et al., 2005; Ekolle Ndode-Ekane et al., 2017; Tate & Bigler). Furthermore, alterations to the contralateral hippocampus may also contribute to the behavioral results observed in this study. Previously, our laboratory has found fewer healthy neurons and DG network hyperexcitability in the contralateral hippocampus 7 days after LFPI (Tran et al., 2006). Although the present study only examines DG physiological function in the hemisphere ipsilateral to the injury site, our previous work would suggest a similar network excitability shift in the contralateral DG as well. Anatomically, the bilateral dentate gyri are commissurally connected by glutamatergic and GABAergic interneuron

projections (Berger et al., 1981; Buckmaster et al., 1996; Deller et al., 1995; Frotscher et al., 1991; Goodman & Sloviter, 1992; Helen E Scharfman & Myers, 2012; Zimmer, 1971). Therefore, it is possible that dysfunction of interneuron subtypes may affect commissural communication between dentate gyri and coordination of behavior after injury.

In examining the underlying physiology, we observed that the DG experienced an increase in network excitability as visualized by higher VSD fluorescence signals and increased fEPSP slopes in LFPI slices. These data corroborate previous work from our laboratory and others that demonstrates increased DG network excitability with extracellular field recordings (Butler et al., 2015; Gupta et al., 2012; Hunt et al., 2010; Lowenstein et al., 1992; Vijayalakshmi Santhakumar et al., 2001; Toth et al., 1997; Witgen et al., 2005). VSD imaging provides additional information about the spatiotemporal spread of perforant path activation, and its enhancement of activity throughout the DG-CA3 network after injury. In sham control slices, excitation was predominantly limited to the DG anatomical region. However, in LFPI slices, perforant path activation lead to the propagation of depolarization through the DG hilus—the location of the mossy fiber pathway—into area CA3. Furthermore, the results of extracellular recordings in CA3 stratum pyramidale demonstrated larger amplitude perforant pathway-evoked population spikes from LFPI slices (Figure 5F), which suggests that upstream DG network perturbations can have functional consequences downstream in area CA3. These results are the first to describe aberrant propagation of perforant path input from DG into area CA3, and provide insight into how the flow of information between hippocampal sub-regions can be affected by brain injury.

Our goal in utilizing a paired-pulse stimulation protocol was to reliably evoke population spikes in area CA3. Mossy fiber-CA3 synapses are known be “conditional detonators”, whose neurotransmitter release depends on granule cell firing pattern (D. a Henze et al., 2002). Single DG granule cell action potentials generally fail to discharge a CA3 pyramidal neuron, however trains of granule cell action potentials reliably and effectively discharge CA3 cells. It has been previously shown that granule cells increase the number of action potentials fired in response to perforant path stimulation one week after LFPI (V Santhakumar et al., 2000; Toth et al., 1997). In response to the first stimulation pulse, DG population spikes had larger amplitudes after LFPI (Figure 5D). However, the second stimulation pulse elicited no difference in DG population spikes between sham and LFPI slices (Figure 5E). We believe that this lack of effect in the second DG population spike is most likely due to maximal signal saturation in the hyperexcitable DG of LFPI slices.

Diminished DG filtering of cortical excitability to CA3 could also affect synaptic plasticity within the circuit, and contribute to learning and memory disruption. In area CA1, we previously showed an inability to induce and maintain long-term potentiation (LTP) at the Schaeffer collateral synapse at 7 days after LFPI (Schwarzbach et al., 2006). In separate study, we were able to restore contextual fear conditioning behavior, as well as CA1 network excitability using a dietary therapy, however found that the dietary therapy did not restore LTP in CA1 (unpublished observations, Cole et al., 2010) Recently, Titus and colleagues were able to reinstate CA1 LTP and contextual fear conditioning behavior with the use of a phosphodiesterase inhibitor after FPI (Titus et al., 2013). Taking the results of these studies together, it seems behavior restoration after injury can be achieved with or without LTP in CA1. Therefore, the role of CA1 LTP in recovery of hippocampal-mediated behavior after injury remains unclear.

Loss of LTP at the Schaeffer collateral synapse does not necessarily relate to loss of LTP in the dentate gyrus, as synaptic potentiation in these regions have different mechanisms, and depends on which DG synapse type is being examined. At the perforant path-granule cell synapse, loss of LTP has been demonstrated at 7 days after injury (White et al., 2016; Yamashita et al., 2011; B.-L. Zhang et al., 2011; B. Zhang et al., 2011). Within the DG, LTP involving hilar excitatory circuitry (i.e., mossy cells) has been shown to modulate gating of cortical input into the dentate gyrus via an NMDA-independent presynaptic mechanism (Hashimotodani et al., 2017; Wright & Jackson, 2014). One week after LFPI, mossy cells were shown to be hyperexcitable and exert aberrant excitation onto granule cells (V Santhakumar et al., 2000). Therefore, mossy cell dysfunction could play a major part in DG hyperexcitability and diminished filtering efficacy, as well as disruption of synaptic plasticity mechanisms.

Our results demonstrating enhanced synaptic efficacy in CA3 stratum lucidum suggests that mossy fiber synaptic transmission is more pronounced after injury. The effect of TBI on LTP at the mossy fiber-CA3 pyramidal cell synapse has yet to be examined. LTP at this synapse is unique from that of other hippocampal synapses: it is NMDA receptor-independent, and involves cyclic AMP-activated presynaptic calcium influx, resulting in enhanced neurotransmitter release (Nicoll et al., 2005). We would hypothesize that enhanced mossy fiber excitatory transmission after LFPI would increase the probability of opening presynaptic voltage-gated calcium channels, likely leading to increased transmitter release. However, whether this activates the long-term molecular machinery necessary for sustained synaptic potentiation remains to be seen. In mouse models of epilepsy, which also exhibit a hyperexcitable DG network phenotype, LTP is induced at

the mossy fiber-CA3 pyramidal cell synapse, similar to high-frequency stimulation of mossy fiber axons (Anderson et al., 1987; Ben-Ari & Gho, 1988; Cherubini et al., 1988). The role of aberrant induction of LTP at this synapse could have major implications for learning and memory disruption. Future experiments are warranted in order to elucidate the maintenance of LTP at the mossy fiber-CA3 pyramidal cell synapse after LFPI.

Within the CA3 network, no significant change in fEPSPs were observed in stratum radiatum, the site of CA3 pyramidal cell recurrent A/C axon collateral synapses. This finding suggests that injury may not necessarily affect intrinsic excitability or synaptic output of CA3 pyramidal neurons within the network, however further work is needed to directly support this hypothesis. A previous study in a closed head injury model found no changes in the intrinsic membrane properties of CA3 pyramidal neurons (Griesemer & Mautes, 2007). However, it is well established that CA3 neurons are vulnerable to cell loss following TBI (Baldwin et al., 1997; Y Chen et al., 1996; Golarai et al., 2001; Lowenstein et al., 1992; Tang et al., 1997; Witgen et al., 2005). While further investigation of posttraumatic alterations within area CA3 itself is needed, the results of this study specifically demonstrate that in response to afferent excitation, mossy fiber transmission from the DG is a major source of CA3 network hyperexcitability.

The most parsimonious explanation of our data is that CA3 excitability is due to electrical stimulation of the perforant path branch projecting to DG (recall that our stimulating electrode was placed in DG stratum moleculare), that then relays information to CA3 via the mossy fiber pathway. Intracellular labelling studies show that entorhinal cortex neurons with axons in the perforant path, have collaterals that reach both dentate gyrus and CA3 (Tamamaki & Nojyo, 1993; Witter, 2007b). In the VSD data, we do not observe

depolarizing spatiotemporal propagation along the CA field stratum lacunosum moleculare where perforant path axons travel directly to area CA3. Additionally, spread of depolarization into CA3 is evident through the DG hilus, where mossy fiber axons project. In slices with a hilar transection, no population spike activity was evident in area CA3 (Figure 5C). Therefore, our data strongly suggest that the majority of stimulus-induced excitation in CA3 was orthodromic firing from DG granule cells, as opposed to antidromic firing of perforant path axons directly projecting to area CA3.

There are considerable mechanistic possibilities to explain the posttraumatic disruption of DG filtering function and subsequent CA3 hyperexcitability. After FPI, the DG experiences overt cell death, including loss of many interneuron subtypes (Lowenstein et al., 1992; V Santhakumar et al., 2000; Toth et al., 1997; Witgen et al., 2005). Within the DG, neuronal loss may contribute to E/I imbalance by disappearance of synaptic connections. Our laboratory and others have shown a decrease in the frequency of inhibitory synaptic currents onto dentate granule cells, reflecting a potential loss of GABAergic synapses (Toth et al., 1997; Witgen et al., 2005). Prior studies have also reported alterations in synaptic inputs onto other dentate cell types, such as hilar interneurons and semilunar granule cells, which may be due to reorganization of structural network connections (Gupta et al., 2012; Hunt et al., 2011; V Santhakumar et al., 2000). Physiologically, surviving neurons in the DG may experience shifts in intrinsic membrane properties or synaptic inputs, resulting in E/I imbalance at the cellular level. For example, a decrease in the potassium-chloride transporter protein KCC2 occurs at 7 days post-LFPI, leading to reduced $GABA_A$-mediated inhibition onto granule cells(Bonislawski et al., 2007). The complex DG interneuron network has also been shown to experience shifts in intrinsic excitability and synaptic inputs after TBI (Howard et al., 2007; Hunt et al., 2011;

Lowenstein et al., 1992; V Santhakumar et al., 2000; Vijayalakshmi Santhakumar et al., 2001; Toth et al., 1997; Tsuda et al., 2016; Witgen et al., 2005). Thus, an imbalance in excitatory/inhibitory neurotransmission throughout the DG after injury most likely contributes to the breakdown of DG filter function.

At the cellular level, TBI has been shown to cause alterations in ion channel function. Previous studies in *in vitro* injury models have shown that disruptions in voltage-gated sodium channel function after TBI leads to aberrant activation of voltage-gated calcium channels and increased calcium influx (Iwata et al., 2004; Wolf et al., 2001; Yuen et al., 2009). Changes to voltage-gated channels could affect action potential propagation and initiation at the axon initial segment, as seen in cortical neurons (Vascak et al., 2017). Action potential propagation can be functionally evaluated by measuring pre-synaptic fiber volley amplitude. Previously, we have shown there is no change in the fiber volley amplitude of perforant path axons into DG (Witgen et al., 2005). Therefore, we do not believe that our model contains net physiological changes in voltage-gated sodium channel properties of DG afferents. However, as mossy fiber synaptic transmission from DG to area CA3 was elicited di-synaptically in this study—as designed to assess dentate network filtering function—we do not know if fiber volley amplitudes of mossy fibers are changed after injury. Additionally, modulation of mossy fiber release probability or membrane properties in CA3 neurons may also contribute to the observed downstream hyperexcitability. Future studies would benefit to examine changes in synaptic efficacy within the DG-CA3 di-synaptic pathway, as well as regulation by interneuron subtypes within both hippocampal sub-regions.

In conclusion, the results of this study show that 1) behavioral spatial information processing is impaired after mTBI and 2) the neuronal circuit within the DG has a diminished physiological “filtering” function, allowing too much excitation into area CA3 via the mossy fiber pathway. These novel findings expand on the current mechanisms of hippocampal circuit dysfunction after experimental mTBI and provide a physiological correlate of posttraumatic deficits in spatial information processing for encoding into memory. Forthcoming studies aim to identify mechanisms of posttraumatic DG dysfunction in order to restore DG filter function, and ultimately, the effects on episodic memory impairment.

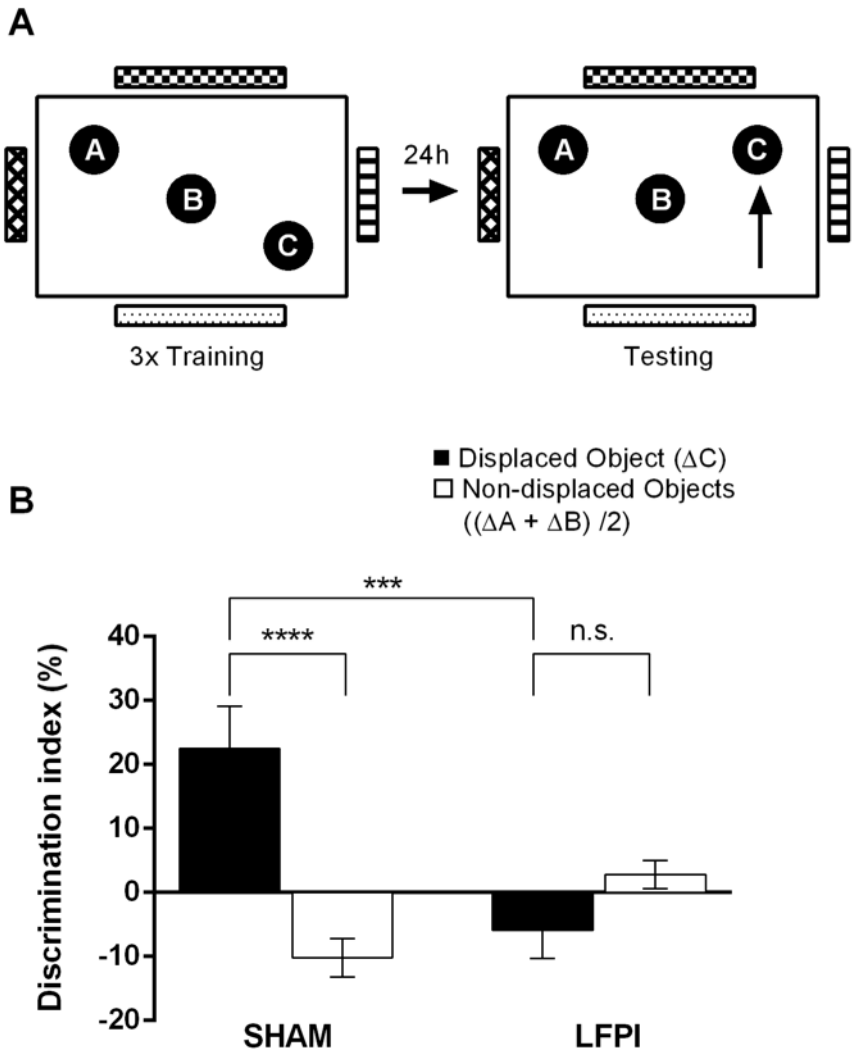

Figure 1. LFPI animals show impairment in object-place recognition task. A) The task consisted of familiarization training with 3 identical objects each in a distinct spatial location. In the testing trial, one object was displaced to a novel location. B) The normalized difference in the time spent exploring the displaced and non-displaced objects in testing and training was calculated as a discrimination index (i.e., positive index scores signify more time spent exploring the object in testing). If the animal showed a preference for the displaced object in the test trial over the non-displaced objects, this was considered a demonstration of spatial novelty detection. (Sham: displaced vs. non-displaced objects,

p=0.0004; LFPI: displaced vs. non-displaced objects, p = 0.5970; Sham displaced vs. LFPI displaced, p =0.0019. n=10 animals for each condition). Discrimination index calculation as follows: Discrimination index = ((Object X interaction $time_{testing}$/Total Interaction $time_{testing}$) * 100) – ((Object X interaction $time_{training}$ / Total Interaction $time_{training}$) * 100).

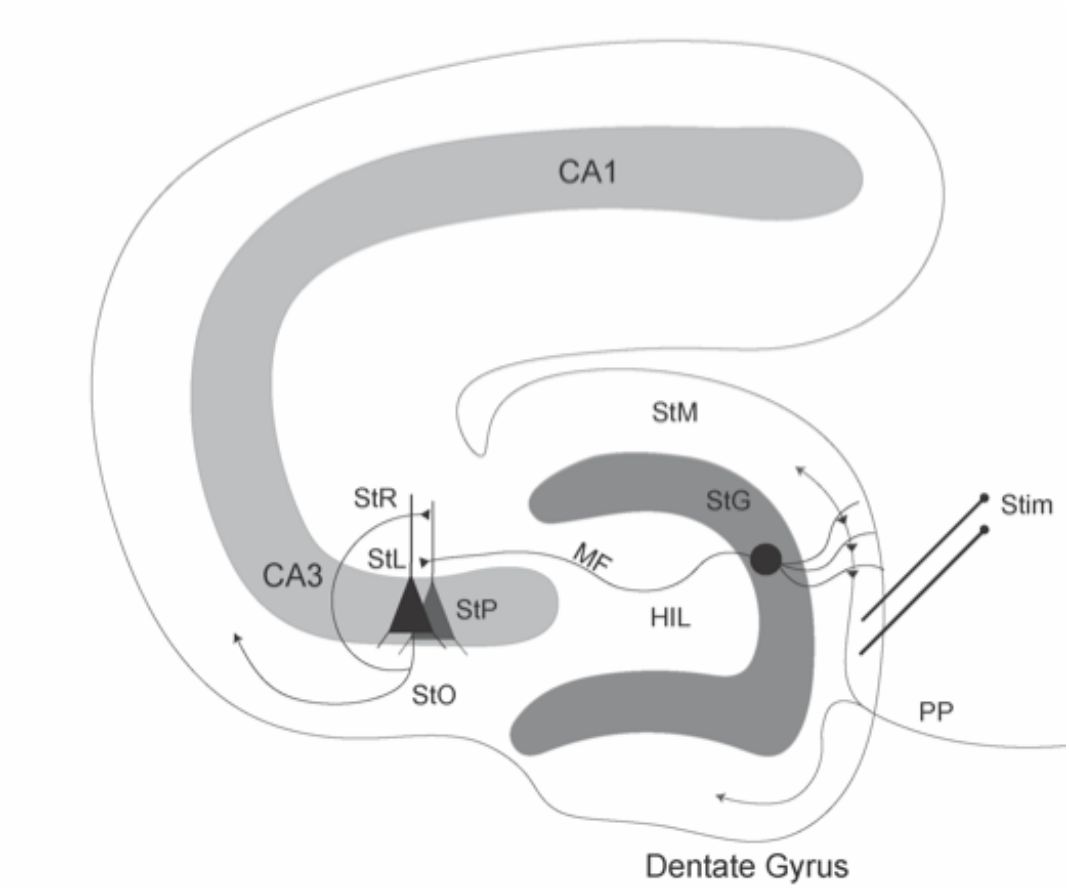

Figure 2. Anatomy of the dentate gyrus and area CA3 in a hippocampal-entorhinal cortex (HEC) brain slice. The perforant path (PP) is comprised of axons from layer II of entorhinal cortex which traverse the subiculum and then enter the stratum moleculare (StM) of dentate gyrus, also known as the molecular layer, to synapse onto distal dendrites of granule cells. Granule cell bodies are located in stratum granulosum (StG), i.e., granule cell layer. Granule cell axons pass through the dentate hilus (HIL) forming the mossy fiber pathway (MF). Mossy fibers synapse onto CA3 pyramidal cell proximal dendrites in the stratum lucidum (StL) of area CA3. Pyramidal cell bodies are situated in stratum pyramidale (StP), i.e., pyramidal cell layer. Pyramidal cell axons project into stratum oriens (StO). Pyramidal cells additionally send recurrent associational/commissural axon

collaterals to stratum radiatum (StR) where they synapse onto other pyramidal cells, forming the CA3 autoassociational network. In all experiments described, a non-concentric bipolar stimulating electrode was placed in the dentate ML at the apex to stimulate perforant path fibers (Stim).

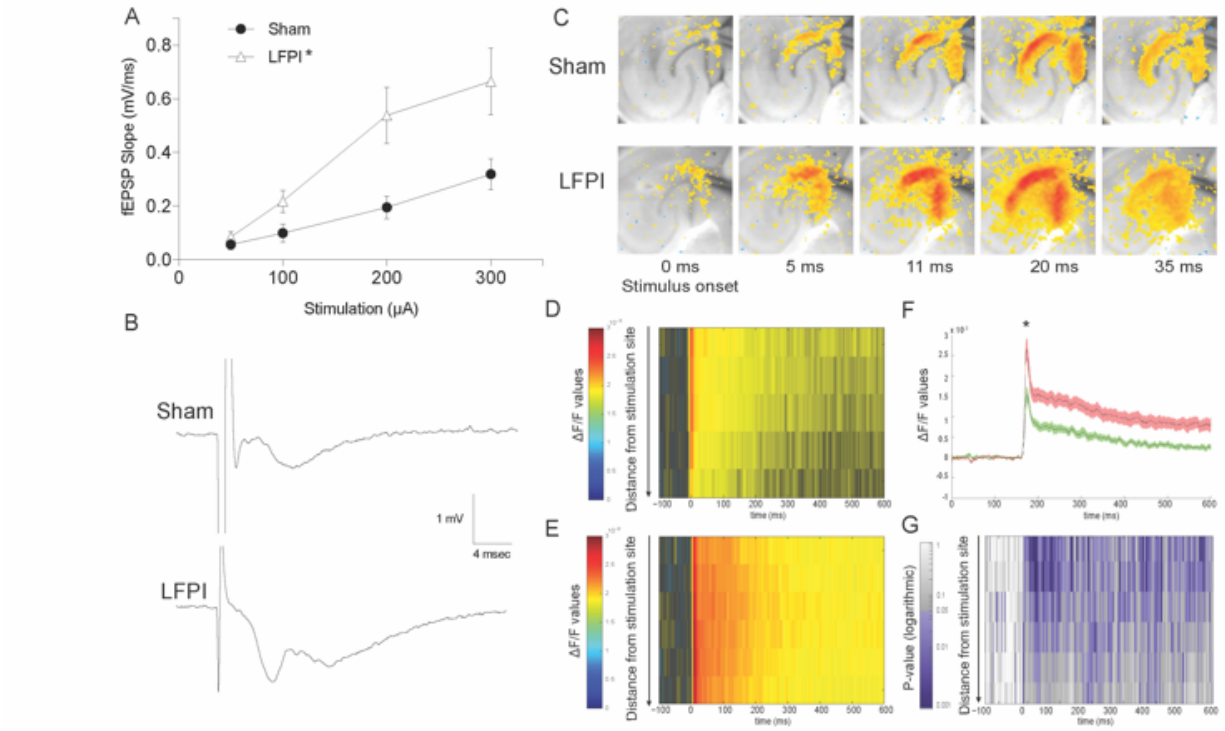

Figure 3. Increase in dentate gyrus net excitability. A) Extracellular I/O curves recorded from molecular layer in response to incremental perforant path stimulation from 50- 300 μA. (LFPI: n= 8, Sham: n= 7; two-way repeated measures ANOVA, (injury effect) $F(1,13) = 8.694$, $p=0.0113$; (stimulus intensity effect) $F(3,39) = 23.48$, $p <0.0001$; (interaction) $F(3,39) = 4.099$, $p=0.0127$). Multiple comparisons show a statistically significant shift in the fEPSP response to the upper range of stimulation intensities shown (Sidak's multiple comparisons test, 200μA, $p = 0.0042$; 300μA, $p = 0.0038$). B) Representative fEPSP traces from sham and LFPI slices at 200μA. C) Representative VSD movie frames from a sham and an LFPI slice at respective time points after 200μA perforant path stimulation. Raster plots for the D) granule cell layer and E) molecular layer

show the group average fluorescence signals for 100μm segments along the longitudinal axis at each sample time point during the 200μA trial. F) Multi-segment regional average line plots from the granule cell layer demonstrate the fast depolarizing peak of the fluorescence signal in slices from the LFPI group (red) versus sham controls (green). Sham mean: 0.001594 ± 0.0002656, LFPI mean: 0.002254 ± 0.0001531, $p = 0.0369$; Sham n = 11, LFPI n = 9 animals. G) Raster indicating the statistical difference between the sham and LFPI group rasters at each spatiotemporal point in the trial with representative pseudocoloring of bootstrapped p-values (shades of purple indicate significance of $p < 0.05$ or more).

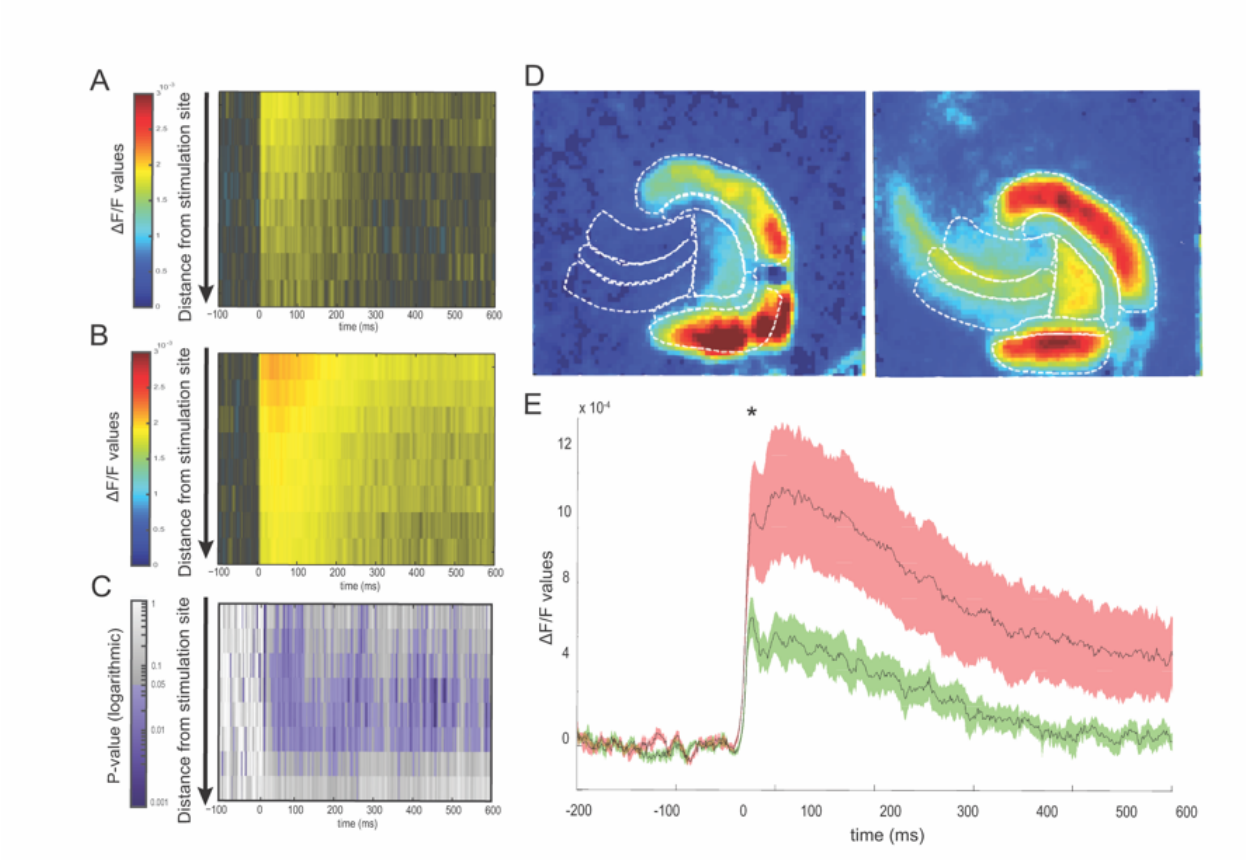

Figure 4. Perforant path stimulation leads to aberrant propagation of depolarization into area CA3. Group raster plots from A) sham and B) LFPI slices. C) Raster plot of the statistical significance comparing the groups at each spatiotemporal point in the trial with representative pseudocoloring of the bootstrapped p-values (shades of purple indicate significance of $p < 0.05$ or more). D) Heat maps of representative sham (left) and LFPI (right) slices demonstrate the spread of activity in area CA3 after injury. E) Multi-segment regional average line plots from the pyramidal cell layer of area CA3 depicts the increase in the fast depolarizing peak of the fluorescence signal in the LFPI group (red) versus shams (green); (all $\Delta F/F$ values in 10^{-4} notation) Sham mean: 4.9 $\pm$ 0.73, LFPI mean: 11.7 $\pm$ 2.62, $p = 0.0329$; n = 6 animals per condition.

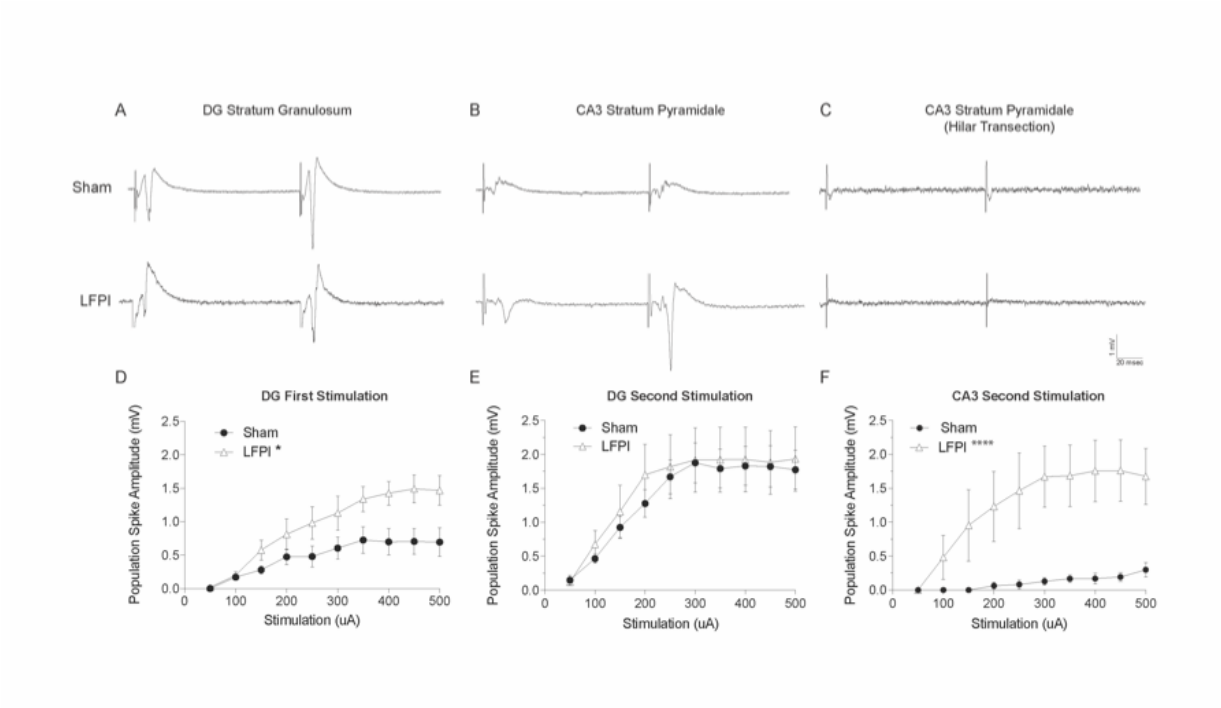

Figure 5. Increase in CA3 population spike activity after LFPI. Population spike traces from sham (top) and LFPI (bottom) slices recorded simultaneously in A) dentate granule cell layer and B) CA3 pyramidal cell layer in response to paired-pulse stimulation (100-ms interval) in the perforant path. C) Hilar transection eliminated CA3 population spike activity in both sham and injured slices. D) I/O curves for 50-500 μA perforant path stimulation show a significant change in DG population spike amplitude after LFPI in the first pulse (Two-way ANOVA, *$p<0.05$), but E) saturated at the second pulse (Two-way ANOVA, n.s., $p = 0.5531$). F) Second stimulation demonstrated a marked increase in CA3 population spike amplitude (Two-way ANOVA, ****$p < 0.0001$).

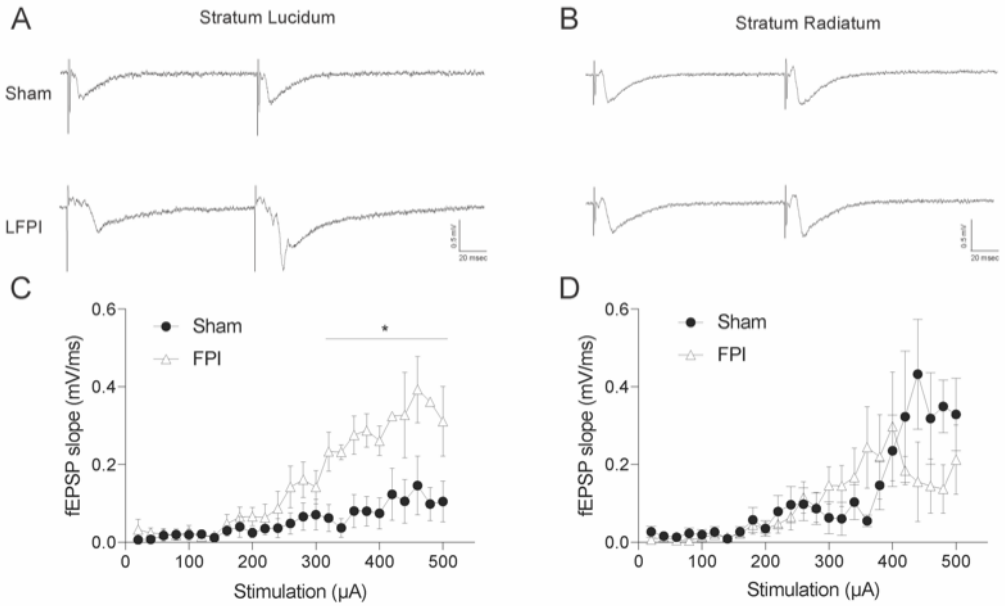

Figure 6. LFPI leads to increased synaptic efficacy in CA3 stratum lucidum but not stratum radiatum. Representative fEPSP traces from sham (top) and LFPI (bottom) slices in response to paired-pulse stimulation (100 msec interstimulus-interval) of the perforant path at 400 μA in A) CA3 stratum lucidum and B) CA3 stratum radiatum. I/O curves (20-500μA) of first pulse fEPSP slopes from 20-500 μA in C) stratum lucidum (Two-way Repeated Measures ANOVA: Injury Factor: $F(1, 135) = 108.2$, $p<0.0001$; Stimulus Intensity Factor: $F(24, 135) = 10.25$, $p<0.0001$; Interaction: $F(24, 135) = 3.426$, $p<0.0001$) and D) stratum radiatum (Two-way Repeated Measures ANOVA: Injury Factor: $F(1, 135) = 1.419$, $p = 0.2356$; Stimulus Intensity Factor: $F(24, 135) = 5.209$, $p<0.0001$; Interaction: $F(24, 135) = 1.276$, $p = 0.1922$). N = 4 animals per condition.

			FDP ΔF/F values ($x10^{-4}$)				
			Sham		LFPI		
			Mean	SEM	Mean	SEM	P-value
Dentate Gyrus	St. Moleculare	Suprapyramidal Blade	23.5	3.9	33.9	3.7	0.070
		Infrapyramidal Blade	30.4	3.8	31.6	4.5	0.840
	St. Granulosum	Suprapyramidal Blade	15.9	26.6	22.5	1.5	0.030
		Infrapyramidal Blade	16.0	1.9	26.7	2.8	0.007
	Hilus		13.7	2.3	21.8	2.1	0.019
Area CA3	St. Pyramidale		4.9	0.73	11.7	2.6	0.033
	St. Radiatum/Lucidum		5.1	0.68	9.9	2.1	0.050
	St. Oriens		4.7	0.61	8.3	1.3	0.029

Table 1. Fast depolarizing peak (FDP) ΔF/F values from voltage-sensitive dye fluorescence in response to perforant path stimulation. Sham and Injured group means and standard error of the mean (SEM) are reported for each anatomically-defined cell layer. The both the DG molecular and granule cell layers (st. moleculare and st. granulosum) were divided based on their anatomical position in the suprapyramidal or infrapyramidal blade. DG, Sham n = 11, LFPI n = 9 animals; CA3, Sham n = 6, LFPI n = 6 animals.

CHAPTER 3

TRAUMATIC BRAIN INJURY REDUCES FEEDFORWARD ACTIVATION OF PARVALBUMIN-EXPRESSING INTERNEURONS IN THE DENTATE GYRUS

Kaitlin A. Folweiler,[1,2,3] Guoxiang Xiong,[1,2] Hannah E. Metheny,[1,2] Gabriel Nah,[1,2] Akiva S. Cohen[1,2,3]

[1]Department of Anesthesiology and Critical Care Medicine, Children's Hospital of Philadelphia, Philadelphia, PA 19104. [2]Department of Anesthesiology, Perelman School of Medicine, University of Pennsylvania, Philadelphia, PA 19104. [3]Neuroscience Graduate Group, University of Pennsylvania, Philadelphia, PA 19104

Abstract

Traumatic brain injury (TBI) is associated with network hyperexcitability in the dentate gyrus and a loss of inhibition onto dentate granule cells. GABAergic parvalbumin-expressing interneurons (PV-INs) in the dentate gyrus regulate granule cell excitability with strong, perisomatic inhibition, however the posttraumatic effects on PV-IN function after TBI are not well understood. In this study, we investigated physiological alterations in PV-INs one week after lateral fluid percussion injury from whole-cell patch clamp recordings in acute brain slices. PV-IN cell counts in LFPI animals demonstrated selective cell loss in the dentate hilus compared to counts in sham controls. Surviving PV-INs showed no change in their intrinsic membrane properties, however did experience alterations in spontaneous and miniature excitatory and inhibitory postsynaptic currents (EPSCs/IPSCs). Specifically, PV-INs in LFPI slices were observed to have larger amplitude EPSCs, but opposing shifts in the frequency of spontaneous and miniature EPSCs. The amplitude of miniature IPSCs was also increased after injury, though only spontaneous IPSCs showed an increase in event frequency. Perforant path stimulation of PV-INs showed a decrease in evoked EPSC amplitude and charge transfer in LFPI slices, which returned to sham control level with bicuculline methiodide wash-in. Current-clamp recordings additionally found that perforant path minimal stimulation results in a decreased likelihood of PV-INs from LFPI slices to fire action potentials. When GABAergic transmission was pharmacologically blocked, PV-IN evoked firing likelihood returned to sham levels. These data suggest that feedforward activation of surviving dentate PV-INs is diminished due to increased network inhibition onto these cells. This suggests that circuit level synaptic alterations may dial down PV-IN firing activity after injury and

contribute to the loss of GABAergic regulatory control of dentate granule cells and overall network excitability.

Introduction

Fast-spiking, parvalbumin-expressing GABAergic interneurons (PV-INs) are powerful regulators of excitability in neural networks and play an important role in mediating hippocampal-dependent cognitive behaviors (Armstrong & Soltesz, 2012; Freund & Buzsáki, 1996; Fuchs et al., 2007; Hu et al., 2014; Nitz & Mcnaughton, 2004). In the hippocampus, PV-INs contribute to the ability of the dentate gyrus sub-region to act as a filter or gate of incoming sensory information from the cortex by providing strong feedforward inhibition onto granule cells (Coulter & Carlson, 2007). In combination with the low intrinsic membrane excitability of granule cells, PV-IN GABAergic inhibition contributes to sparse granule cell action potential firing under normal conditions (Ewell & Jones, 2010; Kraushaar & Jonas, 2000).

After traumatic brain injury (TBI), the dentate gyrus experiences network hyperexcitability (Cole et al., 2010; Lowenstein et al., 1992; V Santhakumar et al., 2000; Toth et al., 1997; Witgen et al., 2005). Granule cells no longer sparsely fire action potentials, and evoked extracellular burst discharges are increased in the granule cell layer *in vivo* (Lowenstein et al., 1992). This shift toward a hyperexcitable network state leads to a break down in the physiological filtering function of the dentate gyrus and is associated with spatial memory impairments (Folweiler et al., 2018).

One week after TBI, the frequency of miniature inhibitory postsynaptic currents (mIPSCs) is reduced in granule cells signaling, suggesting that a loss of synaptic inhibition is contributing to granule cell hyperexcitability (Toth et al., 1997; Witgen et al., 2005). Previous studies have looked at other populations of dentate inhibitory interneurons after

TBI (Butler et al., 2017; Hunt et al., 2011), but none so far have examined changes in PV-INs and their potential role in dentate network hyperexcitability after injury. In this study, we investigated physiological alterations in PV-IN intrinsic membrane properties, as well as afferent synaptic inputs onto PV-INs in the dentate gyrus one week after mild lateral fluid percussion injury (LFPI). The data demonstrate that injury leads to a synaptic E/I imbalance in inputs onto PV-INs, and that feedforward activation of PV-INs is compromised by augmented network inhibition. These findings suggest that the propensity for PV-INs to provide feedforward inhibition onto granule cells is diminished after mild TBI, and contributes to posttraumatic network hyperexcitability in the dentate gyrus overall.

Materials and Methods

Mice

All experiments were performed in accordance with protocols approved by the Institutional Animal Care and Use Committee of Children's Hospital of Philadelphia and the guidelines established by the National Institutes of Health (NIH) Guide for the Care and Use of Laboratory Animals. Experiments were designed to minimize the number of animals required and those used were cared for, handled, and medicated as appropriate to minimize pain and suffering. In order to visually identify PV-INs, PV^{CRE} transgenic mice, which express Cre recombinase in parvalbumin-expressing neurons ($129P2^{Pvalbtm1(cre)Arbr}$/J; Jackson Laboratory, Bar Harbor, ME, USA. Stock number 008069) were crossed with tdTomato reporter mice ($129S6\text{-}Gt(ROSA)26Sor^{m14(CAG\text{-}tdTomato)Hze}$/J; Jackson Laboratory, stock number 007908) to generate PV^{CRE};$tdTomato^{+/-}$ (i.e., PV-

Tomato) transgenic animals which express tdTomato fluorescence in PV+ cells. All experiments were performed on 6-8 week-old male and female PV-Tomato mice.

Surgical procedures

Animals were anesthetized with a mixture of ketamine (2.6mg/kg) and xylazine (0.16 mg/kg) via intraperitoneal injection. Once fully anesthetized, animals were placed in a stereotaxic frame (Stoetling, Wood Dale, IL, USA), the scalp was incised and pulled away to fully expose the right parietal bone. An ultra-thin Teflon disk, with an outer diameter equal to the inner diameter of a trephine was glued to the skull with Vetbond (3M, St. Paul, MN, USA) between lambda and bregma sutures, and between the sagittal suture and the lateral ridge over the right hemisphere. Guided by the Teflon disk, a trephine was used to perform a 3-mm diameter craniectomy over the right parietal area. Following craniectomy, a Luer-lock needle hub (3-mm inner diameter) was secured above the skull opening with Loctite superglue and dental acrylic, filled with saline and capped. Lastly, animals were removed from stereotaxis, placed on a heating pad until fully recovered from anesthesia, and then returned to their respective home cage.

Lateral fluid percussion injury (LFPI)

Twenty-four hours following craniectomy, animals were placed under isoflurane anesthesia (2% oxygen in 500ml/min) in a chamber and respiration was visually monitored until animals reached a surgical plane of anesthesia (one respiration per 2 s). At this point, animals were removed from isoflurane, the needle hub was refilled with saline and connected to the fluid percussion injury device (Department of Biomedical Engineering, Virginia Commonwealth University, Richmond, VA, USA) via high-pressure tubing. The animal was placed onto a heating pad on its left side and upon resumption of normal

breathing pattern but before sensitivity to stimulation, the injury was induced by a 20-millisecond pulse of saline onto the intact dura. The pressure transduced onto the dura was monitored with an oscilloscope, with injury severity ranging between 1.4 and 1.6 atmospheres. Immediately after injury, the hub was removed from the skull and the animal was placed in a supine position to assess righting reflex. After righting, the animal was subjected to inhaled isoflurane to suture the scalp. Animals were allowed to recover on a heating pad until mobile, at which point they were returned to their home cage. Sham animals underwent all surgical procedures including attachment to the FPI device with exclusion of the actual fluid pulse.

Cell counts

Seven days after LFPI or sham procedure, a subset of animals was anesthetized with 5% chloral hydrate and perfused with 10 ml of saline, followed by 50 ml of paraformaldehyde (4% in phosphate buffer, pH 7.4; Sigma-Aldrich). Brains were post-fixed for 90 min at room temperature (RT) and 50 µm thick coronal sections were cut with a VT1000S vibratome (Leica Microsystems Inc.). Fixed sections were counterstained with Hoechst. Fluorescent images were acquired with the Olympus BX-51 microscope at 10X magnification. Cell counts were quantified in slices containing the dorsal dentate gyrus in 300 um increments. Cell anatomical location was considered by both dentate blade (suprapyramidal or infrapyramidal) and cellular layer, including: molecular layer, granule cell layer, subgranular zone, and hilus.

Electrophysiology

All recordings were made 5–9 days after LFPI or sham surgery. Mice were anesthetized with isoflurane, and the brains were quickly and carefully removed, then placed into ice-

cold oxygenated (95% O_2/5% CO_2) sucrose artificial cerebral spinal fluid (aCSF) containing (in millimolar): sucrose 202, KCl 3, NaH_2PO_4 1.25, $NaHCO_3$ 26, glucose 10, $MgCl_2$ 1, and $CaCl_2$ 2. Coronal slices 350 µM thick containing the dorsal hippocampus were cut on a VT1200S vibratome (Leica Microsystems Inc., Buffalo Grove, IL, USA) and transferred to 33–37°C normal aCSF containing (in millimolar): NaCl 130, KCl 3, NaH_2PO_4 1.25, $NaHCO_3$ 26, glucose 10, $MgCl_2$ 1, $CaCl_2$ 2, for at least 45 minutes.

Extracellular field recordings

Electrodes for recording field excitatory post-synaptic potentials (fEPSPs) were fabricated from borosilicate glass (World Precision Instruments, Sarasota, FL, USA, #1B150F-4), pulled to a tip resistance of 2–6 MΩ and filled with aCSF. fEPSPs were recorded from an electrode placed in the dentate molecular layer of the dentate gyrus. Stimulating electrodes were non-concentric bipolar (World Precision Instruments, Sarasota, FL, USA, #ME12206) and placed at the apex of the molecular layer. Electrical stimuli were 100 µs in duration. Field potential input–output relationships were conducted by recording the response to increasing stimulating intensities (20–400 µA stimulation, 20 µA increments, 8 second inter-stimulus interval). Recordings were obtained with an Axoclamp 900A amplifier and pClamp10 data acquisition software (Molecular Devices, Sunnyvale, CA, USA), filtered at 2 kHz. Field potential data was analyzed using pClamp10 and custom-written MATLAB scripts.

Whole-cell patch clamp recordings

Patch electrodes with resistances of 4–7 MΩ were pulled from borosilicate glass (World Precision Instruments, Sarasota, FL, USA). Series resistance was monitored throughout the experiment and recordings were discontinued if series resistance exceeded 25 MΩ at

any point. Series resistance was compensated for at 70-80% compensation. All recordings were made using a Multiclamp 700B (Molecular Devices, Palo Alto, CA, USA) sampled at 20 kHz, filtered at 2 kHz. Electrophysiological data were analyzed using Clampfit 10 (Molecular Devices) and MATLAB R2012b (Mathworks, Natick, MA, USA). Synaptic events were determined via the Template Search algorithm in Clampfit 10.

PV-Ins were visually identified by fluorescent *tdTomato* expression in cells within the granule cell layer, subgranular zone, or hilar subregions. In order to confirm that tdTomato-expressing neurons were also fast-spiking, experiments began with a series of depolarizing current steps. Any neurons that failed to demonstrate non-accommodating trains of action potentials with a maximum spiking frequency greater than 30Hz (Kawaguchi & Kubota, 1997), in response to depolarizing current injections, or demonstrating baseline instability, were excluded from further analysis.

Resting membrane potential was computed as the average voltage in the first 2 seconds immediately after whole-cell configuration was achieved. All other intrinsic excitability measures were computed from current clamp recordings consisting of a series of ten 500 ms current steps, from −100 to 250 pA in 50 pA increments. Constant holding current was applied to maintain the neuron at −65 mV before and after current steps. Action potential threshold was computed by taking dV/dt of the voltage trace at 175 pA in the intrinsic excitability experiments and then averaging the corresponding voltage values for the first 10 spikes where dV/dt exceeded 30 mV/ms (Howard et al., 2007). Input resistance was determined from the steady-state voltage response for the four initial current steps (-100 pA to 50 pA). Action potential frequency and corresponding inter-spike-intervals were calculated for all current steps resulting in action potential firing.

For whole-cell patch-clamp recording of spontaneous- and miniature excitatory postsynaptic currents (sEPSCs and mEPSCs) and intrinsic excitability measures electrode internal solution contained (in millimolar): K-Gluconate 140, EGTA 5, HEPES 10, $MgCl_2$ 1, $CaCl_2$ 1, KOH 3, Mg-ATP 2, and was titrated to a final pH of 7.1–7.3 with KOH and osmolality of 290-300 mOsm. Bicuculline methiodide (30 µM, BMI) was added before voltage clamp recordings, and tetrodotoxin (0.4 µM, TTX) was added to isolate mEPSCs. Neurons were voltage-clamped at −65 mV for all EPSC voltage-clamp experiments. Liquid junction potential of 16.9 mV (calculated in Clampex) was corrected for in all data reported from these experiments. For whole-cell patch-clamp recording of inhibitory currents, internal solution contained (in millimolar): Cs-gluconate 140, NaCl 1, EGTA 5, $MgCl_2$ 1, $CaCl_2$ 1, KOH 3, Mg-ATP 2, and was titrated to a final pH of 7.2-7.3 with CsOH and an osmolality of 290-300 mOsm. APV (50 µM), CNQX (6 µM), and QX-314 (5 mM) were added before voltage clamp recordings, and TTX (0.4 µM) was added to isolate mIPSCs. Liquid junction potential of 2.0 mV (calculated in Clampex) was corrected for in all data reported from these experiments. Neurons were voltage-clamped at 0 mV for all voltage clamp experiments of inhibitory currents. The slice chamber temperature for all recordings was set to 29-31°C.

To record perforant path-evoked excitatory postsynaptic currents (eEPSCs), a non-concentric bipolar placed in at the apex of the molecular layer was used to stimulate afferent axons onto patch-clamped PV-INs held at -65 mV in voltage-clamp. Evoked potentials were recorded in response to electrical stimulation from 10–100 µA in 10 µA incremental steps. Extracellular fEPSPs were simultaneously recorded in the molecular

layer during evoked voltage-clamp and current-clamp experiments and eEPSC for each recorded cell were normalized to the fiber volley amplitude of the slice.

For current-clamp experiments, an electrode was placed in the perforant path at the apex of the molecular layer. Minimal current stimulation was adjusted to find the lowest current intensity parameter that could elicit at least one action potential (10-50 μA) in a series of 20 stimulations. Once the minimal stimulation current intensity was set, three series of 20 stimulations (12 second interstimulus interval) were administered and the number of stimulus-evoked action potentials (APs) for each series was recorded and reported as a percentage of the total number of stimulations in that series (20 stimulations per series). Throughout current-clamp recordings, a slow injection of current was given to maintain a membrane potential of -65 mV.

Statistical procedures

A priori power calculations were performed using G*Power based on variability from similar previous experiments (Faul et al., 2007). Electrophysiological and cell count data were analyzed using pClamp 10 and Graphpad Prism 7.0 software. Statistics were performed using either Mann–Whitney U-tests, or two-way repeated measures ANOVA with Sidak's multiple comparison test in order to test for injury effect and stimulation intensity effect with significance set at $P < 0.05$. The Kolmogorov-Smirnov test was used for statistical comparison of synaptic current measurements. *N* refers to number of cells (for physiology) or number of animals (cell counts). Statistical significance was $p < 0.05$ ($p < 0.05$*, $p < 0.01$**, $p < 0.001$***. Data in the figures are presented as group means ± SEM unless otherwise stated.

Results

Mild LFPI induces selective loss of hilar tdTomato-expressing neurons

Previous studies found fewer hilar GABA-expressing neurons, including PV-INs, one week after fluid percussion injury (Lowenstein et al., 1992; V Santhakumar et al., 2000; Toth et al., 1997; Witgen et al., 2005), however these studies utilized a moderate (2.0-2.2 atm) pressure impact. To test if hilar PV-IN cell loss occurred in our mild (1.4-1.6 atm) LFPI model, we counted the number of tdTomato-expressing cells in the dorsal dentate gyrus ipsilateral to the injury site in sham (n = 8) and LFPI (n = 9) mice (Figure 1). At one week after injury, there were significantly less tdTomato-positive cells in the hilus (Figure 1B and 1D; mean ± SEM = 17.2 ± 2.4 cells in sham and 10.2 ± 1.8 in LFPI; $p < 0.05$). The total number of dentate PV-INs appeared to trend downward but did not result in a statistically significant change after injury (Figure 1C, mean ± SEM = 108.4 ± 10.8 cells in sham; 80.8 ± 9.1 in LFPI; $p = 0.067$). PV-IN cell counts remained unchanged in the subgranular zone, granule cell layer, and molecular layer when respectively counted (data not shown, $p > 0.05$), indicating that mild LFPI also induces selective hilar cell loss for the PV-IN population.

Dentate network hyperexcitability persists in PV-Tomato mouse line

Our laboratory has previously shown that dentate network hyperexcitability after LFPI in acute brain slices from C57Bl6/J mice (Cole et al., 2010; Folweiler et al., 2018; Witgen et al., 2005). To ensure that injury also alters dentate excitability in PV-Tomato transgenic mice, input/output (I/O) curves were generated by stimulating the perforant path (stimulation intensity range: 20-400 μA, 20 μA increments, 100 μs duration) and recording extracellular field potentials in the molecular layer one week after LFPI (n = 3) or sham (n = 2) surgery on transgenic animals. In brain slices from sham animals, fEPSP slope

increased almost linearly as perforant path stimulation intensity increased (Figure 2A). Slices from LFPI animals demonstrated significantly larger fEPSP slopes with increasing stimulation intensity compared with sham (Two-way ANOVA, $F(1, 3) = 508.7$; $p < 0.001$). This injury-induced shift in the I/O curve suggests that dentate post-traumatic hyperexcitability is present in the transgenic mouse line used for further experiments in this study.

PV-IN intrinsic membrane properties are unaffected by injury

Neuronal intrinsic membrane properties, dictated predominantly by membrane proteins and their subsequent activity, play a significant role in a neuron's propensity to fire action potentials. After experimental TBI, alterations in intrinsic properties have been observed in other dentate interneurons (Gupta et al., 2012; Howard et al., 2007). To investigate the intrinsic properties of dentate PV-INs, we performed whole-cell patch clamp recordings one week after LFPI or sham surgery (Figure 2B-F, n = 10 cells in each group). Passive properties such as membrane input resistance (Figure 2C; sham: 92.2 ± 6.3 MΩ; LFPI: 88.6 ± 7.5 MΩ; $p = 0.71$), and resting membrane potential (Figure 2D; mean ± SEM = -65.3 ± 1.4 mV in sham and -62.9 ± 1.2 mV in LFPI; $p = 0.22$), were not significantly different between cells from sham and LFPI groups. Additionally, PV-IN active firing properties were not affected by injury. PV-INs from sham animals had on average an action potential threshold of -29.8 ± 1.0 mV, while cells from LFPI animals had an average firing threshold of -32.7 ± 2.1 mV (Figure 2E; $p = 0.23$). Action potential firing frequency in response to depolarizing current steps (400 – 550 nA, 50 nA steps) was unaltered by injury (Figure 2B and 2F; sham: n = 8 cells, LFPI: n = 7 cells; two-way ANOVA: $F(1,13) = 0.42$; $p = 0.53$). Lastly, action potential half-width, was not significantly different between sham and injured

groups (mean ± SEM= 0.74 ± 0.06 ms in sham and 0.69 ± 0.04 ms in LFPI; p = 0.55, data not shown). These findings suggest that there is no net change in either passive or active intrinsic membrane properties of PV-INs after injury.

Excitatory synaptic inputs onto PV-INs exhibit posttraumatic changes

In addition to intrinsic membrane properties, the balance of excitatory and inhibitory (E/I) synaptic transmission onto cells determines their firing output. To examine whether overall excitatory synaptic input to dentate PV-INs was altered after LFPI, whole-cell voltage-clamp recordings of spontaneous excitatory postsynaptic currents (sEPSCs) were obtained from sham (n = 8 cells) and LFPI (n=7 cells) acute brain slices in the presence of the $GABA_A$-receptor antagonist bicuculline methiodide (BMI). Representative recordings for each group are shown in Figure 3A-B. The median sEPSC amplitude was significantly larger in cells recorded from LFPI animals compared to sham (Figure 3C; Sham: median = 40.25 pA, IQR = 31.4—56.8; LFPI: median = 49.4 pA, IQR = 39.1—64.3, $p < 0.0001$, K-S test). However, the frequency of sEPSCs was reduced in LFPI cells as demonstrated by prolonged inter-event intervals (Figure 3D; Sham: median = 212 ms, IQR = 79.8—492.8; LFPI: median = 346.5 ms, IQR = 113—830.3, $p < 0.0001$, K-S test). Spontaneous excitatory currents also had slower decay kinetics after injury, signifying an increase in the duration of individual glutamatergic events (decay τ, sham: median = 1.25 ms, IQR = 0.51—2.84, LFPI: median = 1.58 ms, IQR = 0.75—3.48, $p < 0.001$, K-S test).

The reduced sEPSC frequency in PV-INs after LFPI could be attributable to fewer glutamatergic synapses onto surviving PV-INs, in which case the frequency of action-potential-independent miniature excitatory postsynaptic currents (mEPSCs) would likely also be affected. mEPSCs were further isolated by the addition of tetrodotoxin (TTX) to

the extracellular solution, eliminating synaptic transmission resulting from pre-synaptic action potentials in sham and LFPI brain slices (n = 7 cells in each group). Representative recordings for each group are shown in Figure 4A. Contrary to spontaneous glutamatergic events, the frequency of mEPSCs was increased in PV-INs after injury as observed by a decrease in inter-event intervals (Figure 4B; Sham: median = 291 ms, IQR = 87.3—832, LFPI: median = 192 ms, IQR = 75.5—673, $p < 0.01$, K-S test). This suggests that there might not necessarily be a loss of glutamatergic synapses onto PV-INs, but a reduction in spontaneous, action potential-dependent transmitter release. On the other hand, mEPSC event amplitudes were larger after LFPI, similar to sEPSCs (Figure 4C; Sham: median = 31.1 pA, IQR = 25.6— 48, LFPI: median = 35.4, IQR = 27.1— 49.25, $p < 0.001$, K-S test). However, no change in glutamatergic channel decay kinetics was observed (decay τ, sham: median = 0.89 ms, IQR = 0.27—2.61, LFPI: median = 1.15 ms, IQR = 0.32—2.84, $p = 0.13$, K-S test).

PV-INs receive less feed-forward excitation from the perforant path after injury

Decreased sEPSC frequency could also indicate diminished presynaptic firing activity or recruitment of afferent glutamatergic neurons. Since local dentate glutamatergic neurons have demonstrated increased activity after experimental TBI (Gupta et al., 2012; Lowenstein et al., 1992; V Santhakumar et al., 2000), it is likely that a decrease in action potential-mediated excitatory drive is coming from perforant path synapses. To test the effect of injury on feed-forward excitation of PV-INs, we examined the I/O relationship of evoked EPSCs (eEPSCs) by electrical stimulation of the perforant path at incremental stimulus intensities (Figure 5; 10-100 μA). While the slope of perforant path eEPSCs was not significantly different between PV-INs from sham (n = 12 cells) and injured (n = 11 cells) (Figure 5B; Two-way ANOVA, $F(1, 270) = 0.036$, $p = 0.85$), there was a decrease

in eEPSC amplitude and charge transfer with increasing stimulus intensities (Figure 5C; Two-way ANOVA, amplitude: $F(1,22) = 4.715$, $p < 0.05$); charge transfer: Figure 5D; $F(1,21) = 5.426$, $p < 0.05$). We next washed in BMI to block local GABAergic inhibition onto PV-INs, and re-measured the evoked synaptic currents (Figure 5A, right trace). In the absence of inhibition, LFPI eEPSCs I/O curves were similar to sham (eEPSC slope: $F(1,10) = 0.005$, $p = 0.94$; eEPSC amplitude: $F(1, 10) = 0.86$, $p = 0.37$; eEPSC charge transfer: $F(1, 10) = 0.95$, $p = 0.35$, I/O curves not shown). These data suggest that diminished feed-forward excitatory synaptic transmission from the perforant path onto dentate PV-INs is due to increased inhibition one week after LFPI.

Increased synaptic inhibitory input onto PV-INs after LFPI

To understand how brain injury affects inhibitory synaptic transmission onto dentate PV-INs, we performed whole-cell voltage-clamp recordings in the presence of the glutamatergic antagonists APV (blocks NMDA receptor–mediated currents) and CNQX (blocks AMPA receptor-mediated currents) to isolate spontaneous inhibitory postsynaptic currents (Figure 6A, sIPSCs). No change in the amplitude of sIPSC events was observed after injury (Figure 6B, Sham: median =32.5 pA, IQR = 19.7—55.6, LFPI: median =33.1, IQR =21.8—59.6, $p = 0.11$, K-S test). However, PV-INs from LFPI mice demonstrated a significant increase in sIPSC event frequency (Figure 6C; reported as inter-event intervals; Sham: median = 174.5 ms, IQR = 89.9—344.5, LFPI: median = 137 ms, IQR = 63.2—343.5, $p < 0.01$, K-S test). Furthermore, a reduction in the decay tau of sIPSCs was also seen in cells from LFPI slices, signifying more rapid channel decay kinetics (Figure 6D; decay τ, sham: median = 7.2 ms, IQR = 4.4—13.2, LFPI: median = 5.8 ms, IQR = 3.4—15.0, $p < 0.001$, K-S test).

To examine miniature independent inhibitory events (mIPSCs), we next bath applied TTX to block action-potential mediated synaptic transmission (Figure 7A). Unlike spontaneous events, we found an increase in the amplitude of mIPSCs after injury (Figure 7B; Sham: median = 18.3 pA, IQR = 13.3—24.9, LFPI: median = 19.6 pA, IQR = 14.4—31.2, $p < 0.001$, K-S test). Injury did not affect mIPSC event frequency however, as the inter-event interval between events was not significantly different between PV-INs from sham and injured slices (Figure 7C; Sham: median = 268 ms, IQR = 124—592.3, LFPI: median = 237, IQR = 102—514.3, $p = 0.26$, K-S test). Miniature IPSC decay tau also remained intact after injury (Sham: median = 5.6 ms, IQR = 3.1—11.5, LFPI: median = 7.8 ms, IQR = 5.0—14.7, LFPI: median = 7.6 ms, IQR = 4.9—13.5, $p = 0.85$, K-S test). These results suggest that PV-INs receive larger basal inhibitory events after LFPI, but that the frequency or chloride channel kinetics is unchanged.

PV-IN decreased firing propensity is due to net GABAergic inhibition

The results of the whole-cell patch clamp recordings indicate that there are changes in both excitatory and inhibitory synaptic inputs onto PV-INs after brain injury. These alterations affect the synaptic E/I balance of PV-INs, and influence the cells' propensity to fire an action potential by depolarizing or hyperpolarizing the membrane potential. To understand what the net effect of posttraumatic E/I synaptic alterations are on feed-forward activation of PV-IN neurons, we performed a series of perforant path minimal stimulations and counted the number of PV-INs evoked action potentials recorded in current-clamp (Figure 8; n = 5 cells in each group). In normal aCSF solution, PV-INs from LFPI slices had a significantly lower percentage of evoked action potentials than cells from sham slices (% evoked APs, sham: mean ± SEM: 57.8% ± 6.3, LFP: mean ± SEM: 12.0% ± 4.0, $p < 0.001$, unpaired t-test). We then washed in 100 nM of picrotoxin to remove

$GABA_A$-mediated inhibition from PV-INs being recorded. After picrotoxin application, there was no difference in the percentage of PV-IN evoked action potentials in sham and LFPI groups (% evoked APs, sham: mean ± SEM = 92.6% ± 6.2, LFPI: mean ± SEM = 78.6% ± 10.6, p = 0.29). These findings suggest that the feed-forward activation of PV-IN inhibition is compromised by network inhibition.

Discussion

In the dentate gyrus, GABAergic basket cells and axo-axonic cells (i.e., PV-INs) are important drivers of feedforward inhibition onto granule cells (Ewell & Jones, 2010; Kraushaar & Jonas, 2000). Previous work has demonstrated that feedforward inhibitory control of dentate granule cell firing is compromised after LFPI (Toth et al., 1997; Witgen et al., 2005). In seeking to identify potential cellular sources of granule cell disinhibition, this study is the first to demonstrate altered excitability of dentate gyrus PV-INs following experimental TBI. First, we showed that mild LFPI induced a loss of PV-INs in the hilus, recapitulating hilar interneuron loss observed in previous studies using moderate LFPI (Lowenstein et al., 1992; V Santhakumar et al., 2000; Toth et al., 1997; Witgen et al., 2005). While surviving PV-INs have normal intrinsic membrane properties, the balance of excitatory and inhibitory synaptic input onto these cells is shifted after injury. Furthermore, the data revealed that cortical feedforward activation of PV-INs is diminished due to a net inhibitory effect and decreased the likelihood of evoked PV-IN firing. Together, these findings suggest that TBI causes a decrease in PV-IN activation which may contribute to the loss of inhibition onto granule cells.

In our study, we replicated the findings that PV-INs are significantly decreased in the hilus, previously reported in studies using higher (2.0-2.2 atm) injury levels of LFPI (Lowenstein et al., 1992; V Santhakumar et al., 2000; Toth et al., 1997; Witgen et al., 2005). This demonstrates that hilar cells—at least PV+ neurons—are vulnerable to cell death even in a milder model of LFPI (1.4-1.6 atm). The steady number of PV-INs in the subgranular zone and granule cell layers also supports findings by Toth and colleagues, who proposed that laminar cell density plays a role in injury-induced neuronal loss, and that loose cell packing in the hilus increases cell death susceptibility (Toth et al., 1997). An advantage of cell counts in our PV-Tomato transgenic mice is that fluorescence protein expression is controlled by the *CAG* promoter, and was not directly linked to PV-expression after injury. Therefore, it is unlikely that the decrease in tdTomato-positive cell bodies is due to reduced PV protein expression or immunoreactivity (Nichols et al., 2018); however, we cannot rule out that brain injury may negatively affect CAG promotor activation and interfere with fluorescent protein expression.

When we examined the intrinsic membrane excitability of PV-INs, we observed no differences in passive or active properties following injury. Other dentate cells types have also been shown retain their intrinsic properties, suggesting that the composition of membrane leak and voltage-gated channels are not overtly altered by LFPI (Howard et al., 2007; V Santhakumar et al., 2000; Vijayalakshmi Santhakumar et al., 2001). This could reflect homeostatic compensation by opposing modifications of intrinsic currents, as was previously observed in mossy cells after injury (Howard et al., 2007). Further inspection of isolated ionic currents may be required to rule out the contribution of homeostatic mechanisms to maintaining PV-IN intrinsic excitability.

While the intrinsic properties of PV-INs remained intact, changes in both excitatory and inhibitory synaptic currents reflected posttraumatic circuit-level alterations. On the excitatory side, both spontaneous and miniature EPSCs had larger amplitude events, suggesting a larger postsynaptic response (e.g., increased insertion of receptors into the membrane) or larger presynaptic quantal size. Spontaneous and miniature EPSCs also showed opposing shifts in event frequency, with a decrease in sEPSC and increase in mEPSC frequencies, respectively. A decrease in spontaneous synaptic transmission could indicate several possible mechanisms including fewer excitatory synapses, altered probability of release, and the reduced activity of presynaptic neurons. Miniature events would be expected to decrease as well if a loss of synapses were to occur. The observed increase in mEPSC events in this study does not appear to support synaptic loss, unless the increase in basal excitatory transmission reflects a compensatory mechanism, leaving changes in release probability or presynaptic activity as untested possibilities. Reduced firing activity of presynaptic excitatory neurons does seem unlikely, since previous studies have found that local dentate glutamatergic neurons are more excitable after injury (Gupta et al., 2012; V Santhakumar et al., 2000). This suggests that the frequency of perforant path glutamatergic projects could be affected by mTBI, and suggests that alterations in excitatory synaptic events reflect changes in different presynaptic glutamatergic cell populations. Additionally, it is possible that TBI may affect specific pools of synaptic vesicles used for spontaneous versus miniature glutamate release differently, as these events have been shown to originate from divergent presynaptic mechanisms of neurotransmission (Fredj & Burrone, 2009; Mathew et al., 2008; Sara et al., 2005).

On the inhibitory side, recorded spontaneous IPSCs demonstrated no change in their amplitude but did show a marked increase in event frequency. This suggests that

presynaptic inhibitory activity is increased onto PV-INs after injury. Somatostatin-positive hilar interneurons, which synapse onto PV-INs (Savanthrapadian et al., 2014), have previously shown increased spontaneous firing activity after TBI and may therefore be a potential source of increased sIPSC frequency, though other GABAergic interneuron types have yet to be examined (Hunt et al., 2011). Miniature IPSC events on the other hand, demonstrated larger amplitudes but did not alter their frequency of occurrence, suggesting either an increase in postsynaptic response such as more $GABA_A$-receptors inserted into the postsynaptic membrane, or the presynaptic packaging of larger GABA quantal sizes.

Changes in spontaneous E/I synaptic input is important for understanding how PV-IN firing activity is regulated by its circuit connections. However, the opposing, complicated changes in synaptic transmission we observed in this study made it difficult to infer the net effect on PV-IN firing, and specifically their feedforward activation by perforant path synapses. After LFPI, perforant path-evoked EPSCs onto PV-INs were smaller than sham controls, but returned to sham levels when GABAergic inhibition was blocked by BMI wash-in. No change in eEPSC slopes indicated that the activation of the evoked response was not affected, but the amplitude and overall charge transfer are decreased because of enhanced inhibitory tone.

Minimal stimulation experiments further demonstrated that net augmentation of GABAergic inhibition decreased the likelihood of PV-INs to fire action potentials in response to entorhinal afferent input. This finding has major implications for predicting the activity of PV-INs in the posttraumatic dentate gyrus. It also provides additional evidence that injury-induced granule cell disinhibition may be attributed to decreased activation of feedforward GABAergic sources. While the results of our study do not provide a direct link

between altered likelihood of PV-IN firing and diminished GABAergic synaptic transmission onto granule cells, they do demonstrate network alterations in E/I balance that affect the functional activation of PV-INs. The posttraumatic decrease in mIPSC frequency onto granule cells seen previously suggests that there is a decrease in presynaptic firing of interneurons that synapse perisomatically onto granule cells, including PV-INs (Soltesz et al., 1995; Toth et al., 1997).

At the circuit level, loss of perisomatic inhibitory control of dentate granule cells is likely to disrupt the gating function of the dentate gyrus after TBI. Additionally, decreased feedforward recruitment of PV-INs could have cognitive consequences. Fuchs and colleagues demonstrated in mice where excitatory drive onto PV-INs was knocked out, that loss of PV-IN recruitment lead to impaired performance on hippocampal-dependent behavioral task (Fuchs et al., 2007). Therefore, alterations in PV-IN activation and network recruitment could have profound effects on cognitive processes and potentially underlie hippocampal-dependent cognitive deficits experienced by TBI patients. Future studies would benefit from investigating potential changes in the properties of PV-IN synapses onto granule cells, as previous work suggests that these synapses may have higher failure rates and smaller pools of readily releasable vesicles in a model of dentate network hyperexcitability (W. Zhang & Buckmaster, 2009).

There are several additional limitations of this study. It is important to note that perisomatic inhibitory control of dentate granule cells is provided by nonoverlapping populations of PV+ *and* CCK+ basket and axo-axonic cells (Freund & Buzsáki, 1996; Soriano et al., 1990). While this study only examined PV+ interneurons after TBI, understanding the effects of CCK+ basket cell inhibition will provide a complete picture of alterations in

granule cell perisomatic inhibition. Another limitation of this study is that we did not investigate possible mechanisms of synaptic alterations such as the number of synapses, presynaptic probability of release, or firing activity of presynaptic neurons. Future investigation of the mechanisms of E/I imbalance are crucial to understanding the overall shift in network excitability.

In conclusion, our data show that synaptic E/I balance onto dentate PV-INs is shifted toward a net inhibitory effect one week after experimental mild TBI. Net inhibition decreases the likelihood of action potential initiation, and suggest that activation of PV-IN-mediated feedforward inhibition onto granule cells in the dentate gyrus is compromised. These results demonstrate posttraumatic alterations in inhibitory function which do contribute to dentate network hyperexcitability and hippocampal dysfunction after TBI.

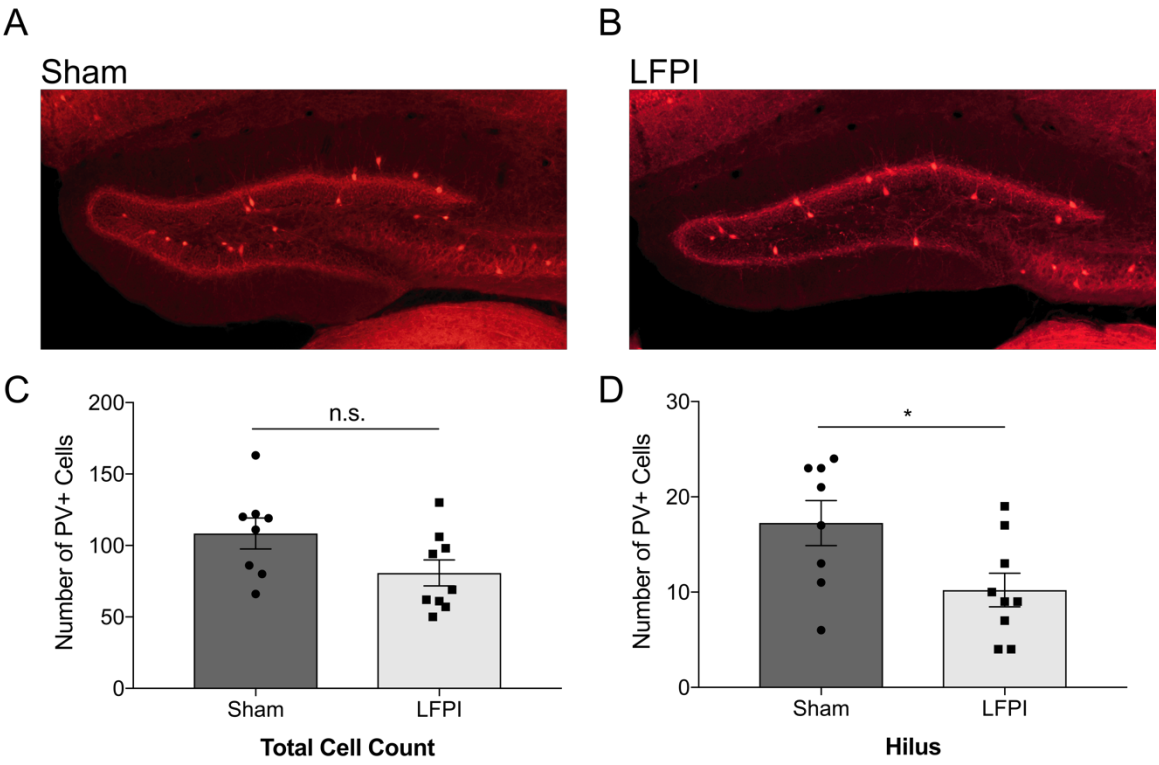

Figure 1. PV-IN cell loss in the dentate hilus occurs one week after mild LFPI. Parvalbumin-positive (PV+) inhibitory interneurons expressing the fluorescent marker tdTomato in the dentate gyrus one week after A) sham surgery or B) LFPI. C) Total number of PV+ cell bodies in the dentate gyrus are not significantly different between sham (mean ± SEM = 108.4 ± 10.8 cells) and LFPI (mean ± SEM = 80.8 ± 9.1 cells; $p = 0.067$). D) The hilus experiences a significant loss of PV+ interneurons (Sham: mean ± SEM = 17.2 ± 2.4 cells, LFPI: mean ± SEM = 10.2 ± 1.8 cells, $p < 0.05$). n.s., non-significant; * $p < 0.05$

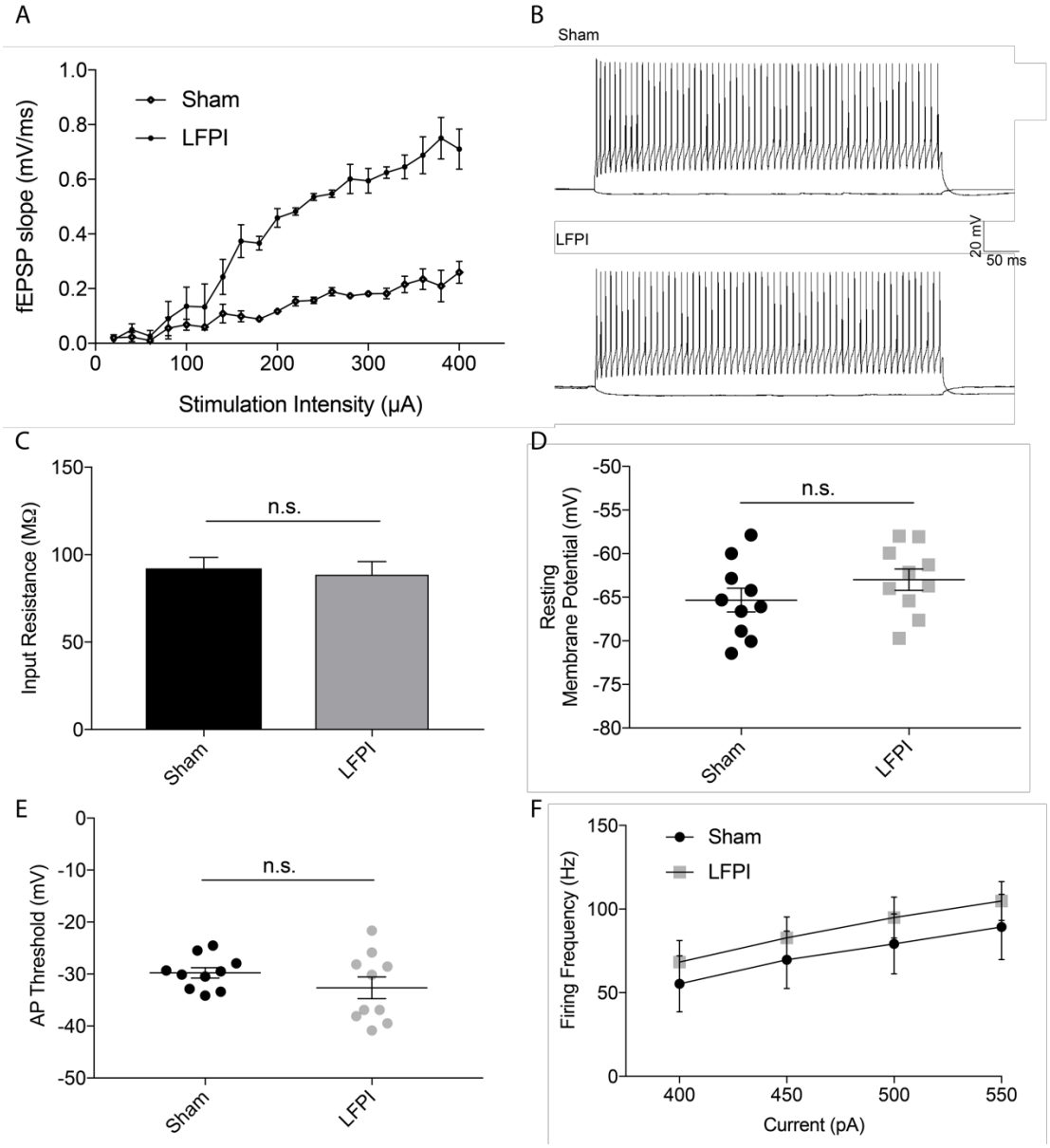

Figure 2. PV-IN intrinsic membrane excitability remains intact after LFPI. A) Dentate network hyperexcitability is replicated in trangenic PV-Tomato mouse line. The slopes of field excitatory postsynaptic potentials (fEPSPs) recorded from dentate molecular layer are plotted for sham (n = 2 mice) and LFPI (n = 3 mice) groups in response to perforant path electrical stimulation. Stimulation intensity range: 20-400 μA, 20 μA increments, 100 μs duration. Two-way ANOVA, F (1, 3) = 508.7; **p < 0.001. B) Example membrane

voltage traces from sham (top trace) and LFPI (bottom trace) PV-INs in response to -50 pA and +100 pA current injections. Passive membrane properties of PV-INs are unchanged by injury as exemplified by C) membrane input resistance and D) resting membrane potential. Active firing properties also show no significant difference between sham (black points) and injured (gray points) on E) action potential threshold and F) PV-IN firing frequency in response to increasing depolarizing current injections.

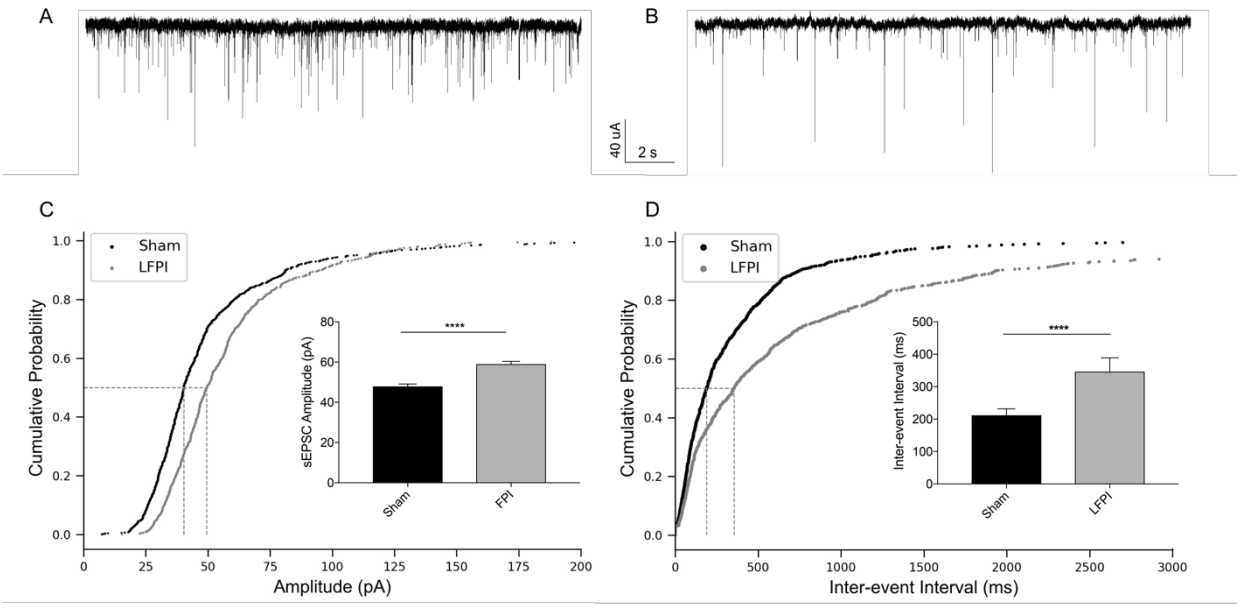

Figure 3. PV-INs have less frequent sEPSCs with larger amplitudes after LFPI. A) Representative traces of voltage-clamp recordings from A) sham PV-IN cell and B) LFPI PV-IN cell show a decrease in event frequency but an increase in the size of individual events after injury. Cumulative probability plots of C) sEPSC amplitude and D) inter-event interval of sEPSCs recorded in the presence of 30 μM bicuculline methiodide from sham PV-INs (black) and LFPI PV-INs (gray). Vertical dashed lines indicate the median of the distribution at probability, p = 0.5. Insets: bar graphs of the median and 95% confidence intervals of C) sEPSC amplitude and D) sEPSC inter-event interval in sham (black) and LFPI (gray) PV-INs. ****, $p < 0.0001$

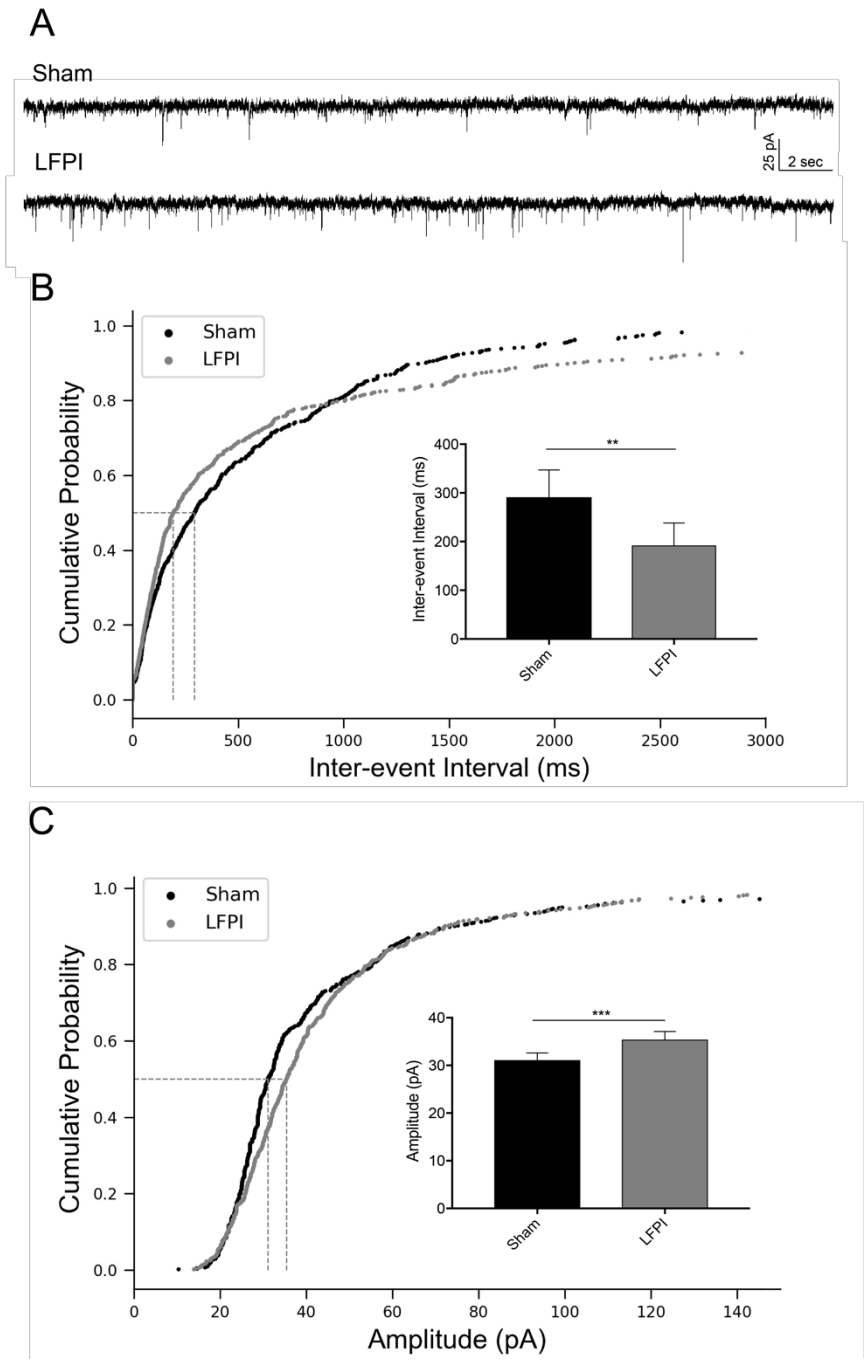

Figure 4. PV-IN mEPSCs are larger and more frequent after LFPI. A) Representative traces of voltage-clamp recordings from sham (top trace) and LFPI (bottom trace) PV-IN cells in the presence of 30 μM bicuculline methiodide and 0.4 μM tetrodotoxin to block presynaptic action potential-dependent synaptic transmission. Cumulative probability

plots of C) mEPSC inter-event interval and D) event amplitude from sham PV-INs (black) and LFPI PV-INs (gray). Vertical dashed lines indicate the median of the distribution at probability, p = 0.5. Insets: bar graphs of the median and 95% confidence intervals of B) mEPSC inter-event interval and C) mEPSC amplitude in sham (black) and LFPI (gray) PV-INs. ***, $p < 0.001$, **, $p < 0.01$

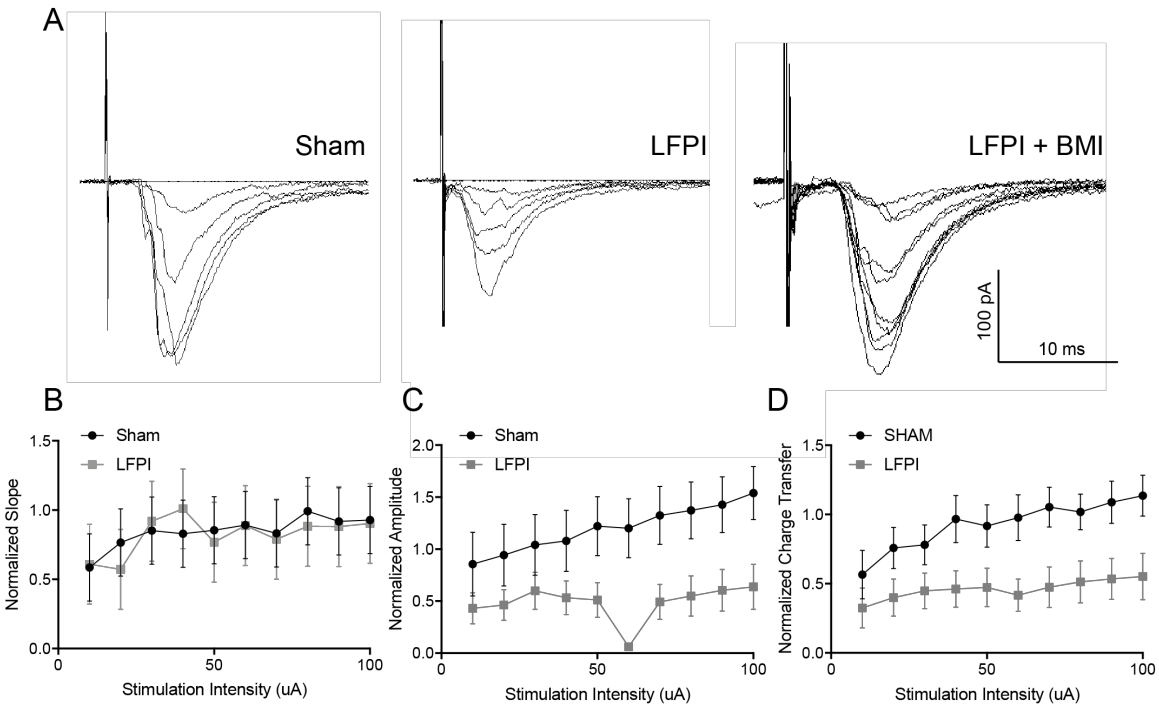

Figure 5. Decreased perforant path evoked EPSCs onto PV-INs after LFPI. A) Representative traces of perforant path evoked EPSCs onto PV-INs from sham (left), LFPI (center), and same LFPI cell with the addition of bicuculline methiodide (BMI). Evoked EPSCs were normalized to the fiber volley (FV) amplitude of the extracellular field response of that brain slice. The FV-normalized B) slope (Two-way ANOVA, $F(1, 270) = 0.036$, $p = 0.85$, n.s.), C) amplitude (Two-way ANOVA, $F(1,22) = 4.715$, $^*p < 0.05$), and D) charge transfer (Two-way ANOVA, $F(1,21) = 5.426$, $^*p < 0.05$), of eEPSCs in sham (black) and LFPI (gray) PV-INs.

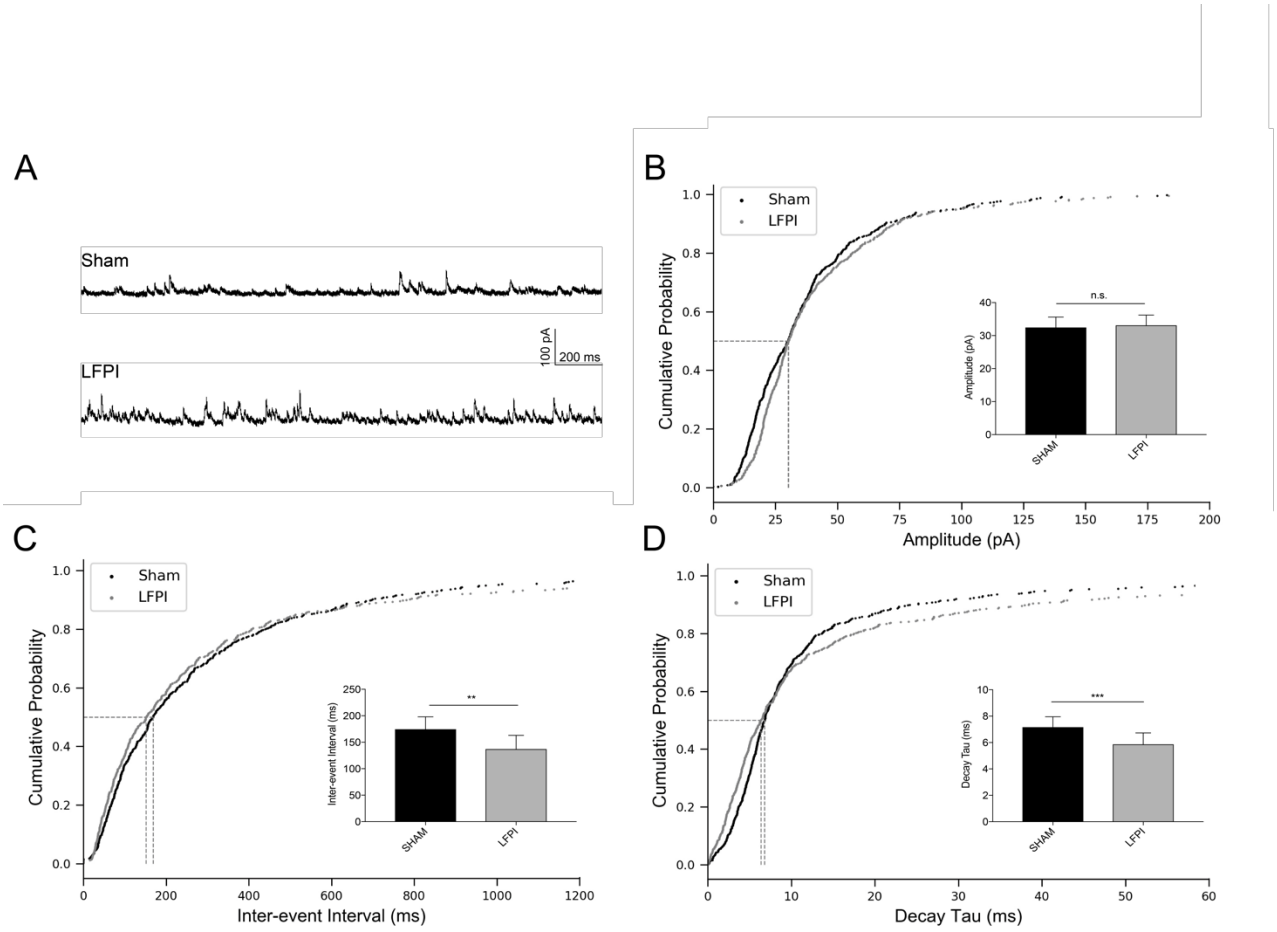

Figure 6. Increase in PV-IN spontaneous IPSC frequency and decay kinetics after LFPI. A) Representative traces of voltage-clamp recordings at 0 mV from sham (top trace) and LFPI (bottom trace) PV-IN cells in the presence of 50 µM APV and 6 µM CNQX to block glutamatergic synaptic transmission. Cumulative probability plots of B) sIPSC amplitude, C) inter-event interval and D) decay tau from sham PV-INs (black) and LFPI PV-INs (gray). Vertical dashed lines indicate the median of the distribution at probability, p = 0.5. Insets: bar graphs of the median and 95% confidence intervals for respective event measurements in sham (black) and LFPI (gray). n.s., no significance, **, $p < 0.01$, ***, $p < 0.001$.

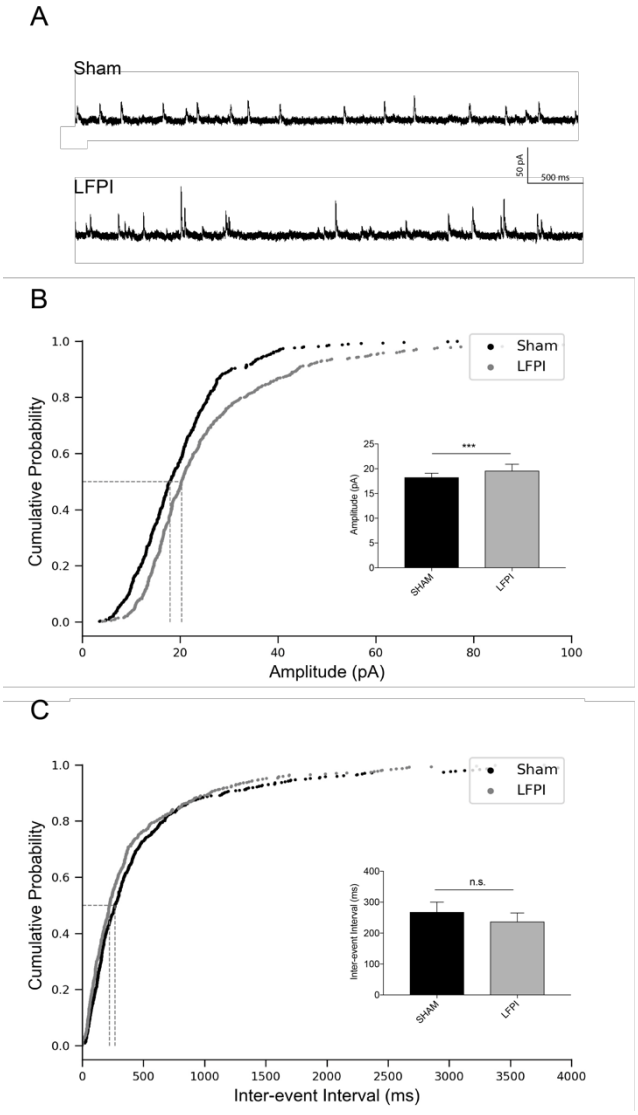

Figure 7. Increase in PV-IN miniature IPSC amplitude after LFPI. A) Representative traces of voltage-clamp recordings at 0 mV from sham (top trace) and LFPI (bottom trace) PV-IN cells in the presence of glutamatergic blockers, APV and CNQX, and 0.4 μM TTX to isolate action-potential-independent synaptic transmission. Cumulative probability plots of B) mIPSC amplitude, C) inter-event interval from sham PV-INs (black) and LFPI PV-INs (gray). Vertical dashed lines indicate the median of the distribution at probability, p =

0.5. Insets: bar graphs of the median and 95% confidence intervals for respective event measurements in sham (black) and LFPI (gray). n.s., no significance, ***, $p < 0.001$.

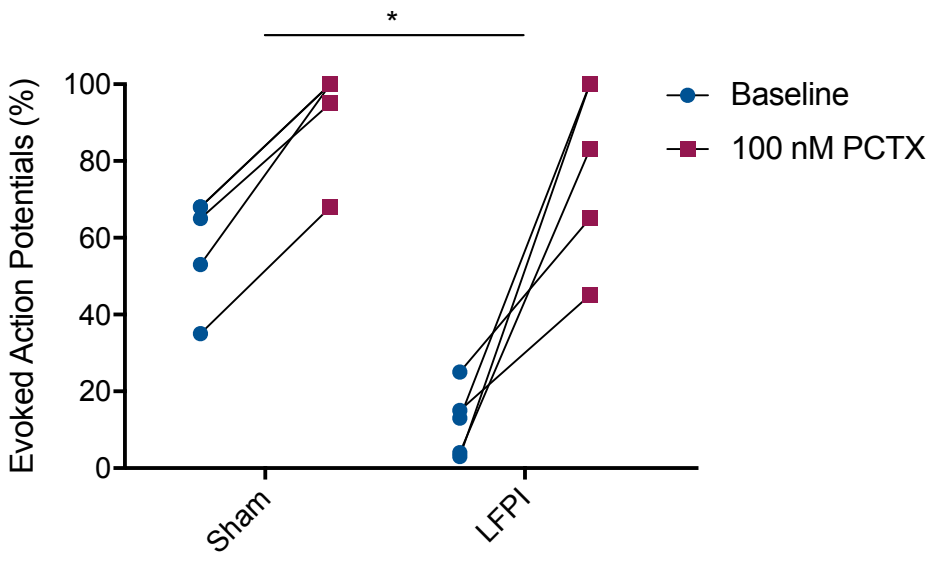

Figure 8. Feed-forward activation of PV-INs is diminished by increased network inhibitory input. Evoked responses for individual cells in sham (left) and LFPI (right) slices during whole-cell current-clamp recordings demonstrate that PV-INs fired less action potentials from perforant path minimal stimulation after LFPI in baseline aCSF (blue circles). After wash-in of the $GABA_A$-receptor antagonist picrotoxin (red squares), sham and LFPI PV-INs had comparable evoked firing responses. Y-axis depicts the percentage of evoked action potentials elicited in response to a sequency of 20 stimulations (i.e., 10 evoked APs in 20 stimulations = 50%), 12 second inter-stimulus intervals. Percent differences in evoked responses for sham (mean ± SEM): 34.8% ± 3.1 (n = 5 cells), and for LFPI (mean ± SEM): 66.6% ± 13.31 (n = 5 cells). *, $p < 0.05$, unpaired t-test.

CHAPTER 4

CONCLUSIONS AND FUTURE DIRECTIONS

The purpose of the work presented in this doctoral thesis is to gain a better understanding of the functional implications and potential mechanisms of neural circuit dysfunction underlying the cognitive symptoms of patients with mild traumatic brain injury (mTBI). Our choice of focus was on the dentate gyrus sub-region of the hippocampus, which acts as a filter or gate of entorhinocortical input to the hippocampus and is involved in cognitive computations such as pattern separation, which play an important role in hippocampal-dependent learning and memory. The dentate gyrus experiences an increased shift in network excitability after experimental TBI. Though dentate hyperexcitability has been known for decades (Cole et al., 2010; Lowenstein et al., 1992; V Santhakumar et al., 2000; Vijayalakshmi Santhakumar et al., 2001; Witgen et al., 2005), the mechanisms which lead to pathological circuit hyper-activation are not well understood.

In Chapter 2, we investigated the functional consequences of dentate network hyperexcitability on hippocampal function. We first established a behavioral deficit in mice after lateral fluid percussion injury (LFPI) in recognizing the displacement of an object in a modified spatial object recognition task (Oliveira et al., 2010). Data from lesion studies demonstrate that the hippocampus is important for spatial novelty detection and specifically that lesions to the dentate gyrus disrupts spatial information processing (Gilbert et al., 2001; Hunsaker et al., 2008; Kesner, 2013a; I. Lee et al., 2005; Morris et al., 2012). We also presented electrophysiological data which showed an association between dysfunctional spatial information processing and network hyperexcitability of the

dentate gyrus. Voltage-sensitive dye imaging revealed the aberrant propagation of depolarization from the dentate gyrus into downstream area CA3 in response to perforant path stimulation in acute brain slices from LFPI animals. To assess if the spread of depolarization had a functional effect on CA3 activity, we measured population spikes in area CA3 pyramidal cell layer in response to upstream perforant path stimulation. Area CA3 population spikes from LFPI animals had significantly higher amplitudes, which was due to increased synaptic efficacy of mossy fiber synaptic transmission rather than recurrent CA3 axon collateral excitation. The results of these experiments provided evidence that the “buck” does not stop at the dentate gyrus in the injured brain, but that propagation of excitation through the dentate gyrus leads to abnormal network excitability in vulnerable downstream hippocampal areas. This demonstrates that disruption in the regulation of cortical input to the hippocampus, via breakdown of the dentate filter function, has consequences in downstream hippocampal circuit function and interhippocampal communication.

In Chapter 3 we shifted the focus of our investigation toward understanding potential mechanisms underlying dentate hyperexcitability. Because previous evidence suggests this is due to a decrease in GABAergic inhibition onto granule cells, we looked at parvalbumin-expressing basket and axo-axonic cells (i.e., PV-INs), which provide robust perisomatic inhibition onto granule cells and are a likely source of reduced inhibition onto these cells. One week after LFPI, selective loss of hilar PV-INs occurs. Passive and active intrinsic membrane properties of surviving PV-INs demonstrated no change after LFPI. When we examined the balance of excitatory-inhibitory synaptic transmission onto PV-INs, we found alterations which suggest that both pre- and post-synaptic mechanisms are affected by TBI. Evoked stimulation experiments revealed that feedforward activation of

PV-INs was significantly reduced after LFPI, and that this reduction was due to a larger influence of local inhibition. Lastly, current-clamp minimal stimulation experiments demonstrated that network inhibition decreases the probability of PV-IN action potential firing, thus demonstrating a functional consequence of posttraumatic alterations in E/I synaptic inputs. The results of this chapter provide evidence for a potential mechanism of reduced granule cell excitability after injury.

The research presented in Chapters 2 and 3 represent a comprehensive examination of dentate gyrus circuit function and its implications after TBI. These data provide further insight that injury-induced E/I imbalance that occurs within the neural circuits underlie behavioral symptoms of injury. Furthermore, these results emphasize the complicated effects of altered E/I balance: alterations in individual neuron populations can have profound effects on the activity of their postsynaptic targets and the downstream output of the circuit. Interestingly, the direction of injury-associated network shifts in excitability (i.e., toward network hyperexcitability or hypoexcitability) are properties of individual microcircuits within anatomical sub-regions. For example, hippocampal area CA1 actually exhibits network hypoexcitability one week after LFPI (D'Ambrosio et al., 1998; Johnson et al., 2014; Reeves et al., 1997; Titus et al., 2013; Witgen et al., 2005). It is possible that the directionality of E/I network shifts represents the mixture of circuit-level pathological and homeostatic mechanisms. As such, pathophysiology may actually provide a better understanding of the normal functioning of neural circuits; by breaking them we can understand how the individual parts work.

So out of all the areas of the brain to study the effects of TBI—why the dentate gyrus? If we think of the simplified analogy of the brain as an electrical circuit board, we can think

of the many anatomical regions and sub-regions as electrical switches, or check points, which control current flow in the circuit. Based on their positioning within the circuit, some switches have more control over circuit output than others. Because of its anatomical location and unidirectional input-output connections, the dentate gyrus represents a crucial 'switch' within the central nervous system. If this check point becomes dysfunctional, it not only affects the sub-region itself, but also has downstream consequences beyond its local circuit connections. Intriguingly, dentate gyrus hyperexcitability is not just a phenomenon that occurs after TBI; it is also present in other disorders with associated cognitive impairments such as epilepsy and Alzheimer's disease (Chin & Scharfman, 2013; Noebels, 2011; Palop et al., 2007). While these pathologies may have different origins and mechanisms of action, the fact that they result in similar dentate circuit dysfunction suggests that the dentate gyrus is a highly vulnerable checkpoint whose network excitability may be easily perturbed.

The theory of the dentate gyrus as a crucial check point on neural communication and excitability within the brain also implies that if hyperexcitability can be fixed, so can cognitive impairments. A study by Kahn and colleagues using a mouse model of epilepsy found that chemogenetic deactivation (i.e., hyperpolarization) of dentate granule cells restored behavioral performance in a hippocampal-dependent spatial object recognition task (Kahn et al., 2016). Future directions of our work would also benefit from optogenetic or chemogenetic investigation of the direct role of PV-INs in dentate hyperexcitability and behavioral performance after TBI. Additionally, our previous work from our laboratory has demonstrated that administration of branched chain amino acids (BCAAs) acutely after injury reversed injury-induced shifts in dentate excitability and hippocampal cognitive impairments (Cole et al., 2010; Elkind et al., 2015). This work has led to an ongoing clinical

trial assessing the efficacy of BCAAs in improving neurocognitive recovery in human mTBI patients. BCAAs, which are important precursors of GABA and glutamate, are thought to restore presynaptic neurotransmitter pools. Currently it is not well understood which populations of neurons, including PV-INs, in the dentate gyrus benefit from BCAA administration. Future investigation of the effects of BCAA treatment on dentate inhibitory interneurons may provide insight into BCAA mechanisms of restoring circuit E/I balance and associated behavior.

Another potential point of future direction is to further investigate the mechanisms of E/I synaptic imbalance onto PV-INs after LFPI, as shown in Chapter 3. There has been relatively little previous work to understand how different interneuron populations, interneuron-interneuron networks, and interneuron-granule cell communication are affected by TBI. To comprehensively survey the posttraumatic landscape within the dentate gyrus, a systematic assessment of individual dentate cell types would be warranted. This would provide important information about how specific populations are disrupted by injury and provide insight into whether these changes reflect homeostatic, compensatory processes or uncontrolled pathophysiology.

Dentate PV-INs as potential therapeutic target

If granule cell firing controls the output of the dentate gyrus, then why bother to indirectly target the inhibitory interneurons that control their firing? It is important to note that GABAergic inhibitory neurons such as PV-INs don't just serve a role in limiting excitation through circuits, but also provide precisely-timed firing that gives rise to oscillatory activity in different frequency bands which are associated with a number of cognitive functions and plasticity in the brain (Buzsáki & Wang, 2012; Cobb et al., 1995; Colgin & Moser,

2010; Kahana, 2006). Therefore, therapeutically targeting PV-IN and GABAergic function via viral technology or precision pharmacology will functionally reintegrate the finely tuned timing of inhibition in the dentate gyrus and restore its role in mediated cognitive behaviors.

The findings of this dissertation work probe a specific, cellular mechanism underlying circuit dysfunction and associated memory impairment after TBI. Specific cellular targets are important for therapeutic translation because they lessen the chance of symptomatic side effects and biological off-target effects. Additionally, PV-INs play an important role in circuits throughout the brain, therefore it is possible that a therapeutic intervention that restores PV-IN function in the dentate gyrus may be beneficial even in circuits with divergent circuit architectures and function. As such, finding specific cellular targets of TBI-induced memory impairment is a promising step toward a translational treatment to restore memory dysfunction and prevent the development of long-term disability following brain injury.

BIBLIOGRAPHY

Acsády, L., Kamondi, A., Sík, A., Freund, T., & Buzsáki, G. (1998). GABAergic cells are the major postsynaptic targets of mossy fibers in the rat hippocampus. *The Journal of Neuroscience : The Official Journal of the Society for Neuroscience*, *18*(9), 3386–403.

Adams, J. H., Doyle, D., Ford, I., Gennarelli, T. A., Graham, D. I., & McLellan, D. R. (1989). Diffuse axonal injury in head injury: definition, diagnosis and grading. *Histopathology*, *15*(1), 49–59.

Aiguo Wu, Zhe Ying, & Gomez-Pinilla, F. (2009). Vitamin E protects against oxidative damage and learning disability after mild traumatic brain injury in rats. *Neurorehabilitation and Neural Repair*, *24*(3), 290–8.

Alger, B. E., & Teyler, T. J. (1976). Long-term and short-term plasticity in the CA1, CA3, and dentate regions of the rat hippocampal slice. *Brain Research*, *110*(3), 463–480.

Amaral, D. G., & Kurz, J. (1985). An analysis of the origins of the cholinergic and noncholinergic septal projections to the hippocampal formation of the rat. *Journal of Comparative Neurology*.

Amaral, D. G., Rempel-Clower, N. L., Zola, S. M., & Squire, L. R. (1996). Three cases of enduring memory impairment after bilateral damage limited to the hippocampal formation. *J Neurosci*, *16*(16), 5233–5255.

Amaral, D. G., Scharfman, H. E., & Lavenex, P. (2007). The dentate gyrus: fundamental neuroanatomical organization (dentate gyrus for dummies). *Progress in Brain Research*.

Amaral, D. G., & Witter, M. P. (1989). The three-dimensional organization of the hippocampal formation: A review of anatomical data. *Neuroscience*.

Amrein, I., Slomianka, L., & Lipp, H. P. (2004). Granule cell number, cell death and cell proliferation in the dentate gyrus of wild-living rodents. *European Journal of Neuroscience*.

Andersen, P., Holmqvist, B., & Voorhoeve, P. E. (1966). Entorhinal Activation of Dentate Granule Cells. *Acta Physiologica Scandinavica*, *66*(4), 448–460.

Anderson, W. W., Swartzwelder, H. S., & Wilson, W. A. (1987). The NMDA receptor antagonist 2-

amino-5-phosphonovalerate blocks stimulus train-induced epileptogenesis but not epileptiform bursting in the rat hippocampal slice. *Journal of Neurophysiology*, *57*(1), 1–21.

Ang, C. W., Carlson, G. C., & Coulter, D. a. (2006). Massive and specific dysregulation of direct cortical input to the hippocampus in temporal lobe epilepsy. *The Journal of Neuroscience : The Official Journal of the Society for Neuroscience*, *26*(46), 11850–11856.

Armstrong, C., & Soltesz, I. (2012). Basket cell dichotomy in microcircuit function. *Journal of Physiology*.

Bakker, A., Kirwan, C. B., Miller, M., & Stark, C. E. L. (2008). Pattern separation in the human hippocampal CA3 and dentate gyrus. *Science (New York, N.Y.)*, *319*(5870), 1640–2.

Bakst, I., Avendano, C., Morrison, J. H., & Amaral, D. G. (1986). An experimental analysis of the origins of somatostatin-like immunoreactivity in the dentate gyrus of the rat. *The Journal of Neuroscience : The Official Journal of the Society for Neuroscience*.

Baldwin, S. A., Gibson, T., Callihan, C. T., Sullivan, P. G., Palmer, E., & Scheff, S. W. (1997). Neuronal cell loss in the CA3 subfield of the hippocampus following cortical contusion utilizing the optical disector method for cell counting. *Journal of Neurotrauma*, *14*(6), 385–98.

Barker, G. R. I., Bird, F., Alexander, V., & Warburton, E. C. (2007). Recognition Memory for Objects, Place, and Temporal Order: A Disconnection Analysis of the Role of the Medial Prefrontal Cortex and Perirhinal Cortex TL - 27. *The Journal of Neuroscience*, *27 VN-r*(11), 2948–2957.

Barker, G. R. I., & Warburton, E. C. (2011). When Is the Hippocampus Involved in Recognition Memory? *Journal of Neuroscience*, *31*(29), 10721–10731.

Beamer, M., Tummala, S. R., Gullotti, D., Kopil, K., Gorka, S., Ted Abel, … Meaney, D. F. (2016). Primary blast injury causes cognitive impairments and hippocampal circuit alterations. *Experimental Neurology*, *283*, 16–28.

Bejanin, A., Viard, A., Chételat, G., Clarys, D., Bernard, F., Pélerin, A., … Desgranges, B. (2012). When Higher Activations Reflect Lower Deactivations: A PET Study in Alzheimer's Disease during Encoding and Retrieval in Episodic Memory. *Frontiers in Human Neuroscience*, *6*,

107.

Ben-Ari, Y., & Gho, M. (1988). Long-lasting modification of the synaptic properties of rat CA3 hippocampal neurones induced by kainic acid. *The Journal of Physiology*, *404*, 365–84.

Berger, T. W., Semple-Rowland, S., & Bassett, J. L. (1981). Hippocampal polymorph neurons are the cells of origin for ipsilateral association and commissural afferents to the dentate gyrus. *Brain Research*, *224*(1), 329–36.

Bohbot, V. D., Allen, J. J. b., & Nadel, L. (2000). Memory Deficits Characterized by Patterns of Lesions to the Hippocampus and Parahippocampal Cortex. *Annals of the New York Academy of Sciences*, *911*(1), 355–368.

Bolton, A. N., & Saatman, K. E. (2014). Regional neurodegeneration and gliosis are amplified by mild traumatic brain injury repeated at 24-hour intervals. *Journal of Neuropathology and Experimental Neurology*, *73*(10), 933–47.

Bonislawski, D. P., Schwarzbach, E. P., & Cohen, A. S. (2007). Brain injury impairs dentate gyrus inhibitory efficacy. *Neurobiology of Disease*, *25*(1), 163–169.

Bourgeois, E. B., Johnson, B. N., McCoy, A. J., Trippa, L., Cohen, A. S., & Marsh, E. D. (2014). A toolbox for spatiotemporal analysis of voltage-sensitive dye imaging data in brain slices. *PLoS ONE*, *9*(9).

Boychuk, J. A., Butler, C. R., Halmos, K. C., & Smith, B. N. (2016). Enduring changes in tonic GABAA receptor signaling in dentate granule cells after controlled cortical impact brain injury in mice. *Experimental Neurology*, *277*, 178–189.

Buckmaster, P. S., Wenzel, H. J., Kunkel, D. D., & Schwartzkroin, P. A. (1996). Axon arbors and synaptic connections of hippocampal mossy cells in the rat in vivo. *The Journal of Comparative Neurology*, *366*(2), 271–92.

Bussey, T. J., Duck, J., Muir, J. L., & Aggleton, J. P. (2000). Distinct patterns of behavioural impairments resulting from fornix transection or neurotoxic lesions of the perirhinal and postrhinal cortices in the rat. *Behavioural Brain Research*, *111*(1–2), 187–202.

Butler, C. R., Boychuk, J. A., & Smith, B. N. (2017). Brain Injury-Induced Synaptic Reorganization in Hilar Inhibitory Neurons Is Differentially Suppressed by Rapamycin. *Eneuro*.

Butler, C. R., Boychuk, J. a, & Smith, B. N. (2015). Effects of Rapamycin Treatment on Neurogenesis and Synaptic Reorganization in the Dentate Gyrus after Controlled Cortical Impact Injury in Mice. *Frontiers in Systems Neuroscience*, *9*(November), 163.

Buzsáki, G., & Wang, X.-J. (2012). Mechanisms of Gamma Oscillations. *Annual Review of Neuroscience*.

CARBONELL, W. S., MARIS, D. O., McCALL, T., & GRADY, M. S. (1998). Adaptation of the Fluid Percussion Injury Model to the Mouse. *Journal of Neurotrauma*.

Card, J. P., Santone, D. J., Gluhovsky, M. Y., & Adelson, P. D. (2005). Plastic reorganization of hippocampal and neocortical circuitry in experimental traumatic brain injury in the immature rat. *Journal of Neurotrauma*, *22*(9), 989–1002.

Cave, C. B., & Squire, L. R. (1991). Equivalent impairment of spatial and nonspatial memory following damage to the human hippocampus. *Hippocampus*, *1*(3), 329–340.

Chawla, M. K., Guzowski, J. F., Ramirez-Amaya, V., Lipa, P., Hoffman, K. L., Marriott, L. K., … Barnes, C. A. (2005). Sparse, environmentally selective expression of Arc RNA in the upper blade of the rodent fascia dentata by brief spatial experience. *Hippocampus*.

Chen, Y., Constantini, S., Trembovler, V., Weinstock, M., & Shohami, E. (1996). An experimental model of closed head injury in mice: pathophysiology, histopathology, and cognitive deficits. *Journal of Neurotrauma*, *13*(10), 557–568.

Chen, Y., Mao, H., Yang, K. H., Abel, T., & Meaney, D. F. (2014). A modified controlled cortical impact technique to model mild traumatic brain injury mechanics in mice. *Frontiers in Neurology*, *5 JUN*.

Cherubini, E., Neuman, R., Rovira, C., & Ben Ari, Y. (1988). Epileptogenic properties of the mast cell degranulating peptide in CA3 hippocampal neurones. *Brain Research*, *445*(1), 91–100.

Chin, J., & Scharfman, H. E. (2013). Shared cognitive and behavioral impairments in epilepsy and Alzheimer's disease and potential underlying mechanisms. *Epilepsy & Behavior*, *26*(3), 343–351.

Cobb, S. R., Buhl, E. H., Halasy, K., Paulsen, O., & Somogyi, P. (1995). Synchronization of neuronal activity in hippocampus by individual GABAergic interneurons. *Nature*.

Cole, J. T., Mitala, C. M., Kundu, S., Verma, A., Elkind, J. A., Nissim, I., & Cohen, A. S. (2010). Dietary branched chain amino acids ameliorate injury-induced cognitive impairment. *Proceedings of the National Academy of Sciences of the United States of America*, *107*(1), 366–71.

Colgin, L. L., & Moser, E. I. (2010). Gamma Oscillations in the Hippocampus. *Physiology*.

Coronado, V. G., McGuire, L. C., Sarmiento, K., Bell, J., Lionbarger, M. R., Jones, C. D., … Xu, L. (2012). Trends in Traumatic Brain Injury in the U.S. and the public health response: 1995-2009. *Journal of Safety Research*.

Coulter, D. A., & Carlson, G. C. (2007). Functional regulation of the dentate gyrus by GABA-mediated inhibition. *Progress in Brain Research*.

D'Ambrosio, R., Maris, D. O., Grady, M. S., Winn, H. R., & Janigro, D. (1998). Selective loss of hippocampal long-term potentiation, but not depression, following fluid percussion injury. *Brain Research*, *786*(1–2), 64–79.

Darwish, H., Mahmood, A., Schallert, T., Chopp, M., & Therrien, B. (2014). Simvastatin and environmental enrichment effect on recognition and temporal order memory after mild-to-moderate traumatic brain injury. *Brain Inj*, *28*(2), 1362–301.

Deller, T., Nitsch, R., & Frotscher, M. (1995). Phaseolus vulgaris -leucoagglutinin tracing of commissural fibers to the rat dentate gyrus: Evidence for a previously unknown commissural projection to the outer molecular layer. *The Journal of Comparative Neurology*, *352*(1), 55–68.

Dengler, C. G., & Coulter, D. A. (2016). Normal and epilepsy-associated pathologic function of the dentate gyrus. In *Progress in brain research* (Vol. 226, pp. 155–178).

Dent, J. A., Galvin, N. J., Stanfield, B. B., & Maxwell Cowan, W. (1983). The mode of termination of the hypothalamic projection to the dentate gyrus: an EM autoradiographic study. *Brain Research*.

Deweer, B., Pillon, B., Pochon, J. B., & Dubois, B. (2001). Is the HM story only a "remote memory"? Some facts about hippocampus and memory in humans. In *Behavioural Brain Research* (Vol. 127, pp. 209–224).

Dixon, C. E., Lyeth, B. G., Povlishock, J. T., Findling, R. L., Hamm, R. J., Marmarou, a, … Hayes, R. L. (1987). A fluid percussion model of experimental brain injury in the rat. *Journal of Neurosurgery*, *67*(1), 110–119.

Eakin, K., & Miller, J. P. (2012). Mild traumatic brain injury is associated with impaired hippocampal spatiotemporal representation in the absence of histological changes. *Journal of Neurotrauma*, *29*(6), 1180–7.

Ekolle Ndode-Ekane, X., Kharatishvili, I., & Pitkänen, A. (2017). Unfolded Maps for Quantitative Analysis of Cortical Lesion Location and Extent after Traumatic Brain Injury. *Journal of Neurotrauma*, *34*(2), 459–474.

Elkind, J. A., Lim, M. M., Johnson, B. N., Palmer, C. P., Putnam, B. J., Kirschen, M. P., & Cohen, A. S. (2015). Efficacy, Dosage, and Duration of Action of Branched Chain Amino Acid Therapy for Traumatic Brain Injury. *Frontiers in Neurology*, *6*, 73.

Ennaceur, A., & Aggleton, J. P. (1997). The effects of neurotoxic lesions of the perirhinal cortex combined to fornix transection on object recognition memory in the rat. *Behavioural Brain Research*, *88*(2), 181–93.

Ewell, L. A., & Jones, M. V. (2010). Frequency-Tuned Distribution of Inhibition in the Dentate Gyrus. *Journal of Neuroscience*.

Faul, F., ErdFelder, E., Lang, A.-G., & Buchner, A. (2007). G*Power 3.1 manual. *Behavioral Research Methods*, *39*(2), 175–191.

Fedor, M., Berman, R. F., Muizelaar, J. P., & Lyeth, B. G. (2010). Hippocampal θ dysfunction after lateral fluid percussion injury. *Journal of Neurotrauma*, *27*(9), 1605–15.

Folweiler, K. A., Samuel, S., Metheny, H. E., & Cohen, A. S. (2018). Diminished dentate gyrus filtering of cortical input leads to enhanced area ca3 excitability after mild traumatic brain injury. *Journal of Neurotrauma*, *35*(11).

Fredj, N. Ben, & Burrone, J. (2009). A resting pool of vesicles is responsible for spontaneous vesicle fusion at the synapse. *Nature Neuroscience*.

Freund, T. F., & Buzsáki, G. (1996). Interneurons of the hippocampus. *Hippocampus*, *6*(4), 347–470.

Fricke, R. a, & Prince, D. a. (1984). Electrophysiology of dentate gyrus granule cells. *Journal of Neurophysiology*, *51*(2), 195–209.

Frotscher, M. (1985). Mossy fibres form synapses with identified pyramidal basket cells in the CA3 region of the guinea-pig hippocampus: a combined Golgi-electron microscope study. *Journal of Neurocytology*, *14*(2), 245–59.

Frotscher, M., Seress, L., Schwerdtfeger, W. K., & Buhl, E. (1991). The mossy cells of the fascia dentata: a comparative study of their fine structure and synaptic connections in rodents and primates. *The Journal of Comparative Neurology*, *312*(1), 145–63.

Fuchs, E. C., Zivkovic, A. R., Cunningham, M. O., Middleton, S., LeBeau, F. E. N., Bannerman, D. M., … Monyer, H. (2007). Recruitment of Parvalbumin-Positive Interneurons Determines Hippocampal Function and Associated Behavior. *Neuron*.

Gilbert, P. E., Kesner, R. P., & Lee, I. (2001). Dissociating hippocampal subregions: A double dissociation between dentate gyrus and CA1. *Hippocampus*, *11*(6), 626–636.

Golarai, G., Greenwood, a C., Feeney, D. M., & Connor, J. a. (2001). Physiological and structural evidence for hippocampal involvement in persistent seizure susceptibility after traumatic brain injury. *The Journal of Neuroscience : The Official Journal of the Society for Neuroscience*, *21*(21), 8523–8537.

Goodman, J. H., & Sloviter, R. S. (1992). Evidence for commissurally projecting parvalbumin-immunoreactive basket cells in the dentate gyrus of the rat. *Hippocampus*, *2*(1), 13–21.

Grady MS, L. A. . (1995). Management of acute head injury. In A. Lam (Ed.), *Anesthetic Management of Head Injury.* (pp. 87–100). New York: McGraw-Hill.

Graham, D. I., Adams, J. H., Nicoll, J. A. R., Maxwell, W. L., & Gennarelli, T. A. (1995). The Nature, Distribution and Causes of Traumatic Brain Injury. *Brain Pathology*, *5*(4), 397–406.

Griesemer, D., & Mautes, A. M. (2007). Closed head injury causes hyperexcitability in rat hippocampal CA1 but not in CA3 pyramidal cells. *Journal of Neurotrauma*, *24*(12), 1823–32.

Gupta, A., Elgammal, F. S., Proddutur, A., Shah, S., & Santhakumar, V. (2012). Decrease in Tonic Inhibition Contributes to Increase in Dentate Semilunar Granule Cell Excitability after Brain Injury. *Journal of Neuroscience*, *32*(7), 2523–2537.

Gurkoff, G. G., Gahan, J. D., Ghiasvand, R. T., Hunsaker, M. R., Van, K., Feng, J.-F., … Folkerts, M. M. (2013). Evaluation of metric, topological, and temporal ordering memory tasks after lateral fluid percussion injury. *Journal of Neurotrauma*, *30*(4), 292–300.

Halasy, K., & Somogyi, P. (1993). Subdivisions in the multiple GABAergic innervation of granule cells in the dentate gyrus of the rat hippocampus. *The European Journal of Neuroscience*, *5*(5), 411–429.

Han, Z.-S., Buhl, E. H., Lorinczi, Z., & Somogyi, P. (1993). A High Degree of Spatial Selectivity in the Axonal and Dendritic Domains of Physiologically Identified Local-circuit Neurons in the Dentate Gyrus of the Rat Hippocampus. *European Journal of Neuroscience*, *5*, 395–410.

Hannesson, D. K. (2004). Interaction between Perirhinal and Medial Prefrontal Cortex Is Required for Temporal Order But Not Recognition Memory for Objects in Rats. *Journal of Neuroscience*, *24*(19), 4596–4604.

Hashimotodani, Y., Nasrallah, K., Jensen, K. R., Chávez, A. E., Carrera, D., & Castillo, P. E. (2017). LTP at Hilar Mossy Cell-Dentate Granule Cell Synapses Modulates Dentate Gyrus Output by Increasing Excitation/Inhibition Balance. *Neuron*, *95*(4), 928–943.e3.

Hasselmo, M. E., Schnell, E., & Barkai, E. (1995). Dynamics of learning and recall at excitatory recurrent synapses and cholinergic modulation in rat hippocampal region CA3. *The Journal of Neuroscience : The Official Journal of the Society for Neuroscience*, *15*(7 Pt 2), 5249–5262.

Heinemann, U., Beck, H., Dreier, J. P., Ficker, E., Stabel, J., & Zhang, C. L. (1992). The dentate gyrus as a regulated gate for the propagation of epileptiform activity. *Epilepsy Research. Supplement*, *7*, 273–80.

Henze, D. A., Urban, N. N., & Barrionuevo, G. (2000). The multifarious hippocampal mossy fiber pathway: A review. *Neuroscience*, *98*(3), 407–427.

Henze, D. a, Wittner, L., & Buzsáki, G. (2002). Single granule cells reliably discharge targets in the hippocampal CA3 network in vivo. *Nature Neuroscience*, *5*(8), 790–795.

Hester, M. S., & Danzer, S. C. (2013). Accumulation of abnormal adult-generated hippocampal granule cells predicts seizure frequency and severity. *The Journal of Neuroscience : The*

Official Journal of the Society for Neuroscience, *33*(21), 8926–36.

Houser, C. R. (2007). Interneurons of the dentate gyrus: an overview of cell types, terminal fields and neurochemical identity. *Progress in Brain Research*.

Howard, A. L., Neu, A., Morgan, R. J., Echegoyen, J. C., & Soltesz, I. (2007). Opposing modifications in intrinsic currents and synaptic inputs in post-traumatic mossy cells: evidence for single-cell homeostasis in a hyperexcitable network. *Journal of Neurophysiology*, *97*(3), 2394–409.

Hsu, D. (2007). The dentate gyrus as a filter or gate: a look back and a look ahead. *Progress in Brain Research*, *163*, 601–613.

Hu, H., Gan, J., & Jonas, P. (2014). Fast-spiking, parvalbumin+ GABAergic interneurons: From cellular design to microcircuit function. *Science*, *345*(6196), 1255263–1255263.

Hunsaker, M. R., Rosenberg, J. S., & Kesner, R. P. (2008). The role of the dentate gyrus, CA3a,b, and CA3c for detecting spatial and environmental novelty. *Hippocampus*, *18*(10), 1064–1073.

Hunt, R. F., Scheff, S. W., & Smith, B. N. (2009). Posttraumatic epilepsy after controlled cortical impact injury in mice. *Experimental Neurology*, *215*(2), 243–252.

Hunt, R. F., Scheff, S. W., & Smith, B. N. (2010). Regionally localized recurrent excitation in the dentate gyrus of a cortical contusion model of posttraumatic epilepsy. *Journal of Neurophysiology*, *103*(3), 1490–500.

Hunt, R. F., Scheff, S. W., & Smith, B. N. (2011). Synaptic reorganization of inhibitory hilar interneuron circuitry after traumatic brain injury in mice. *The Journal of Neuroscience : The Official Journal of the Society for Neuroscience*, *31*(18), 6880–6890.

Hylin, M. J., Orsi, S. a, Zhao, J., Bockhorst, K., Perez, A., Moore, A. N., & Dash, P. K. (2013). Behavioral and histopathological alterations resulting from mild fluid percussion injury. *Journal of Neurotrauma*, *30*(9), 702–15.

Iwata, A., Stys, P. K., Wolf, J. A., Chen, X., Taylor, A. G., Meaney, D. F., & Smith, D. H. (2004). Traumatic Axonal Injury Induces Proteolytic Cleavage of the Voltage-Gated Sodium Channels Modulated by Tetrodotoxin and Protease Inhibitors, *24*(19), 4605–4613.

Johnson, B. N., Palmer, C. P., Bourgeois, E. B., Elkind, J. A., Putnam, B. J., & Cohen, A. S. (2014). Augmented Inhibition from Cannabinoid-Sensitive Interneurons Diminishes CA1 Output after Traumatic Brain Injury. *Frontiers in Cellular Neuroscience*, *8*(December), 435.

Josselyn, S. A., Köhler, S., & Frankland, P. W. (2015). Finding the engram. *Nature Reviews Neuroscience*, *16*(9), 521–534.

Jung, M. W., & McNaughton, B. L. (1993). Spatial selectivity of unit activity in the hippocampal granular layer. *Hippocampus*.

Kahana, M. J. (2006). The Cognitive Correlates of Human Brain Oscillations. *Journal of Neuroscience*.

Kahn, J., Yue, C., Takano, H., & Coulter, D. (2016). Dentate granule cell hyperactivity contributes to cognitive comorbidities in temporal lobe epilepsy. In *The 46th Annual Meeting of the Society for Neuroscience*.

Katona, I., Acsády, L., & Freund, T. F. (1999). Postsynaptic targets of somatostatinimmunoreactive interneurons in the rat hippocampus. *Neuroscience*.

Kawaguchi, Y., & Kubota, Y. (1997). GABAergic cell subtypes and their synaptic connections in rat frontal cortex. *Cerebral Cortex (New York, N.Y. : 1991)*, *7*(6), 476–86.

Kay, T., Harrington, D. E., Adams, R., Anderson, T., Berrol, S., Cicerone, K., … Malec, J. (1993). American Congress of Rehabilitation Medicine Mild Traumatic Brain Injury Committee of the Head Injury Interdisciplinary Special Interest Group. Definition of mild traumatic brain injury. *Journal of Head Trauma Rehabilitation*.

Kempermann, G., & Gage, F. H. (2000). Neurogenesis in the adult hippocampus. *Neural Transplantation in Neurodegenerative Disease: Current Status and New Directions*, *231*(12), 220–235.

Kesner, R. P. (2013a). An analysis of the dentate gyrus function. *Behavioural Brain Research*.

Kesner, R. P. (2013b). Role of the hippocampus in mediating interference as measured by pattern separation processes. *Behavioural Processes*, *93*, 148–154.

Kesner, R. P., & Ragozzino, M. E. (2003). The role of the prefrontal cortex in object-place learning: a test of the attribute specificity model. *Behavioural Brain Research*, *146*(1–2),

159–65.

Kesner, R. P., Taylor, J. O., Hoge, J., & Andy, F. (2015). Role of the dentate gyrus in mediating object-spatial configuration recognition. *Neurobiology of Learning and Memory*, *118*, 42–48.

Kim, D., Nishida, H., An, S. Y., Shetty, A. K., Bartosh, T. J., & Prockop, D. J. (2016). Chromatographically isolated CD63 $^{+}$ CD81 $^{+}$ extracellular vesicles from mesenchymal stromal cells rescue cognitive impairments after TBI. *Proceedings of the National Academy of Sciences*, *113*(1), 170–175.

Koster, R., Chadwick, M. J., Chen, Y., Berron, D., Banino, A., Düzel, E., … Kumaran, D. (2018). Big-Loop Recurrence within the Hippocampal System Supports Integration of Information across Episodes. *Neuron*, *99*(6), 1342–1354.e6.

Kraushaar, U., & Jonas, P. (2000). Efficacy and stability of quantal GABA release at a hippocampal interneuron-principal neuron synapse. *The Journal of Neuroscience : The Official Journal of the Society for Neuroscience*.

Krook-Magnuson, E., Armstrong, C., Bui, A., Lew, S., Oijala, M., & Soltesz, I. (2015). *In vivo* evaluation of the dentate gate theory in epilepsy. *The Journal of Physiology*, *593*(10), 2379–2388.

Langlois, J. A., Rutland-Brown, W., Wald, M. M., Li, N., Yang, Y., Glover, D. P., … Shahlaie, K. (2015). Decrease in Tonic Inhibition Contributes to Increase in Dentate Semilunar Granule Cell Excitability after Brain Injury. *Journal of Neurotrauma*, *32*(1), 1–13.

Langston, R. F., & Wood, E. R. (2010). Associative recognition and the hippocampus: Differential effects of hippocampal lesions on object-place, object-context and object-place-context memory. *Hippocampus*, *20*(10), 1139–1153.

Larimer, P., & Strowbridge, B. W. (2010). Representing information in cell assemblies: Persistent activity mediated by semilunar granule cells. *Nature Neuroscience*.

Lee, D. J., Gurkoff, G. G., Izadi, A., Seidl, S. E., Echeverri, A., Melnik, M., … Shahlaie, K. (2015). Septohippocampal Neuromodulation Improves Cognition after Traumatic Brain Injury. *Journal of Neurotrauma*, *11*, 150902125930001.

Lee, I., Hunsaker, M. R., & Kesner, R. P. (2005). The Role of Hippocampal Subregions in

Detecting Spatial Novelty. *Behavioral Neuroscience*, *119*(1), 145–153.

Lee, I., & Kesner, R. P. (2004). Differential contributions of dorsal hippocampal subregions to memory acquisition and retrieval in contextual fear-conditioning. *Hippocampus*, *14*(3), 301–10.

Leranth, C., Malcolm, A. J., & Frotscher, M. (1990). Afferent and efferent synaptic conncetions sof somatostatin-immunoreactive neurons in the rat fascia dentata. *Journal of Comparative Neurology*.

Leutgeb, J. K., Leutgeb, S., Moser, M.-B., & Moser, E. I. (2007a). Pattern separation in the dentate gyrus and CA3 of the hippocampus. *Science (New York, N.Y.)*, *315*(5814), 961–6.

Leutgeb, J. K., Leutgeb, S., Moser, M.-B., & Moser, E. I. (2007b). Pattern Separation in the Dentate Gyrus and CA3 of the Hippocampus. *Science*, *315*, 961–966.

Li, Y., Stam, F. J., Aimone, J. B., Goulding, M., Callaway, E. M., & Gage, F. H. (2013). Molecular layer perforant path-associated cells contribute to feed-forward inhibition in the adult dentate gyrus. *Proceedings of the National Academy of Sciences*, *110*(22), 9106–9111.

Lothman, E. W., Stringer, J. L., & Bertram, E. H. (1992). The dentate gyrus as a control point for seizures in the hippocampus and beyond. *Epilepsy Research. Supplement*, *7*, 301–13.

Lowenstein, D. H., Thomas, M. J., Smith, D. H., & McIntosh, T. K. (1992). Selective vulnerability of dentate hilar neurons following traumatic brain injury: a potential mechanistic link between head trauma and disorders of the hippocampus. *The Journal of Neuroscience : The Official Journal of the Society for Neuroscience*, *12*(12), 4846–4853.

Lübke, J., Deller, T., & Frotscher, M. (1997). Septal innervation of mossy cells in the hilus of the rat dentate gyrus: An anterograde tracing and intracellular labeling study. *Experimental Brain Research*.

Maglóczky, Z., Acsády, L., & Freund, T. F. (1994). Principal cells are the postsynaptic targets of supramammillary afferents in the hippocampus of the rat. *Hippocampus*.

Marr, D. (1971). Simple Memory: A Theory for Archicortex. *Source: Philosophical Transactions of the Royal Society of London. Series B, Biological Sciences*, *262*(841), 23–81.

Marucci, G., Rubboli, G., & Giulioni, M. (n.d.). Role of dentate gyrus alterations in mesial temporal

sclerosis. *Clinical Neuropathology*, *29*(1), 32–5.

Mathew, S. S., Pozzo-Miller, L., & Hablitz, J. J. (2008). Kainate Modulates Presynaptic GABA Release from Two Vesicle Pools. *Journal of Neuroscience*, *28*(3), 725–731.

McHugh, T. J., Jones, M. W., Quinn, J. J., Balthasar, N., Coppari, R., Elmquist, J. K., … Tonegawa, S. (2007). Dentate gyrus NMDA receptors mediate rapid pattern separation in the hippocampal network. *Science (New York, N.Y.)*, *317*(5834), 94–9.

McIntosh, T. K., Vink, R., Noble, L., Yamakami, I., Fernyak, S., Soares, H., & Faden, A. L. (1989). Traumatic brain injury in the rat: Characterization of a lateral fluid-percussion model. *Neuroscience*, *28*(1), 233–244.

McNaughton, B. L., & Morris, R. G. M. (1987). Hippocampal synaptic enhancement and information storage within a distributed memory system. *Trends in Neurosciences*.

Miller, L. a, Lai, R., & Munoz, D. G. (1998). Contributions of the entorhinal cortex, amygdala and hippocampus to human memory. *Neuropsychologia*, *36*(11), 1247–1256.

Milman, A., Rosenberg, A., Weizman, R., & Pick, C. G. (2005). Mild traumatic brain injury induces persistent cognitive deficits and behavioral disturbances in mice. *Journal of Neurotrauma*, *22*(9), 1003–10.

Moore, R. Y., & Halaris, A. E. (1975). Hippocampal innervation by serotonin neurons of the midbrain raphe in the rat. *Journal of Comparative Neurology*.

Morris, A. M., Churchwell, J. C., Kesner, R. P., & Gilbert, P. E. (2012). Selective lesions of the dentate gyrus produce disruptions in place learning for adjacent spatial locations. *Neurobiology of Learning and Memory*, *97*(3), 326–331.

Moser, E. I., Kropff, E., & Moser, M.-B. (2008). Place Cells, Grid Cells, and the Brain's Spatial Representation System. *Annual Review of Neuroscience*.

Mtchedlishvili, Z., Lepsveridze, E., Xu, H., Kharlamov, E. A., Lu, B., & Kelly, K. M. (2010). Increase of GABAA receptor-mediated tonic inhibition in dentate granule cells after traumatic brain injury. *Neurobiology of Disease*, *38*(3), 464–475.

Nakashiba, T., Cushman, J. D., Pelkey, K. A., Renaudineau, S., Buhl, D. L., McHugh, T. J., … Tonegawa, S. (2012). Young dentate granule cells mediate pattern separation, whereas old

granule cells facilitate pattern completion. *Cell*, *149*(1), 188–201.

Nenov, M. N., Laezza, F., Haidacher, S. J., Zhao, Y., Sadygov, R. G., Starkey, J. M., … Denner, L. (2014). Cognitive enhancing treatment with a PPARγ agonist normalizes dentate granule cell presynaptic function in Tg2576 APP mice. *The Journal of Neuroscience : The Official Journal of the Society for Neuroscience*, *34*(3), 1028–36.

Neuberger, E. J., Abdul Wahab, R., Jayakumar, A., Pfister, B. J., & Santhakumar, V. (2014). Distinct effect of impact rise times on immediate and early neuropathology after brain injury in juvenile rats. *Journal of Neuroscience Research*, *92*(10), 1350–1361.

Nicholl, J., & LaFrance, W. C. (2009). Neuropsychiatric sequelae of traumatic brain injury. *Seminars in Neurology*.

Nichols, J., Bjorklund, G. R., Newbern, J., & Anderson, T. (2018). Parvalbumin fast-spiking interneurons are selectively altered by paediatric traumatic brain injury. *The Journal of Physiology*, *596*(7), 1277–1293.

Nicoll, Schmitz, Nicoll, R. A., & Schmitz, D. (2005). Synaptic plasticity at hippocampal mossy fibre synapses. *Nature Reviews Neuroscience*, *6*(11), 863–876.

Nitz, D., & Mcnaughton, B. (2004). Interneurons During Exploration of Novel Environments Differential Modulation of CA1 and Dentate Gyrus Differential Modulation of CA1 and Dentate Gyrus Interneurons During Exploration of Novel Environments. *J Neurophysiol*, *91*, 863–872.

Noebels, J. (2011). A perfect storm: Converging paths of epilepsy and Alzheimer's dementia intersect in the hippocampal formation. *Epilepsia*, *52*, 39–46.

O'Reilly, R. C., & McClelland, J. L. (1994). Hippocampal conjunctive encoding, storage, and recall: Avoiding a trade-off. *Hippocampus*, *4*(6), 661–682.

Oliveira, A. M. M., Hawk, J. D., Abel, T., & Havekes, R. (2010). Post-training reversible inactivation of the hippocampus enhances novel object recognition memory. *Learning & Memory (Cold Spring Harbor, N.Y.)*, *17*(3), 155–60.

Palmer, C. P., Metheny, H. E., Elkind, J. A., & Cohen, A. S. (2016). Diminished amygdala activation and behavioral threat response following traumatic brain injury. *Experimental*

Neurology, *277*, 215–226.

Palop, J. J., Chin, J., Roberson, E. D., Wang, J., Thwin, M. T., Bien-Ly, N., … Mucke, L. (2007). Aberrant Excitatory Neuronal Activity and Compensatory Remodeling of Inhibitory Hippocampal Circuits in Mouse Models of Alzheimer's Disease. *Neuron*, *55*(5), 697–711.

Patel, T. P., Gullotti, D. M., Hernandez, P., O'Brien, W. T., Capehart, B. P., Morrison, B., … Meaney, D. F. (2014). An open-source toolbox for automated phenotyping of mice in behavioral tasks. *Frontiers in Behavioral Neuroscience*, *8*, 349.

Paterno, R., Folweiler, K. A., & Cohen, A. S. (2017). Pathophysiology and Treatment of Memory Dysfunction After Traumatic Brain Injury. *Current Neurology and Neuroscience Reports*, *17*(7), 52.

Pause, B. M., Zlomuzica, A., Kinugawa, K., Mariani, J., Pietrowsky, R., & Dere, E. (2013). Perspectives on episodic-like and episodic memory. *Frontiers in Behavioral Neuroscience*, *7*(April), 33.

Pavlov, I., Huusko, N., Drexel, M., Kirchmair, E., Sperk, G., Pitkänen, A., & Walker, M. C. (2011). Progressive loss of phasic, but not tonic, GABAA receptor-mediated inhibition in dentate granule cells in a model of post-traumatic epilepsy in rats. *Neuroscience*, *194*, 208–219.

Pickel, V. M., Segal, M., & Bloom, F. E. (1974). A radioautographic study of the efferent pathways of the nucleus locus coeruleus. *Journal of Comparative Neurology*.

Pierce, J. E. S., Smith, D. H., Trojanowski, J. Q., & McIntosh, T. K. (1998). Enduring cognitive, neurobehavioral and histopathological changes persist for up to one year following severe experimental brain injury in rats. *Neuroscience*, *87*(2), 359–369.

Prince, C., & Bruhns, M. (2017). Evaluation and Treatment of Mild Traumatic Brain Injury: The Role of Neuropsychology. *Brain Sciences*.

Putcha, D., Brickhouse, M., O'Keefe, K., Sullivan, C., Rentz, D., Marshall, G., … Sperling, R. (2011). Hippocampal hyperactivation associated with cortical thinning in Alzheimer's disease signature regions in non-demented elderly adults. *The Journal of Neuroscience : The Official Journal of the Society for Neuroscience*, *31*(48), 17680–8.

Reed, J. M., & Squire, L. R. (1997). Impaired recognition memory in patients with lesions limited

to the hippocampal formation. *Behav Neurosci*, *111*(4), 667–675.

Reeves, T. M., Lyeth, B. G., Phillips, L. L., Hamm, R. J., & Povlishock, J. T. (1997). The effects of traumatic brain injury on inhibition in the hippocampus and dentate gyrus. *Brain Research*, *757*(1), 119–132.

Ruff, R. (2005). Two decades of advances in understanding of mild traumatic brain injury. *Journal of Head Trauma Rehabilitation*.

Ruff, R. M., Iverson, G. L., Barth, J. T., Bush, S. S., & Broshek, D. K. (2009). Recommendations for diagnosing a mild traumatic brain injury: A national academy of neuropsychology education paper. *Archives of Clinical Neuropsychology*.

Rutland-Brown, W., Langlois, J. A., Thomas, K. E., & Xi, Y. L. (2006). Incidence of traumatic brain injury in the United States, 2003. *J Head Trauma Rehabil*, *21*(6), 544–548.

Santhakumar, V., Bender, R., Frotscher, M., Ross, S. T., Hollrigel, G. S., Toth, Z., & Soltesz, I. (2000). Granule cell hyperexcitability in the early post-traumatic rat dentate gyrus: the "irritable mossy cell" hypothesis. *The Journal of Physiology*, *524 Pt 1*(Pt 1), 117–34.

Santhakumar, V., Ratzliff, A. D. H., Jeng, J., Toth, Z., & Soltesz, I. (2001). Long-term hyperexcitability in the hippocampus after experimental head trauma. *Annals of Neurology*, *50*(6), 708–717.

Santhakumar, V., Voipio, J., Kaila, K., & Soltesz, I. (2003). Post-traumatic hyperexcitability is not caused by impaired buffering of extracellular potassium. *The Journal of Neuroscience : The Official Journal of the Society for Neuroscience*, *23*(13), 5865–76.

Sara, Y., Virmani, T., Deák, F., Liu, X., & Kavalali, E. T. (2005). An isolated pool of vesicles recycles at rest and drives spontaneous neurotransmission. *Neuron*.

Savanthrapadian, S., Meyer, T., Elgueta, C., Booker, S. A., Vida, I., & Bartos, M. (2014). Synaptic Properties of SOM- and CCK-Expressing Cells in Dentate Gyrus Interneuron Networks. *Journal of Neuroscience*, *34*(24), 8197–8209.

Scharfman, H. E. (1992). Differentiation of rat dentate neurons by morphology and electrophysiology in hippocampal slices: granule cells, spiny hilar cells and aspiny "fast-spiking" cells. *Epilepsy Research. Supplement*, *7*, 93–109.

Scharfman, H. E. (1994). Evidence from simultaneous intracellular recordings in rat hippocampal slices that area CA3 pyramidal cells innervate dentate hilar mossy cells. *Journal of Neurophysiology*.

Scharfman, H. E. (2016). The enigmatic mossy cell of the dentate gyrus. *Nat Rev Neurosci*, *17*(9), 562–575.

Scharfman, H. E., & Myers, C. E. (2012). Hilar mossy cells of the dentate gyrus: a historical perspective. *Frontiers in Neural Circuits*, *6*, 106.

Scharfman, H. E., & Myers, C. E. (2013). Hilar mossy cells of the dentate gyrus: a historical perspective. *Frontiers in Neural Circuits*, *6*.

Schwarzbach, E., Bonislawski, D. P., Xiong, G., & Cohen, A. S. (2006). Mechanisms underlying the inability to induce area CA1 LTP in the mouse after traumatic brain injury. *Hippocampus*, *16*(6), 541–550.

Shum, D., Valentine, M., & Cutmore, T. (1999). Performance of Individuals with Severe Long-Term Traumatic Brain Injury on Time-, Event-, and Activity-Based Prospective Memory Tasks. *Journal of Clinical and Experimental Neuropsychology (Neuropsychology, Development and Cognition: Section A)*.

Smith, C. J., Xiong, G., Elkind, J. A., Putnam, B., & Cohen, A. S. (2015). Brain injury impairs working memory and prefrontal circuit function. *Frontiers in Neurology*, *6*(NOV), 1–13.

Smith, D. H., Okiyama, K., Thomas, M. J., Claussen, B., & McIntosh, T. K. (1991). Evaluation of memory dysfunction following experimental brain injury using the Morris water maze. *Journal of Neurotrauma*, *8*(4), 259–269.

Soltesz, I., Smetters, D. K., & Mody, I. (1995). Tonic Inhibition Originates from Synapses Close to the Soma. *Neuron*, *14*, 1273–1283.

Soriano, E., & Frotscher, M. (1993). Spiny nonpyramidal neurons in the CA3 region of the rat hippocampus are glutamate???like immunoreactive and receive convergent mossy fiber input. *Journal of Comparative Neurology*, *333*(3), 435–448.

Soriano, E., Nitsch, R., & Frotscher, M. (1990). Axo-axonic chandelier cells in the rat fascia

dentata: Golgi-electron microscopy and immunocytochemical studies. *Journal of Comparative Neurology*.

Staley, K. J., Otis, T. S., & Mody, I. (1992). Membrane properties of dentate gyrus granule cells: comparison of sharp microelectrode and whole-cell recordings. *Journal of Neurophysiology*, *67*(5), 1346–1358.

Swanson, L. W., & Hartman, B. K. (1975). The central adrenergic system. An immunofluorescence study of the location of cell bodies and their efferent connections in the rat utilizing dopamine-B-hydroxylase as a marker. *Journal of Comparative Neurology*.

Tamamaki, N., & Nojyo, Y. (1993). Projection of the entorhinal layer II neurons in the rat as revealed by intracellular pressure???injection of neurobiotin. *Hippocampus*, *3*(4), 471–480.

Tang, Y. P., Noda, Y., Hasegawa, T., & Nabeshima, T. (1997). A concussive-like brain injury model in mice (I): impairment in learning and memory. *Journal of Neurotrauma*, *14*(11), 851–862.

Tate, D. F., & Bigler, E. D. (n.d.). Fornix and hippocampal atrophy in traumatic brain injury. *Learning & Memory (Cold Spring Harbor, N.Y.)*, *7*(6), 442–6.

Taylor, C. A., Bell, J. M., Breiding, M. J., & Xu, L. (2017). Traumatic Brain Injury–Related Emergency Department Visits, Hospitalizations, and Deaths — United States, 2007 and 2013. *MMWR. Surveillance Summaries*, *66*(9), 1–16.

Teyler, T. J., & Alger, B. E. (1976). Monosynaptic habituation in the vertebrate forebrain: The dentate gyrus examined in vitro. *Brain Research*, *115*(3), 413–425.

Thomas R. Frieden, Debra Houry, G. B. (2015). Traumatic Brain Injury In the United States: Epidemiology and Rehabilitation. *Centers for Disease Control and Prevention (CDC)*.

Thompson, H. J., Lifshitz, J., Marklund, N., Grady, M. S., Graham, D. I., Hovda, D. A., & McIntosh, T. K. (2005). Lateral Fluid Percussion Brain Injury: A 15-Year Review and Evaluation. *Journal of Neurotrauma*.

Titus, D. J., Sakurai, A., Kang, Y., Furones, C., Jergova, S., Santos, R., … Atkins, C. M. (2013). Phosphodiesterase Inhibition Rescues Chronic Cognitive Deficits Induced by Traumatic

Brain Injury. *Journal of Neuroscience*, *33*(12), 5216–5226.

Tonegawa, S., Pignatelli, M., Roy, D. S., & Ryan, T. J. (2015). Memory engram storage and retrieval. *Current Opinion in Neurobiology*.

Toth, Z., Hollrigel, G. S., Gorcs, T., & Soltesz, I. (1997). Instantaneous perturbation of dentate interneuronal networks by a pressure wave-transient delivered to the neocortex. *The Journal of Neuroscience : The Official Journal of the Society for Neuroscience*, *17*(21), 8106–17.

Tran, L. D., Lifshitz, J., Witgen, B. M., Schwarzbach, E., Cohen, A. S., & Grady, M. S. (2006). Response of the contralateral hippocampus to lateral fluid percussion brain injury. *Journal of Neurotrauma*, *23*(9), 1330–42.

Treves, a, Treves, a, Rolls, E. T., & Rolls, E. T. (1994). Computational analysis of the role of the hippocampus in memory. *Hippocampus*, *4*(3), 374–391.

Treves, A., & Rolls, E. T. (1994). Computational analysis of the role of the hippocampus in memory. *Hippocampus*, *4*(3), 374–391.

Tsirka, V., Simos, P., Vakis, A., Vourkas, M., Arzoglou, V., Syrmos, N., … Micheloyannis, S. (2010). Material-specific difficulties in episodic memory tasks in mild traumatic brain injury. *International Journal of Neuroscience*, *120*(3), 184–191.

Tsuda, S., Hou, J., Nelson, R. L., Wilkie, Z. J., Mustafa, G., Sinharoy, A., … Bose, P. K. (2016). Prolonged hippocampal cell death following closed-head traumatic brain injury in rats. *Neuroreport*, *27*(10), 724–729.

Tulving, E. (1972). Episodic and semantic memory. *Organization of Memory*.

Tulving, E. (1985). How many memory systems are there? *American Psychologist*, *40*, 385–398.

Tulving, E., & Markowitsch, H. J. (1998). Episodic and declarative memory: role of the hippocampus. *Hippocampus*, *8*(3), 198–204.

Tweedie, D., Rachmany, L., Rubovitch, V., Lehrmann, E., Zhang, Y., Becker, K. G., … Pick, C. G. (2013). Exendin-4, a glucagon-like peptide-1 receptor agonist prevents mTBI-induced changes in hippocampus gene expression and memory deficits in mice. *Experimental Neurology*, *239*(1), 170–182.

Vascak, M., Jin, X., Jacobs, K. M., & Povlishock, J. T. (2018). Mild Traumatic Brain Injury Induces Structural and Functional Disconnection of Local Neocortical Inhibitory Networks via Parvalbumin Interneuron Diffuse Axonal Injury. *Cerebral Cortex*, *28*(5), 1625–1644.

Vascak, M., Sun, J., Baer, M., Jacobs, K. M., & Povlishock, J. T. (2017). Mild Traumatic Brain Injury Evokes Pyramidal Neuron Axon Initial Segment Plasticity and Diffuse Presynaptic Inhibitory Terminal Loss. *Frontiers in Cellular Neuroscience*, *11*, 157.

Wammes, J. D., Good, T. J., & Fernandes, M. A. (2017). Autobiographical and episodic memory deficits in mild traumatic brain injury. *Brain and Cognition*, *111*, 112–126.

White, E. R., Pinar, C., Bostrom, C. A., Meconi, A., & Christie, B. R. (2016). Mild Traumatic Brain Injury Produces Long-Lasting Deficits in Synaptic Plasticity in the Female Juvenile Hippocampus. *Journal of Neurotrauma*, neu.2016.4638.

Williams, P. A., Larimer, P., Gao, Y., & Strowbridge, B. W. (2007). Semilunar Granule Cells: Glutamatergic Neurons in the Rat Dentate Gyrus with Axon Collaterals in the Inner Molecular Layer. *Journal of Neuroscience*, *27*(50), 13756–13761.

Williamson, A., Spencer, D. D., & Shepherd, G. M. (1993). Comparison between the membrane and synaptic properties of human and rodent dentate granule cells. *Brain Research*, *622*(1–2), 194–202.

Wilson, D. I. G., Langston, R. F., Schlesiger, M. I., Wagner, M., Watanabe, S., & Ainge, J. A. (2013). Lateral entorhinal cortex is critical for novel object-context recognition. *Hippocampus*, *23*(5), 352–366.

Witgen, B. M., Lifshitz, J., Smith, M. L., Schwarzbach, E., Liang, S. L., Grady, M. S., & Cohen, A. S. (2005). Regional hippocampal alteration associated with cognitive deficit following experimental brain injury: A systems, network and cellular evaluation. *Neuroscience*, *133*(1), 1–15.

Witter, M. P. (2007a). Intrinsic and extrinsic wiring of CA3: indications for connectional heterogeneity. *Learning & Memory (Cold Spring Harbor, N.Y.)*, *14*(11), 705–713.

Witter, M. P. (2007b). The perforant path: projections from the entorhinal cortex to the dentate gyrus. *Progress in Brain Research*, *163*, 43–61.

Wolf, J. A., Stys, P. K., Lusardi, T., Meaney, D., & Smith, D. H. (2001). Traumatic Axonal Injury Induces Calcium Influx Modulated by Tetrodotoxin-Sensitive Sodium Channels, *21*(6), 1923–1930.

Wright, B. J., & Jackson, M. B. (2014). Long-term potentiation in hilar circuitry modulates gating by the dentate gyrus. *The Journal of Neuroscience : The Official Journal of the Society for Neuroscience*, *34*(29), 9743–53.

Wyss, J. M., Swanson, L. W., & Cowan, W. M. (1979). Evidence for an input to the molecular layer and the stratum granulosum of the dentate gyrus from the supramammillary region of the hypothalamus. *Anatomy and Embryology*.

Yamashita, S., Hasuo, H., Tokutomi, T., Shigemori, M., & Akasu, T. (2011). Edaravone attenuates impairment of synaptic plasticity in granule cell layer of the dentate gyrus following traumatic brain injury. *The Kurume Medical Journal*, *58*(2), 47–58.

Yassa, M. A., & Stark, C. E. L. (2011). Pattern separation in the hippocampus. *Trends in Neurosciences*.

Yuen, T. J., Browne, K. D., Iwata, A., & Smith, D. H. (2009). Sodium channelopathy induced by mild axonal trauma worsens outcome after a repeat injury. *Journal of Neuroscience Research*, *87*(16), 3620–5.

Zhang, B.-L., Chen, X., Tan, T., Yang, Z., Carlos, D., Jiang, R.-C., & Zhang, J.-N. (2011). Traumatic brain injury impairs synaptic plasticity in hippocampus in rats. *Chinese Medical Journal*, *124*(5), 740–5.

Zhang, B., Chen, X., Lin, Y., Tan, T., Yang, Z., Dayao, C., … Zhang, J. (2011). Impairment of synaptic plasticity in hippocampus is exacerbated by methylprednisolone in a rat model of traumatic brain injury. *Brain Research*, *1382*, 165–172.

Zhang, W., & Buckmaster, P. S. (2009). Dysfunction of the Dentate Basket Cell Circuit in a Rat Model of Temporal Lobe Epilepsy. *Journal of Neuroscience*.

Zhang, Y., Chopp, M., Meng, Y., & Zhang, Z. G. (2015). Cerebrolysin improves cognitive performance in rats after mild traumatic brain injury, *122*(April), 843–855.

Zimmer, J. (1971). Ipsilateral afferents to the commissural zone of the fascia dentata,

demonstrated in decommissurated rats by silver impregnation. *The Journal of Comparative Neurology*, *142*(4), 393–416.

Zohar, O., Rubovitch, V., Milman, A., Schreiber, S., & Pick, C. G. (2011). Behavioral consequences of minimal traumatic brain injury in mice. *Acta Neurobiologiae Experimentalis*, *71*(1), 36–45.